Trapping and Cooling Atoms at High Densities

by

Michael Arnold Joffe

M.S. Engineering Physics, Moscow Institute of Physics and Technology (1984)

Submitted to the Department of Physics in
partial fulfillment of the requirements
for the degree of

Doctor of Philosophy

at the

Massachusetts Institute of Technology

November, 1993

Signature of the Author

Department of Physics
December, 1993

Certified by

David E. Pritchard
Professor of Physics
Thesis Supervisor

Accepted by

George F. Koster
Chairman, Department Committee
on Graduate Studies

To All From Whom I Have Learned

Trapping and Cooling Atoms at High Densities

by

Michael Arnold Joffe

Submitted to the Department of Physics
in December of 1993 in partial fulfillment
of the requirements for the degree of
Doctor of Philosophy

Abstract

Results of experiments on trapping and cooling of high number of sodium atoms at high densities are presented. Atoms are loaded into a magneto-optical trap from a slow atomic beam. A flux of up to 10^{12} slow atoms/sec was achieved with a Zeeman slower with increasing magnetic field. A new technique combining slowing and transverse cooling of a sodium atomic beam by two-dimensional optical molasses inside the slower was demonstrated. The transverse molasses increases the brightness of the slow beam, and allows it to be deflected out of the intense slowing laser light.

A new magneto-optical trap (**dark SP**ontaneous **O**ptical **T**rap) was demonstrated which confined atoms predominantly in a "dark" hyperfine level, that does not interact with the trapping light. This leads to much higher atomic densities as repulsive forces between atoms due to rescattered radiation are reduced and trap loss due to excited-state collisions is diminished. In such a trap, more than 10^{10} sodium atoms were confined to densities approaching 10^{12} atoms cm^{-3}.

Optically trapped atoms were further cooled with new kind of dark polarization-gradient optical molasses. The scheme overcomes limits on minimum temperature arising at high atomic densities. Temperature of 50 μK was derived from images of the ballistically expanding cloud.

Optically cooled atoms were efficiently reloaded in situ into a spherical-quadrupole magnetic trap. Computer model which was developed to simulate experimental conditions indicated that evaporative cooling of sodium atoms should be possible at present experimental conditions.

Thesis Supervisor: Dr. David E. Pritchard

Title: Professor of Physics

ACKNOWLEDGMENT

I would like to take this rare opportunity to express my gratitude to all those people who, in one way or the other, helped me to come to this point of my life.

I thank my parents for explaining me the importance of education, supporting me in all ways during my schooling, encouraging independence in decisions and choices, and, most importantly, their understanding.

I am extremely grateful to prof. David Pritchard who literally picked me up in a hallway at MIT and gave me this opportunity of a lifetime to work in his exciting, fast-paced, intellectually challenging, and well supported research lab. I would like to thank him for creating a creative environment of independent work, while being a real mentor available for questioning and discussions. I also appreciate prof. Pritchard's intuition that not only allowed him to choose right experiments but also pick right people for the group. As a result, the author had a chance to meet and collaborate with excellent professionals and extraordinary individuals. I would like to specifically thank Dave for sending me to several conferences and Les Houches Summer School. That has been a wonderful and very valuable experience for me.

An opportunity to work with Wolfgang Ketterle is the biggest piece of luck I have had in my professional career. A real team leader he has been the major moving force of the whole project, with whom we shared success and failures, all days and many sleepless nights. He has taught me much more than could be squeezed into a theses but fortunately it will stay with me.

The work was a team effort and I would like to thank Ken Davis for reliably doing the first shift of the round-the-clock runs and getting things going. I wish him a lot of success and interesting discoveries with the beloved machine left in his capable hands.

I am proud of being able to call Alex Martin a colleague of mine. We had (too?) many cups of coffee together and, while the bad parts of the manuscript are the sole responsibility of the author, the good parts should be to a large part credited to Alex.

I have been very happy to work with excellent undergraduate students who made very valuable contributions to the experiment and also quietly allowed me to practice management skills on them. Many thanks to Stan Thompson, John Wuu, Ilya Entin, Dave Pelly, Alex Silitch, Wan Morshidi.

Many thanks to all the students in the group and for setting up a high standard of a Graduate Student and challenging me to live up to it. I am so grateful to Kris Helmerson who patiently introduced me to the lab and taught me by example a lot of survival skills. I felt somewhat uncomfortable asking him a question though because he would drop whatever he was doing at the moment to help me out. And helped he did! Thanks to Chris Ekstrom for being always ready to give an expert advice, volunteer a suggestion and greeting us when he came to the lab very early in the morning. Thanks to David Keith for showing me places in town where one can escape the tough research schedule and talk about life and other less important, but still interesting subjects. Thanks to Vasant Natarajan for always providing words of encouragement and always being able to remind what was the name of that LSC movie that we saw last week. Thanks to Jörg Schmiedmayer who clearly demonstrated that it is possible to do several things simulteneously: talk science, drink beer, shoot pool, and enjoy his company. Ric Stoner,

Bruce Oldaker, Kevin Boyce, Frank DeFilippo, Eric Cornell, Min Xio, Michael Chapman, Troy Hammonds, Mike Bradley made my whole life at MIT not just professionally rewarding but personally pleasurable and joyful.

I would like to acknowledge many members of prof. Daniel Kleppner's group. John Doyle has been indispensable in discussing details of experiment and the model and, furthermore, has become a good personal friend. Robert Lutwak provided reliable electronic contact with the Outside World (it turned out there is one) and always found time to punch in that magic "&%$()" string in UNIX language that actually meant something to the computer. Jeff Holey ("the Coach"), Jon Sandberg, Claudio Cesar, Hong Jiao, Michael Yoo and all the others with whom I overlapped much less.

I would like to thank Warren and Deb Moskowitz for helping me finding my place in a long list of Dave Pritchard's students, providing a link with alumni and great recreation.

There were many people whose everyday support made the work possible, and often enjoyable. Specifically, I would like to thank Carol Costa who not only greatly relieved the burden of navigating through the complicated administrative system but also created a friendly, homey work environment that is so important in life full of problems and stresses. I would like to thank John Peck and Maxine Samuels who often stayed after hours to patiently place a rush order for the part we needed yesterday.

I would also like to thank V. Bulatov, V. Rozenshtein, S. Cheskis, S. Ryabchuk, S. Il'in, O. Kishkovich, A. Iogansen for patiently teaching me the "skills of the trade" of experimental physics on the early stages of my career.

I am very grateful to Peter Dandridge, Sr. and Peter Dandridge, Jr. of Atomic Welding Limited, whose only expertise and skills made it possible to realize some of the author's designs in hardware.

Many thanks to Candy Royer and Jeff Hamilton for teaching me how to stay calm, keep the ballance, maintain the pace and talk to partners (basically, how to remain sane and enjoy it). Their efforts resulted in probably the most visible result of my MIT training: my backhand has improved significantly.

I thank Dr. and Mrs. Bloch who gave me a crush introductory course on American life and education when I so badly needed it.

Many thanks to Dr. and Mrs. Perlov who welcomed me in their home when I just came to Boston and had many other things to worry about besides housing.

I would like to thank my old friend Eugene Gelberger and his wife Masha for being with me during all these years.

The last but not least, I would like to thank Natasha for patiently taking from me all that while I have been busy doing all of the above.

Carol has wisely suggested that I start writing the Acknowledgment section in advance in order not to forget anybody, so I hope I have not:

Gee Thanx, Everybody!

"He had never dined with a duchess, never received a prize, never been interviewed, never produced anything the public could understand, nor experienced anything since his schoolboy amours which nice people could regard as romantic. He was, in fact, an authentic scientist."

S. Lewis

BIOGRAPHICAL NOTE

I, Michael Joffe, was born in 1961 in what was then the USSR. As long as I can remember I always preferred "precise" disciplines, such as math and physics to others. While at school with the extensive science program I was fascinated by the Quest for The Truth. Later on I discovered that, in addition, Science as a full-time occupation is a healthy alternative to the everyday lies of communist propaganda. In pursuit of the dream I graduated from Moscow Institute of Physics and Technology with a degree in Chemical Physics. During a few years that followed I was working in different research labs studying atoms and molecules moving in the gas. Once I heard about experiments where scientists learned how to "tame" atoms and made them "stand still" I knew what I want to do. After coming to the U.S. in 1988 I joined the Neutral Atoms Trapping Group at MIT as a graduate student.

TABLE OF CONTENTS

"Be careful what you ask for, you just may get it"

1. INTRODUCTION

1.1. MOTIVATION

The last decade has witnessed tremendous progress in manipulation of atoms with electromagnetic fields. Fascinated by the idea of "taming" atoms, many groups around the world have developed techniques to slow down atomic beams, confine atoms in a trap, and cool trapped samples to unprecedented temperatures. Just as the achievements of classical mechanics and molecular physics enabled this century's success of quantum mechanics, it was the careful exploitation of the well-understood quantum structure of atoms that allowed scientists to find ways to gain control of the mechanics and thermodynamics of atomic samples.

Themselves a product of atomic physics research, coherent light sources have recently become efficient tools in controlling the translational degrees of freedom of the classical motion of atoms. It is a challenge to make the next step along the eternal spiral of scientific progress - to advance this control to a point where quantum features of translational motion will become observable. Atom traps are perfect instruments for observing these effects.

In order to observe collective quantum effects, such as Bose-Einstein Condensation, atomic samples have to be made sufficiently cold and sufficiently dense so that their phase-space density exceeds the theoretically predicted threshold. Other experiments, such as slow-atom interferometers using intense laser-like atomic beams, might greatly benefit if high densities of cold atoms are achieved. Studies of a whole new class of cold collisions for which quadratic density dependence is expected benefit greatly if high enough densities of cold atoms are reached.

Since trapped atoms necessarily decay with time due to unavoidable losses (e.g. knock-out collisions with background molecules) or desirable effects (e.g. evaporation from a trap), it is highly desirable to start off experiments with a high total number of trapped atoms. This series of experiments has been aimed at achieving the highest possible density of the highest possible total number of trapped atoms cooled to the lowest possible temperature, en route to observation of collective quantum effects.

This chapter will provide a background on trapping and cooling and a general overview of the experimental achievements. The subsequent chapters will describe in greater detail each of the steps towards the set goal.

1.2. TRAPPING AND COOLING BACKGROUND

1.2.1. Sodium

Most of the experiments on trapping and cooling of atoms with light have been performed on alkali atoms because of their simple electronic structure and availability of strong transitions at easily attainable laser wavelenghts. We use sodium for our experiments. The transition between the ground $3S_{1/2}$ and the $3P_{3/2}$ first excited state

(589 nm) falls right into the tunability range of dye lasers where high power single-frequency operation is available. The nucleus of sodium atom carries spin I = 3/2, so the total spin is integral, making sodium a good candidate for observation of Bose-Einstein Statistics.

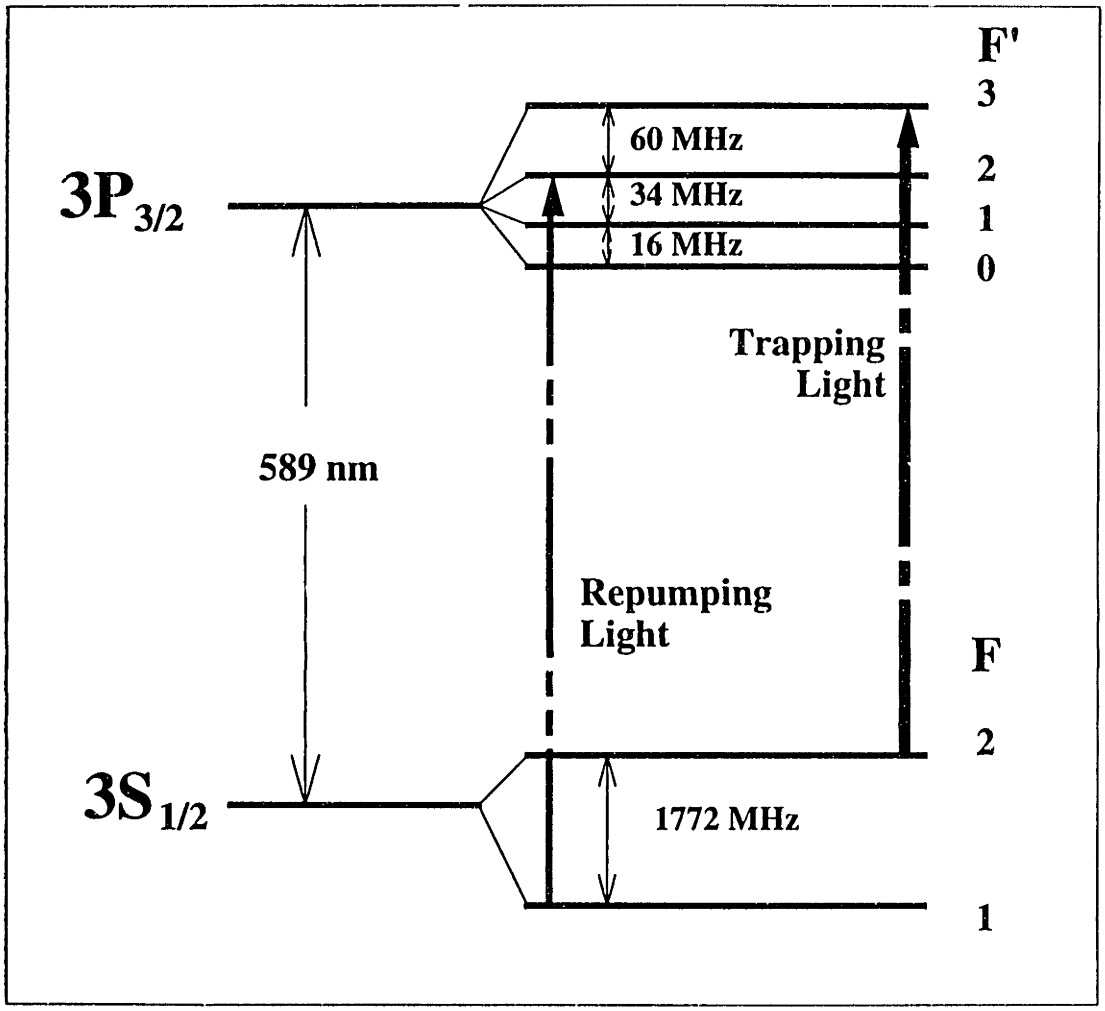

Fig. 1-1: Hyperfine structure of sodium levels.

The hyperfine structure of sodium levels is shown in Fig. 1-1. This omnipresent scheme is sometimes considered a nuisance, but is in fact essential for the described experiments.

Light forces used to cool and confine atoms arise due to the cycling optical transition between the $3S_{1/2}$ (F = 2) and the $3P_{3/2}$ (F' = 3) levels. Due to the finite probability of off-resonant Raman processes involving the F' = 2 or 1 levels, atoms can be optically

pumped into the (F = 1) level of the ground state. They can be brought back to the (F = 2) level by means of repumping light tuned to the (F = 2) → (F' = 2) transition.

In a magnetic field the degenerate Zeeman sublevels of each hyperfine level split according to their respective g-factors. Fig. 1-2 shows the splitting of the (F = 1) level of the ground state.

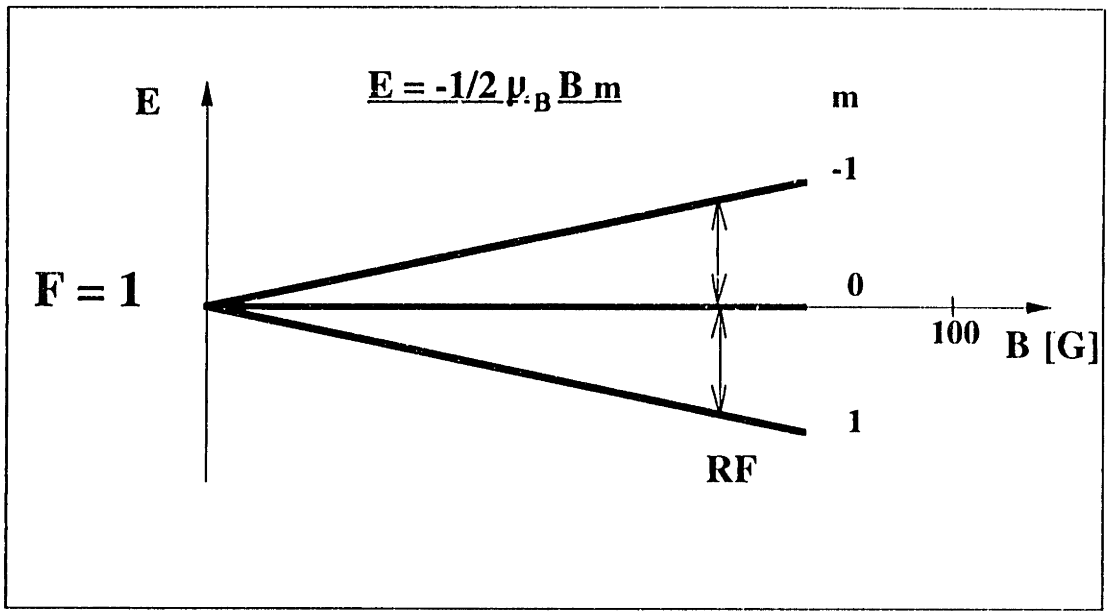

Fig. 1-2: Zeeman splitting of the (F = 1) ground level.

As shown on the picture the potential energy of atoms in (m_F=1) state increases with magnetic field. Consequently, atoms in this "weak-field seeking" state can be (and have been in our experiments) confined in a magnetic field minimum. Furthermore, transitions between neighboring states ($\Delta m_F = \pm 1$) can be induced by a resonant RF radiation.

1.2.2. Forces on Atoms

There are two basic kinds of forces that can be applied to neutral atoms: magnetic forces and light forces.

If an atom has a magnetic dipole moment $\vec{\mu}$ then in an inhomogeneous magnetic field $\vec{B}$ it would experience a force $-\nabla(-\vec{\mu} \cdot \vec{B})$. Obviously, an atom has to be in a state with a non-zero magnetic dipole moment in order to experience such a force.

Light forces with a magnitude of practical interest can be exerted on atoms with resonant laser light. The most commonly used force is the spontaneous light force (also called "scattering" or "radiation-pressure" force). It arises from momentum transfer to atoms from a directed beam of photons [STE86]. Every absorbed photon transfers its momentum to an atom, while recoil momentum due to spontaneous re-emission in random directions averages out to zero. Consequently, when irradiated by a laser, atoms experience a force:

$$\vec{F} = \Gamma \hbar \vec{k}, \tag{1.1}$$

where Γ is a scattering rate and $\hbar\vec{k}$ is photon momentum. Maximum scattering rate is achieved when the transition is saturated and

$$\Gamma_{max} = \frac{1}{2\tau}, \tag{1.2}$$

where τ is spontaneous lifetime of the upper state. In order for the force to be strong and impact significant momentum transfer, atoms have to scatter many photons. To make this possible atoms have to return back to the same initial state after spontaneously emitting a photon. Exiting transitions which have this property are said to be "cycling". While we do not have much command of the spontaneous emission, excitation can be controlled. Since excitation rates are determined by selection rules, selective excitation of cycling transitions can sometimes be achieved by appropriate polarization of the resonant laser light. This is the kind of light force we use in our experiments with sodium.

In a magnetic field F and m_F are not a good quantum numbers, but are commonly used as convinient labels for levels in small magnetic fields. In weak magnetic fields F-levels split into 2F+1 sublevels with different m_F. For sodium, the cycling transition is the transition between $(F=2, m_F=2)$ ground level and $(F'=3, m_F'=3)$ upper level which can be excited by a σ^+ circularly polarized light. Symmetry implies that (2,-2)$\leftrightarrow$(3,-3) is also a cycling transition, provided the exciting light has the opposite helicity σ^-. Leakage out ot the cycling transition occurs predominantly due to spontaneous Raman transitions from (F = 2) to (F = 1) ground level via off-resonanant excitation of $F'=2$ level.

There is another known kind of light force - stimulated (also known as "dipole", "gradient" or "induced") force. This force arises from the interaction of an induced dipole moment of an atom with an inhomogeneous electric field in the intense laser beam of bell-shape profile [CBA86]. Recently, some other new manifestations of light forces have been discovered [GLO92] and even used for trapping atoms [EBS92].

1.2.3. Traps for Neutral Atoms

Confinement of Atoms

If forces acting on an atomic sample are arranged around a point in space $\vec{r}_o$ in such a way that the net force acting on an atom is restoring ($\vec{F}=-k(\vec{r}-\vec{r}_o)$), atoms can be confined in space around this point, provided their energy is sufficiently reduced. In other words, atoms can be trapped in a potential well with a minimum at $\vec{r}_o$. Both optical and magnetic traps have been demonstrated for various atoms. Furthermore, the field of atomic trapping has expanded already to such an extent that several comprehensive reviews on atom trapping are available [PHM89, PRK93], so I will only briefly describe here the fundamentals and the main results of the work that has provided the foundation for our experiment.

Magnetic Traps

Generally speaking a magnetic trap is such a configuration of magnetic fields that an atom with a magnetic moment is trapped in a potential well, or local minimum of the potential energy $-\vec{\mu} \cdot \vec{B}$. The possibility of confinement of "weak-field seekers" (i.e. atoms in a state whose energy increases with increasing magnetic field) has been first pointed out in [HEE63]. In subsequent years, several magnetic field configurations have been suggested [PRI83, BEM87]. The first atom trap demonstrated [MPP85] was a magnetic trap . Later, improved schemes have been implemented for trapping of sodium [BLM87] and hydrogen [HKD87]. While more detailed analysis of these schemes is postponed till Chapter 6 (entirely devoted to magnetic trapping) I would like to discuss here the more general aspects of magnetic confinement of neutral atoms.

While static fields can be arranged so that the weak-field seekers are trapped, the problem is that it is only the weak-field seekers that can be trapped. It is possible, in fact in several ways, to achieve a local minimum of a static magnetic field, so for weak-field seekers this minimum is at the same time a minimum of potential energy (a trap). But, as has been shown by Wing [WIN84] the magnitude of a static magnetic field can not have local maxima in free space. This is unfortunate from the trapping standpoint, since the lowest-energy state is necessarily a strong-field seeker (e.g. Fig. 1-2) and, consequently, a trapped weak-field seeking state is not the lowest-energy state of the system. Consequently, some process can exist that enables atoms to make transition to the lower non-trapped state and leave the trap. Also, the "excessive" potential energy can be released and transformed into kinetic energy of atoms. The atom thus heated easier escape the trap which results in an accelerated trap decay. The most common example of this kind of process is the dipolar trap loss when atoms which populate non-trapped states via exothermic spin-exchange collisions.

Depending on the atomic structure of the trapped species and the trapping conditions this fact constitutes a more (hydrogen) or less (sodium) severe problem. I will discuss the details in Chapter 7 and here will give only qualitative arguments. First, this loss mechanism creates an obstacle for achieving high densities of atoms. Second, the heating associated with the process limits the lowest achievable temperature. One reason for heating of the trapped sample is preferential removal of low-energy atoms: the density of colder atoms is higher according to the Boltzmann distribution and the dipolar loss rate is density-dependent. The other is that the released potential energy is partially transferred into kinetic energy of the remaining atoms, i.e. results in heating.

To overcome this problem and trap atoms magnetically in strong-field seeking states two different approaches have been devised. One proposal was to trap ground-state atoms dynamically, i.e. in stable orbits in an appropriate field configuration [KEP92]. The other was the experimental demonstration of trapping cesium atoms in an AC magnetic trap [CMW91] that employs time-varying fields much like in the Paul trap for charged particles. While both approaches might lead to confinement of high densities of atoms they at the same time suffer from inherent heating arising from micromotion of atoms in the trap. Also, actual realizations of both of these ideas are technologically more complicated. Consequently, in our quest for higher densities and lower temperatures, we took advantage of the fact that dipolar loss is not the limiting process for magnetically trapped sodium (there are others that are worse) and restricted ourselves to just optimizing the static field configuration.

Concluding this section, I would like to mention that MIT is a great place to do experiments on magnetic trapping. Not only there is a lot of expertise on magnetic trapping of sodium within the group [HMP92a], but furthermore right next door there is another excellent resource: the world leading group in hydrogen trapping led by professors T. Greytak and D. Kleppner [DSY91].

Optical Traps

Both stimulated and spontaneous light forces can be used to confine neutral atoms. The stimulated light forces have been successfully used to trap atoms [CBA86, GLJ88] and high densities have been achieved [MCH93]. However, since the atoms are trapped in a waist of a tightly focused laser beam, these traps feature a very small volume (10^{-9} cm^3) and only a relatively small number of atoms can be confined* . Consequently, we have chosen for our experiment the Magneto-Optical Trap (MOT) based on the spontaneous light force. Basing on the elegant idea of J. Dalibard to exploit the internal atomic degrees of freedom to overcome the Optical Earnshaw Theorem [ASG83] D. Pritchard has come up with an one-dimensional trapping scheme which has been generalized to 3D by E. Raab. The first MOT has been first demonstrated in 1987 [RPC87]. Since than it has become the light trap of choice for many atom trappers due to its robustness, simplicity, efficiency in capturing and holding large number of atoms. About a dozen different elements have been trapped in a MOT [PRK93] and it has been used as a source of cold atoms in numerous experiments [CMW91, CSG91, RWM90]

The principle operation of MOT can be qualitatively described using a one-dimensional model and is illustrated on Fig. 1-3. Consider an atom with an S_0 ground state and P_1 excited state placed in an inhomogeneous magnetic field $B_z(z) = bz$ (Fig. 1-3a). If the atom is in a zero magnetic field its Zeeman sublevels are degenerate, but as the atom moves along the z axis the levels split increasingly (Fig. 1-3b). Also, since the magnetic field changes sign, the relative positions of the split levels change too: at $z > 0$ it is the $(m = -1)$ level whose energy shifted down, whereas at $z < 0$ it is the $(m = 1)$ level. Now,

---

* In an optical dipole force trap a high peak density of $8 \cdot 10^{11}$ cm^{-3} has been recently achieved [MCH93] which is comparable to our results. However, only 1300 atoms have been trapped, compared to 10^{11} in our dark SPOT.

the idea of a MOT is to irradiate the atom with two counterpropagating laser lights that are circularly polarized with opposite helicities (σ^+ and σ^-).

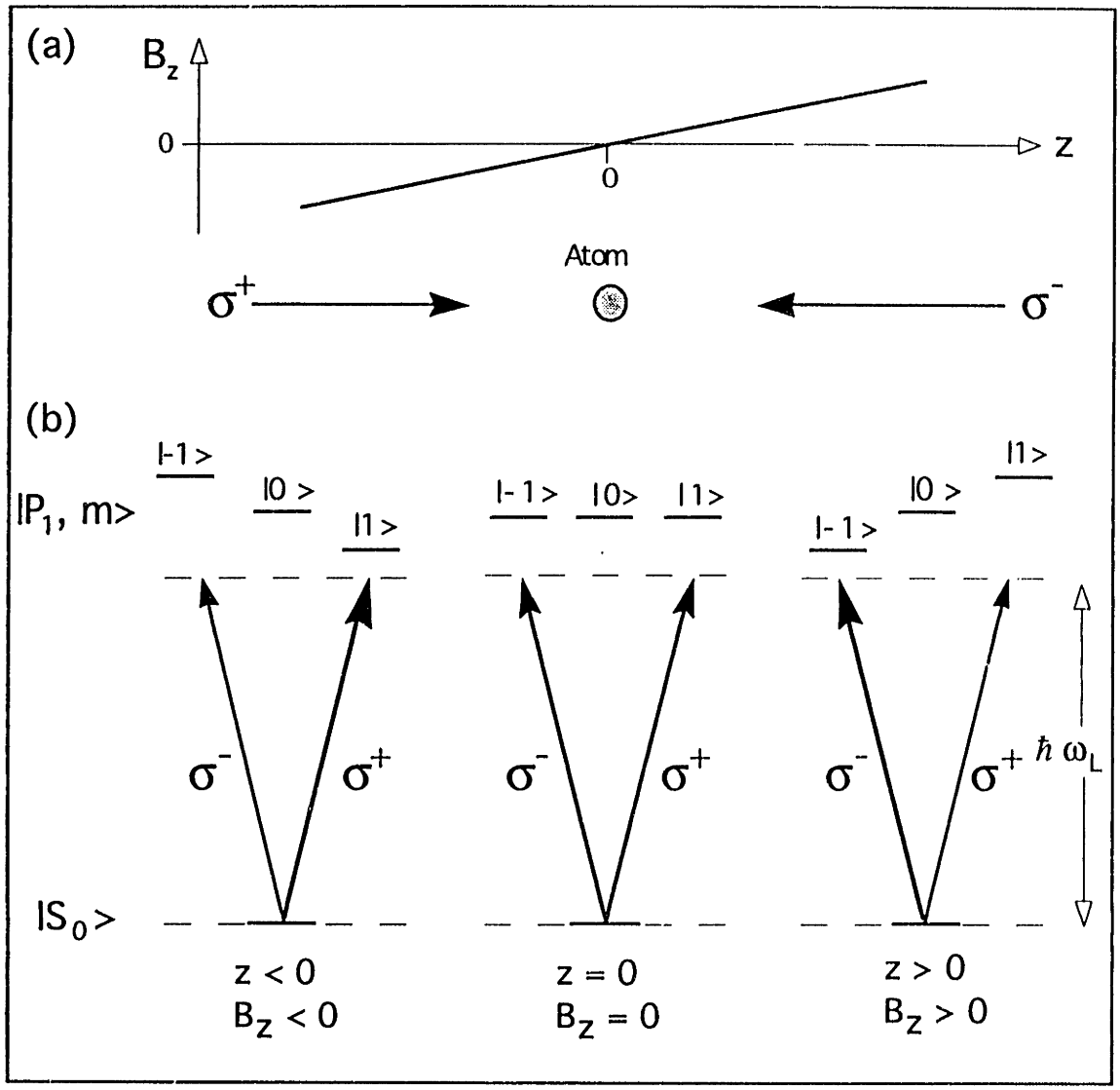

Fig. 1-3: Magneto-Optical Trap: Principle of Operation

Following the conservation of angular momentum selection rules these beams excite transitions to the ($m = 1$) and ($m = -1$) levels respectively. If both beams are detuned to the red of resonance than at $z = 0$ they are equally detuned from their respective transitions and the atom scatters on average equal amounts of photons from the left- and the right-propagating beam. But, as the atom moves along the z axis the Zeeman effect shifts the levels so that the light from a "head-on" laser is closer to the resonance(thick

lines in Fig. 1-3b). Consequently, the net light pressure force is always directed towards the origin and restores the position of the atom. The atom is trapped in one dimension!

Eric Raab has shown [RAA88] that the idea can be generalized to three dimensions for a sodium atom with its more complicated hyperfine structure. Indeed, if three pairs of appropriately polarized laser beam intersect in the center of a spherical quadrupole magnetic field produced by two anti-Helmholtz coils (Fig. 1-4), along each direction the picture looks analogous to the one-dimensional Fig. 1-3. Each of the laser beams (thick arrows on the Fig. 1-3) usually carries two frequencies: one for trapping and one for repumping (see Fig. 1-1). Since the first demonstration of the trap a few modifications of this configuration for magneto-optical trapping have been used by various groups: a tetrahedral beam configuration [SST91] and a vortex-force trap [WHF92]. For our experiments we have used the six-beam configuration as shown on Fig. 1-4.

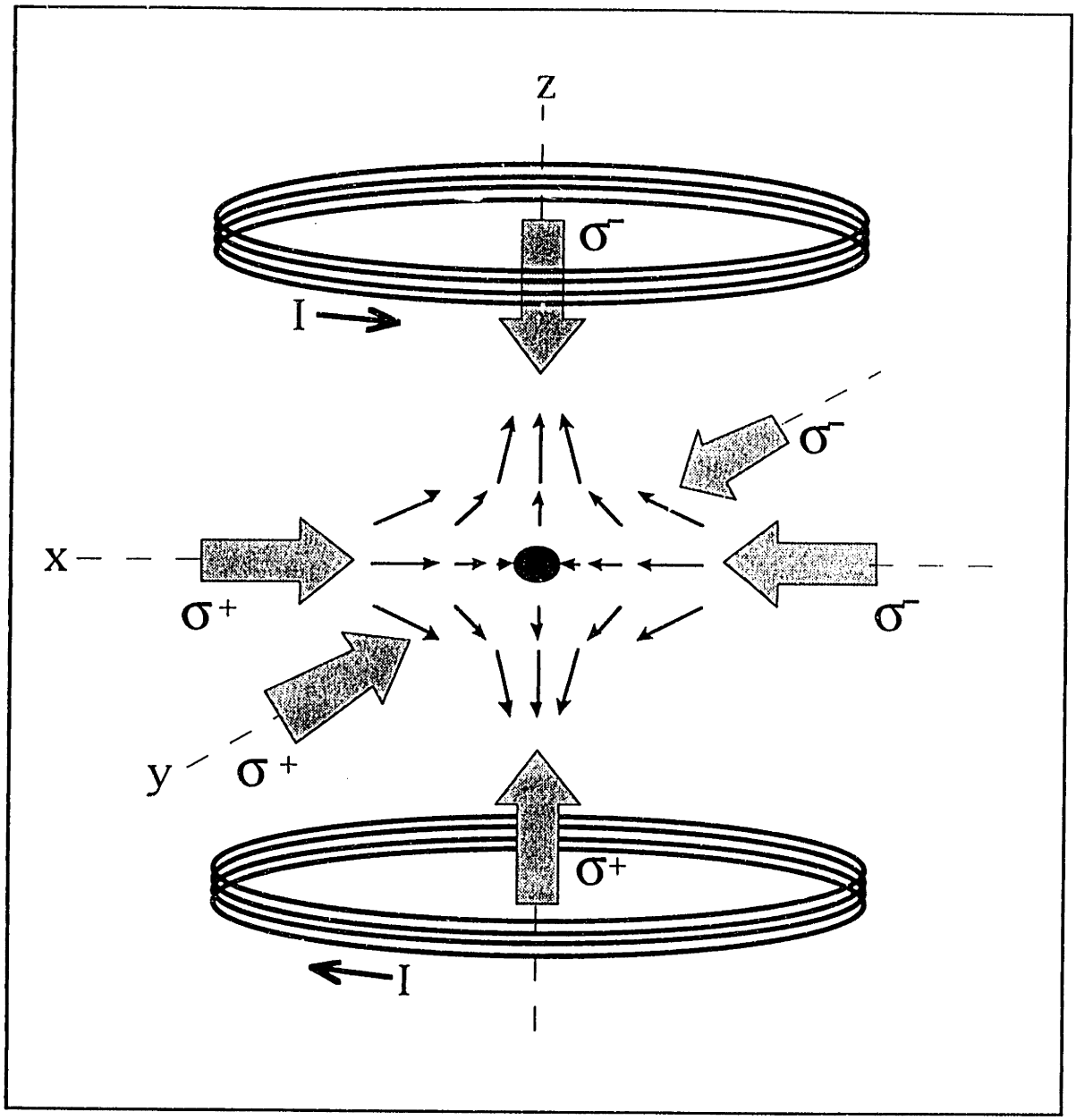

Fig. 1-4: Magneto-Optical Trap: Three-dimensional trapping scheme. The spherical quadrupole field, created by two coils carrying current I, is indicated by thin arrows. Thick arrows denote the laser beams with indicated helicities.

Which Trap is Better?

Comparing optical traps with magnetic ones might look just like comparing apples and oranges. This is to a large extent true but I will attempt to do so anyway. The reason is that comparative analysis of the strong and weak points of each is important for finding the most efficient way to increase the total number and density of trapped atoms and to bring down their temperature.

One advantage that magneto-optical traps for sodium have over magnetic traps is that they are several times deeper. Consequently, they are more robust and more tolerant to such experimental parameters as background pressure. On the other hand, the notable feature of optical traps - presence of a high-intensity resonant light - is a handicap. The problem is that radiation trapping effects, discussed in detail in chapter 4, set hard limits on maximum atomic densities achievable in a MOT. Furthermore, in a MOT atoms spend significant fraction of time in the excited state, so no precision measurements are possible. Also, since many atoms are in the excited state the resulting resonant collisions with ground-state atoms [PCB88, GAP89] introduce an additional loss mechanism limiting the maximum number of atoms.

Generally, a magnetic trap is a "cleaner" system for studying cold atoms. One reason is that laser excitation of atoms is a much stronger perturbation of atoms than a relatively small level shift in a magnetic trap. In addition, while the magnetic field near the trap center can be pretty well calculated using Classical Electricity and Magnetism Laws, the shape of the MOT potential is somewhat a mystery. Not only is it stochastic in nature because of spontaneous decay involved, but it is also subject to ever changing laser beam properties. Every dust particle flowing through the laser beam makes its impact on the shape of the potential well. It is a lot of fun to watch, but hard to describe in quantitative terms. Furthermore, for many experiments such as studies of cold collisions it is highly

desirable to change parameters of the system (temperature, density, etc.) in a controlled way. Magnetic traps whose potential can be pretty accurately changed by (maybe) one knob on the power supply that powers the coils have a big advantage over MOTs. So for actual studies on *cold atoms* rather than atom traps, magnetic traps are much preferred compared to optical traps.

But probably the most important point in comparing these two different techniques of trapping is the question of availability of an efficient cooling scheme. This subject is discussed in the very next section, but it is important to describe here why cooling is necessary anyway. It is easy to understand that a conservative potential would not be able to trap atoms at all. A particle entering the potential well would accelerate towards the center, decelerate along the outbound part of its trajectory to the initial velocity and leave the trap. Thus, it is necessary to provide some dissipation of the atoms' kinetic energy (Dissipation = friction = cooling) while they are in the trap. The most important parameter that characterizes the efficiency of cooling is of course the minimum final temperature of the trapped atoms that one can achieve. The other parameter of merit, however, is probably more important in the early stages of a trapping process: velocity capture range. Depending on how efficient the cooling is, the trap can only capture atoms that have velocity less than a certain value. The better damping the cooling scheme provides, the higher this value is, and so the bigger flux of atoms can be loaded into the trap.

As will be explained in the next section on cooling, MOT has a cooling mechanism "built in": atoms are very efficiently cooled with laser light and even those with relatively high velocity can be captured, cooled, and confined. The coldest temperature one can achieve is, however, limited by the processes discussed in Chapter 5. Conversely, the magnetic potential is conservative and so magnetic traps require external cooling for loading [BLM87]. This is somewhat disadvantageous, but on the other hand, once you get

enough atoms in it, magnetic traps allow for implementation of very efficient cooling scheme - evaporative cooling [MDS88] - that leads to final temperatures much lower than those reachable in optical traps. In our experiments we have attempted to get "the best of two worlds". First, we capture as many atoms as we can in an optical trap exploiting its good capturing and storage capabilities. Then we transfer (reload) the pre-cooled sample into a magnetic trap so that we could take advantage of better control of atoms and the cooling scheme that leads to ultra low temperatures.

1.2.5. Cooling Schemes

A relatively large number of cooling schemes for neutral atoms that have been proposed or even demonstrated can be divided into two groups: Single-atom methods and many-body methods. In the former group some kind of a friction force is applied to every individual atom (e.g. Doppler cooling [LPR89] or polarization-gradient cooling [DAC89, WRS89]) or each atom is continuously run through a closed cycle of events that take out some of its kinetic energy (e.g. Cycling cooling [PRI83]). Since all the single-atom cooling schemes known to date involve lasers, this group can be without loss of generality labeled "Laser Cooling". Conversely, in the latter group cooling mechanism relies on interactions between the atoms (e.g. sympathetic cooling or evaporative cooling [LMT85]).

Laser Cooling

The intuitive method of Doppler Cooling relies on slowing atoms with radiation pressure from a counterpropagating laser beam. The spontaneous light force acts as a friction force, and kinetic energy is carried away by the scattered photons. This idea can be readily generalized to cooling in three dimensions if atoms are irradiated with laser beams from all six directions. In order for the atom to preferentially scatter light from the laser beam opposite to its velocity the light is red-detuned from atomic resonance. The

Doppler shift than brings the counterpropagating beam closer to resonance compared to co-propagating light and gives the name to the cooling scheme. Near-resonant photons coming from all directions create a viscous, dissipative media for atoms called "optical molasses" [LPR89]. As has been mentioned earlier, in a MOT all trapping laser beams are red-detuned so they provide optical cooling *and* trapping at the same time.

A few years after the first demonstration of optical molasses [CHB85] it was discovered that cooling works much better than theoretically predicted in serious violation of Murphy's Law. This later led to a discovery of a much less transparent cooling mechanism - polarization-gradient cooling [DAC89, WRS89]. This more efficient scheme will be discussed in more detail in Chapter 5.

Since both Doppler and polarization-gradient cooling include spontaneous emission their respective temperature limits , albeit much different, have one thing in common. They can not cool below the so-called recoil limit: the kinetic energy of an atom can not be made smaller than the energy of recoil due to photon emission. However, new sub-recoil cooling methods have been demonstrated [KAC92] and may soon be used to efficiently cool atoms in a trap.

Evaporative Cooling

Whoever first thought of this method of cooling atoms did so probably while sipping hot coffee. The idea is to selectively remove hot atoms while keeping the colder ones. If afterwards the sample re-thermalizes the new temperature is lower than it was before. Selective removal can be achieved by lowering the trap so that "hot" atoms from the tail of Maxwell-Boltzmann distribution can escape. At the same time the remaining atoms re-thermalize via elastic collisions and eventually repopulate this "missing" tail. If the density is high enough so that the repopulation is faster than other trap losses - continuous evaporative cooling is possible.

Obviously, some trapped atoms are lost on the way: roughly 20% of atoms per order of magnitude in temperature. But if one has trapped atoms to spare it is a very efficient cooling mechanism with a very low temperature limit. Evaporative cooling naturally requires high densities *and* high number of atoms in a trap. Our experiments have been geared into achieving these parameters. Furthermore, since magnetic traps allow for better control of the trap depth and width it is advantageous to have high densities of *magnetically* trapped atoms. Single-atom cooling is possible for a magnetically trapped sample [HMP92b], but evaporative cooling is the preferred method since much lower ultimate temperatures could be achieved.

1.3. SUMMARY OF THE EXPERIMENTAL ACHIEVEMENTS

In summary, this experiment consisted of a number of steps, all of which were aimed at achieving the goal set above: obtain the highest possible density of the highest possible total number of trapped atoms cooled to the lowest possible temperature. Each individual step is discussed in a separate chapter. Here I will just provide the overall picture that brings them together and summarize the results.

In order to have many atoms in a trap it is necessary to provide for efficient loading of atoms there. Different methods of loading are discussed in Chapter 2, along with the description of our choice - Increasing-field Zeeman Slower. Using this method we have obtained a continuous flux of cold atoms within a velocity capture range of the MOT of $\sim 10^{11}$ atoms/sec.

To accommodate and store all these atoms for a sufficiently long time we have built a special ultra-high vacuum chamber with coils creating strong fields for confinement - the actual trap. This hardware and the diagnostic methods we used to probe the trapped atoms are described in Chapter 3.

In Chapter 4 I will describe the original idea implemented in our group to overcome the severe limitations of a conventional MOT: trapping atoms in a "dark" state. This Dark SPOT (**SP**ontaneous **O**ptical **T**rap) has allowed us to trap more than 10^{10} sodium atoms at densities approaching 10^{12} atoms cm^{-3}, which is a two-order-of-magnitude improvement in the density-number combination .

After the atoms are trapped and accumulated in this dark SPOT it is possible to efficiently cool them using the polarization-gradient cooling. While the scheme itself has been known for a few years, it is a novel achievement to use this method at such high densities. An approach analogous to dark trapping - dark cooling - has enabled us to cool the sample down to 60 μK. This is described in Chapter 5.

The cold sample is then reloaded into a magnetic trap. Different configurations of magnetic traps and the efficiency of the approach compared to other schemes are discussed in Chapter 6 on magnetic trapping. We have reloaded ~25% of our atoms (close to the theoretically predicted 33%) into a magnetic trap without losing density or heating the sample. The result is the densest alkali (and the coldest sodium) atoms in a magnetic trap ever achieved.

Chapter 7 is devoted to evaporative cooling of these magnetically trapped atoms. The theoretical model and the results of the computer simulation are presented along with experimental results.

"All radiation-pressure experiments are basically alike"

A.P. French in "Special Relativity.
The MIT Introductory Physics Series".
(New York, W.W. Norton & Co.), p.13.

2. TRAP LOADING

2.1 LOADING SCHEMES

Before all the exciting experiments can be performed on trapped atoms, the trap has to be loaded, in other words, some atoms have to be put there. Unfortunately, so far all existing traps for neutral atoms are relatively shallow (< 1K). This means that atoms have to be pre-cooled before loading, otherwise the trap will not be able to confine them. Magnetic traps, due to the conservative nature of the potential require that all the cooling is provided externally. Atoms have to be cooled to an energy lower than the trap depth right at or near the trap origin; otherwise, they escape. Magneto-Optical Traps have cooling capabilities built in, so the requirements on loading are somewhat relaxed. The loading requirements of the trap can be characterized by its capture velocity: the maximum velocity of an atom traveling through the trap that can be captured, cooled down and confined by the trap. So an efficient loading source should provide the maximum number of atoms near the trap origin that are slow enough to fall within the

trap capture range. Two kinds of sources of slow atoms have been used for loading a trap: slowed atomic beams and vapor cells.

Slow Beams

In the first approach (slow atomic beam) an atomic beam is slowed down by a counterpropagating laser beam that exerts spontaneous light force on atoms in the beam. The experimental arrangement is such that atoms reach their low (below capture range) final velocity in the vicinity of the trap that captures them.

While many different schemes to slow atoms with laser light have been demonstrated, we were interested in those that produce the largest flux of slow atoms. To date two slowing techniques have been used to load traps with slow atoms: (a) chirp-slowing where the slowing light frequency is swept with a linear ramp to compensate for the changing Doppler shift of decelerated atoms and (b) Zeeman slowing where the Doppler shift is compensated by a specially designed magnetic field. The latter method has the advantage of being continuous, and higher fluxes can be achieved since there is no duty cycle. This chapter will describe our efforts in developing the Zeeman slower for trap loading.

Vapor Cell

The second method of trap loading is a vapor cell. The Magneto-Optical trap is created inside a cell filled with atomic vapor. At any temperature of the vapor, the Maxwell-Boltzmann distribution implies that there are some atoms with very low velocities. These atoms can be directly captured by the trap. Collisional replenishment of this low-velocity tail of the distribution provides a continuous source of slow atoms. Vapor cells have proved to be very reliable, robust and easy-to-make. The problem is that the same vapor that acts as a source of slow atoms for the trap, at the same time creates a trap-loss mechanism. The "cold" minority of atoms in the vapor are captured by the trap, while the "hot" majority collides with trapped atoms and knocks them out of the trap. The

maximum number of atoms in the trap is reached when the background loss grows equal to the loading rate and dynamic equilibrium is achieved.

In order to reach high number of atoms in the trap it is necessary to cut down on these background losses. Hence, It is obviously better to keep the trap in a vacuum and load a trap from the slow beam where the majority (well, at least large fraction) of atoms are within the trap capture range. This was exactly the route we have taken. I will discuss the provisions for the ultra-high vacuum environment in Chapter 3 and the rest of this chapter is devoted to the design and implementation of a beam slower.

2.2 THE ZEEMAN SLOWER

Zeeman slowers [BLM89] have been used by many groups to load a magneto-optical trap [MSR90, SST91] and a magnetic trap [BLM87]. In these slowers, the atoms are slowed with a single-frequency counterpropagating laser beam. As the atoms slow down, their resonant frequency ν_o changes due to the Doppler effect. To keep the decelerating atoms in resonance with the laser frequency ν_l they are passed through a magnetic field profile chosen so that their Doppler shift $\Delta\nu_D$ is compensated by the Zeeman shift $\Delta\nu_Z$. The slower solenoid is designed to create a magnetic field such that:

$$\nu_l = \nu_o + \Delta\nu_D + \Delta\nu_Z. \tag{2.1}$$

The Zeeman slowers for sodium used in earlier works operated on the (2, 2)↔(3, 3). cycling transition. The resonance condition (2.1) in this case looks like:

$$\delta + ku - \frac{\mu}{h}B = 0, \tag{2.2}$$

where $\delta = \nu_l - \nu_o$ is the laser detuning, k is the photon wavevector, u is atomic velocity, μ is the Bohr Magneton, h is the Planck constant, B is the magnetic field. Two conclusions can be derived from (2.2): (a) the decelerating atoms have to be in a

decreasing magnetic field and (b) If the atoms reach their near-zero final velocity in a small magnetic field, the detuning is very small, i.e. the slowing light is close to the atomic resonance of stationary atoms.

The problems with this conventional Zeeman slower arise from these conclusions. In reality small magnetic fields are not abruptly switched off, but rather taper off gradually. Therefore, as the atoms leave the slower they experience off-resonant post-slowing which complicates extraction of a mono-velocity slow beam from the slower. The slowers work great for stopping atoms somewhere inside, but to extract an intense slow atomic beam and direct it to the trap downstream turns out to be all but impossible. So in some previous works [PPM85] the traps were loaded from atoms diffusing away from the stopped beam rather than from the beam. Obviously, the maximum loading rate was somewhat limited. Another approach [BLM87] was to trap atoms downstream in a bias field which required an additional laser frequency to stop atoms when they reached the trap. Furthermore, a MOT does not work in a non-zero field, so it becomes impossible to simply put it downstream from the slower. Another problem with this type of slower is that if the trap is on axis with the near-resonant slowing laser beam, the laser excites atoms and causes additional trap loss.

To overcome these problems while preserving the valuable features of a Zeeman slower (the highest continuos slow atoms flux) we have designed a Zeeman slower with increasing magnetic field [BDR 91]. This slower operates on the (2, -2)↔(3, -3) cycling transition. In this case the resonance condition (2.1) takes form:

$$\delta + ku + \frac{\mu}{h} B = 0, \tag{2.3}$$

Opposite to the previous case, the atoms are slowed as the field increases and they reach their final velocity in the maximum magnetic field. Since on-axis magnetic field scales

as $\frac{B_{max}}{z^3}$ and B_{max} is quite large (650 G in our experiments), the decreasing field falls off rapidly and efficiently switches off off-resonant slowing. This has allowed us to make an intense slow atomic beam for trap loading. Furthermore, the detuning in this case is quite large (~900 MHz or about 100 linewidths) and so the slowing light does not perturb trapped atoms even if it shines right through the trap.

The slower solenoid is wound with 1/8" refrigerator tubing embedded in the epoxy matrix that holds the coils together. To make sure that individual coils are electrically insulated the tubing was wrapped in Kynar heat-shrink tubing rated for high temperatures. The cooling water runs through the tubing, so currents up to 100 A could be run through the solenoid. The operating current was 36 A.

With this slower we have obtained a total continuos flux of cold atoms within the velocity capture range of the MOT of ~10^{11} atoms/sec. By the time the slow atoms reach the trap, which is ~ 20 cm downstream, the beam spreads to a few cm in diameter, so not all atoms are loaded into the trap. We load the trap with more than 10^{10} atoms in ~1 sec, so the loading rate is ~$3 \cdot 10^{10}$ atoms/sec (Fig. 2-1).

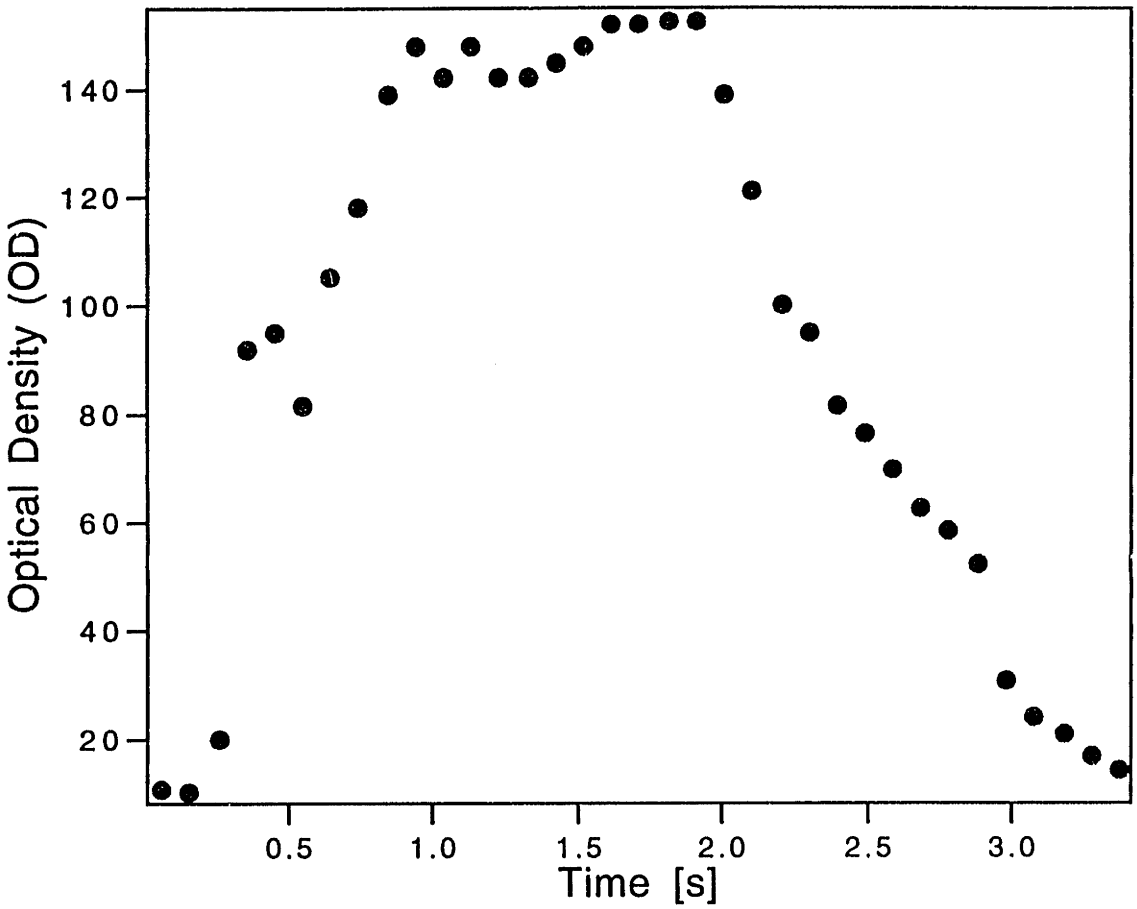

Fig. 2-1. The loading of the dark SPOT trap is turned on at t = 0 and the optical density of the trapped cloud increases as the number of trapped atoms exponentially approaches the maximum value. After the trap is filled to capacity the loading is turned off (t = 2 s) and the number of trapped atoms decays exponentially thereafter.

The rate achieved falls somewhat short of the record loading rate to-date of $2 \cdot 10^{11}$ atoms/sec achieved in a Cs vapor cell [GKC92]. The trap performance is not proportionally worse however, because of the advantages of loading from a slow beam vs. from a vapor. However, it would be highly desirable to get even better rates and a new slower with improvements based on experience with this slower is currently under way in our group. The rest of this Chapter describes our experiments, exploring some ways of improving efficiency of an increasing-field Zeeman slower as a source of slow atoms for loading a trap.

2.3 BRIGHTER AND CLEANER: THE IMPROVED SLOWER

What could be improved?

A significant increase in slow-atom fluxes coming out of Zeeman slowers is hardly expected since their performance is limited by existing technology. Available laser power, achievable magnetic fields, reasonable size, etc. limit the total flux, but significant improvement in performance can be achieved even without resorting to super powerful lasers or superconducting magnets. The most important avenue for improving the Zeeman slower as a trap-loading source is increasing its brightness. If the same flux of slow atoms is delivered as a beam with smaller cross-section area, the trap itself can be substantially improved. For example, in case of a MOT, the diameter of the trapping laser beam could be made smaller. This would relax requirements on the quality of laser beam profiles, bring down the necessary laser power, and slash the cost of optical hardware. Magnetic traps can benefit likewise: for a smaller trap much higher field gradients can be achieved with the same coils technology (see Chapter 3 for details). Consequently, should the slower be made brighter, the trap could be made deeper and trapped clouds could be compressed to higher densities.

Another important aspect of beam-loading that should be considered is the trap loss it induces. In order to fully take advantage of the high loading rate, the trap should be placed right in the center of the slow beam. But, however high the efficiency of the slower is, not all atoms in the the effusive atomic beam are slowed, and there are "hot" atoms in the beam that go right through the trap. These high-temperature atoms from the direct thermal beam have enough energy to knock atoms out of the trap. The resulting trap-loss rate can decrease the background-limited trap lifetime by orders of magnitude (about a thousand times for our slower). The solution we use is to load the trap from the beam and then switch off the beam with a shutter described in the Chapter 3. There is a

better, although more complicated, way to solve this problem. Slow atoms could be selectively deflected from the slowed thermal beam to form a "100% slow" beam. This entirely useful beam could be directed onto the trap, while the loss-inducing hot fraction peacefully passes by the trap. This method is obviously preferred if continuous trap loading is required. Furthermore, higher total numbers can be loaded in the trap since one of the loss mechanisms acting during the loading is eliminated.

We have carried out the experiments investigating possibilities of improving the Zeeman slower along both of the described lines and the results have been reported in a paper. The paper has been accepted for publication and I include its text here as it will appear in the Journal of Optical Society of America B.

JOSA B paper

Transverse Cooling and Deflection of an Atomic Beam Inside a Zeeman Slower

Michael A. Joffe, Wolfgang Ketterle, Alex Martin*,

and David E Pritchard

Department of Physics and Research Laboratory of Electronics, Massachusetts Institute of Technology

Cambridge, MA 02139

Abstract

We demonstrate the combined slowing and transverse cooling of a sodium atomic beam. Atoms have been slowed in a Zeeman slower with increasing magnetic field and transversely cooled by two-dimensional optical molasses inside the slower. The transverse molasses increases the brightness of the slow beam, and allows it to be deflected out of the intense slowing laser light.

1. INTRODUCTION

In many fields of atomic physics it is highly desirable to have a well collimated beam of slow atoms. Bright beams of slow atoms with low divergence should allow experimenters to load traps efficiently[1], develop new atom optics and better atom interferometers[2], and study cold collisions in a single beam[3].

Numerous techniques for slowing atoms have been demonstrated[4-13] to date. These techniques differ in the way they compensate for the changing Doppler shift of the decelerating atoms[4-12]. In all these methods, cooling is provided almost exclusively along the longitudinal direction. The accompanying transverse heating leads to a strong divergence of the slow atomic beam, especially for very low final longitudinal velocities. This effect, colorfully described as "beam explosion"[5], results in inefficient coupling of the slow atoms to subsequent experiments; for example, the efficiency of directly loading a magneto-optical trap from a Zeeman slower is limited typically to a few percent.

2. TRANSVERSE HEATING AND COOLING OF A SLOWED ATOMIC BEAM

Atoms moving in a counterpropagating light beam experience a slowing force due to momentum transfer from scattered photons. These photons are absorbed from the laser beam and rescattered randomly with a dipole radiation pattern. Consequently, the mean longitudinal velocity of the slowed atoms v_z decreases due to the absorbed photons from the initial velocity v_i to the final velocity v_f as

$$v_f(t) = v_i - v_{rec}N(t), \qquad (1)$$

and the transverse velocity components $v_{x,y}$ increase due to heating by spontaneous emission[14]:

$$(v_{x,y}^{rms})^2 = \alpha \frac{v_{rec}^2}{3} N(t), \qquad (2)$$

where v_{rec} is the recoil velocity and $N(t)$ is the number of photons scattered between $t = 0$ and t. The dipole pattern accounts for the factor of α=9/10 in front of the expression for isotropic radiation, but the resulting correction is small and will be neglected. The photon scattering leads to a transverse displacement of an atom given by

$$x(t) = \sum_k \left[(\Delta v_x)_k (t - t_k) \right] , \qquad (3)$$

where the sum is taken over all spontaneous emission events occurring at times t_k and $(\Delta v_x)_k$ is the velocity change due to the photon recoil. Since there is no correlation between different events, one has

$$\left(x^{rms}(t) \right)^2 = \frac{v_{rec}^2}{3} \frac{t}{3\Delta t}^3 = \frac{v_{rec}^2}{3} N(t) \frac{t}{3}^2 = (v_x^{rms})^2 \frac{t}{3}^2 \qquad (4)$$

where Δt is the average time between two excitations. If during the slowing process the longitudinal velocity of the atomic beam v_z reaches a final value v_f, and its transverse velocity v_x^{rms} reaches $v_\perp$, then after the slowing process the atomic beam will spread with a constant divergence angle of $2v_\perp/v_f$. Note, that since the final transverse velocity $v_\perp \propto \sqrt{v_i - v_f}$, it is very insensitive to the final longitudinal velocity v_f, provided the final velocity of atoms v_f is much smaller than their initial velocity v_i.

According to this simple model, slowing a Na atomic beam with counterpropagating light from ~600 m/s to 25 m/s over 0.5 m results in an increase in its average transverse velocity of 2.5 m/s. While during the slowing process the beam has spread by only ~4 mm, afterwards it will spread by 2 mm per cm of flight distance, i.e. the spreading after the slowing is much more significant than that during the slowing process. For other elements with different masses m , if all other relevant parameters (e.g. source temperature and photon momentum) are equal, one expects the initial longitudinal velocity to scale approximately as $m^{-\frac{1}{2}}$, the number of scattered photons N as $m^{\frac{1}{2}}$, and the final transverse velocity $v_\perp$ as $m^{-\frac{1}{2}}$. Therefore, the problem of transverse spreading is even more pronounced for lighter atoms such as Li and He.

A few techniques have been demonstrated which mitigate the problem of the transverse spreading. If the slowing is performed with an intense and tightly focused laser beam, the stimulated force can provide transverse confinement[15]. In isotropic light slowing[12], due to the isotropy of the slowing forces, the transverse heating is less than that given by Eq.2 by a factor of up to $\sqrt{v_i/v_f}$ (Ref. 16).

An obvious way to avoid spreading downstream of the slower is to apply transverse cooling immediately after the slowing. Atomic beams have been collimated with one-[17] or two-dimensional[18] optical molasses, intense standing waves[19,20,21] or magneto-optical compression[22,23]. However, if this is not done very close (~cm) to the

point where atoms have reached their final velocity, the atomic beam will undergo considerable spreading requiring large laser beams to recollimate the atoms. In this paper we report transverse cooling of a slow atomic beam right at this final velocity point.

3. TRANSVERSE COOLING OF AN ATOMIC BEAM INSIDE A ZEEMAN SLOWER

Zeeman slowing is the only demonstrated technique where all the atoms reach their final velocity at the same point in space, regardless of their initial velocity. This is therefore the ideal point to transversely cool and collimate the atomic beam. However, to date this has been performed only several cm after the slower[17], due to geometrical constraints imposed by the slowing magnet and the strong magnetic fields which are present. The optimal solution - transverse cooling inside a Zeeman slower at the final velocity point - is described here.

Zeeman slowing has the further advantage of slowing atoms continuously, and having a large velocity capture range limited only by ΔB, the difference in magnetic field between the start and end of the slower. However, in a conventional Zeeman slower which employs a decreasing magnetic field, there is considerable off-resonant scattering after the steep magnetic field gradient at the end of the slower, causing severe broadening of the resulting velocity distribution, and hindering the efficient extraction of very slow atoms[4,24]. This effect is much less pronounced in the recently demonstrated increasing-field Zeeman slower[25,17], where the atoms reach their final velocity near the maximum of the magnetic field. The fast drop-off of the field after this point rapidly detunes the atoms out of resonance with the slowing light, thereby minimizing subsequent off-resonant slowing.

Transverse cooling inside the Zeeman slower imposes two requirements: (1) the optical pumping of atoms to "wrong" hyperfine sublevels of the ground state by the transverse light must be avoided; (2) the variations in magnetic field over the molasses volume must be small enough so that Zeeman shifts do not undermine the cooling process with large detunings, while transverse optical access to the atoms inside the slower magnet is obviously required.

Optical pumping.

For Na, the increasing-field Zeeman slower operates on the cycling "σ^-" transition $|F = 2, m_F = -2\rangle \leftrightarrow |F' = 3, m_F' = -3\rangle$. In this type of slower, as well as in the conventional Zeeman slower[4], leakage from this quasi-two-level system is possible due to imperfect polarization of the slowing light and the transverse components of the inhomogeneous magnetic field. Sufficient additional suppression is provided by the detuning of other competing transitions by the magnetic field. This suppression is no longer effective in a conventional Zeeman slower when the magnetic field approaches zero; in some cases it turned out to be advantageous to add a bias magnetic field[4,25].

Transverse excitation in a magnetic field is less selective because σ^+ and σ^- light have the same intensity. Unwanted σ^+ transitions can therefore only be supressed by a large enough magnetic field. This issue has been addressed by calculating transition rates for magnetic field values used in the experiment (~650 G).

The only strong σ^+ transition from $|F = 2, m_F = -2\rangle$ state is detuned by 2400 MHz from the cycling transition and therefore suppressed by a factor of $\sim 10^6$. The other

σ^+ transitions (including one which is only ~60 MHz to the red of the cycling transition) contribute to the leakage even less because of small matrix elements. As for longitudinal excitation, leakage due to optical pumping can also occur via a π transition to an excited state, which is only 30 MHz to the red of the $|F = 3, m_F = -3\rangle$ state. This transition has a squared matrix element which is 2500 times smaller than that of the cooling transition. The suppression of this transition depends on the detuning of the laser and the fraction of the π light (on the order of 10^{-3}) and is typically 10^7. Overall, the problem of optical pumping by transverse excitation is only slightly worse compared to longitudinal excitation: leakage rates allow scattering of $\sim 10^6$ photons on the cycling transition, much more than needed for transverse cooling of a slowed atomic beam ($\sim 10^3$). Since Na atoms in a large magnetic field act as a nearly perfect two-level system, the theory of Doppler molasses described in Ref. 26 should be strictly applicable.

Magnetic field design.

The issue of magnetic field inhomogeneity was addressed by using an increasing-field Zeeman slower. The magnetic field *maximum* in this type of slower provides the ideal point for transverse cooling, as all the atoms reach their final velocity close to this point, and as it is an extremum, the field gradients are necessarily small. In order to gain optical access to the atoms in this region of sufficiently uniform field, a gap between the windings of the solenoid is therefore required at the point of the field maximum. The gap had to be sufficiently large (a few mm) so that the slow atomic beam spends enough time in the molasses light for the cooling to be effective, while at the same time not introduce a dip in the magnetic field profile (Fig.1). Careful design of the solenoid windings allowed us to meet both requirements simultaneously.

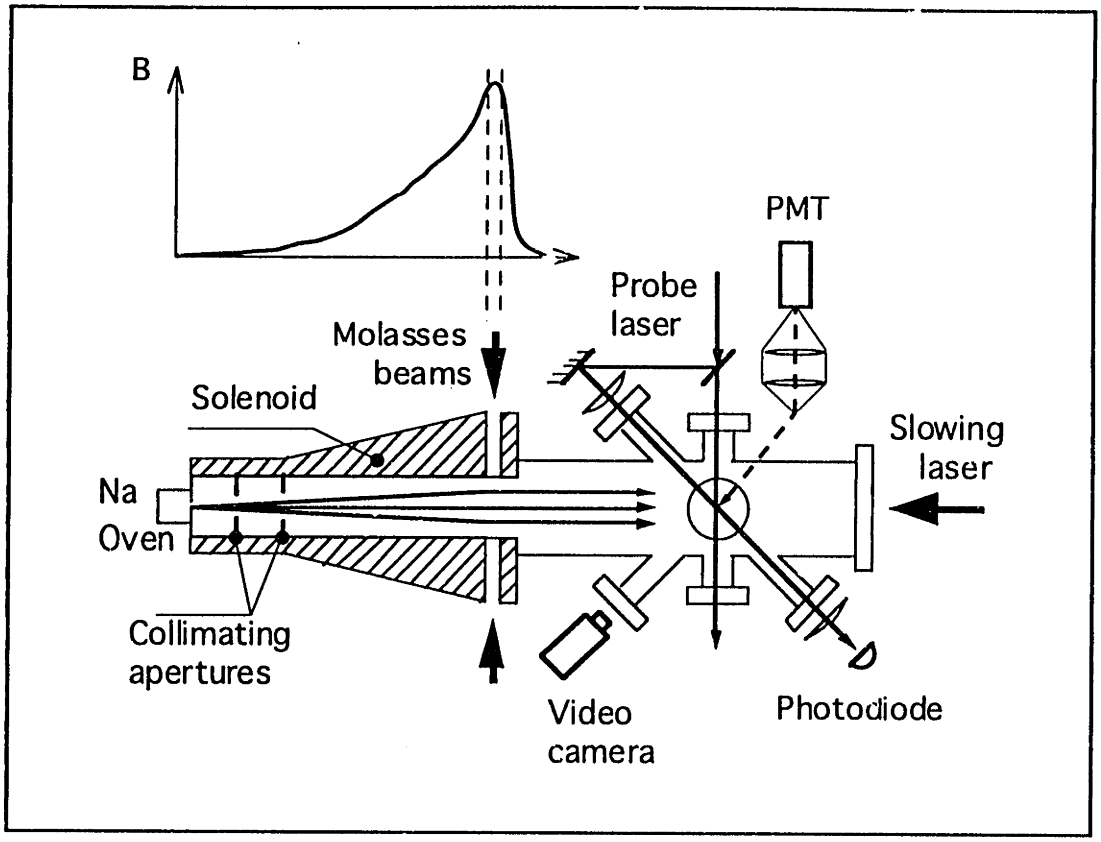

Figure 1. Experimental setup: A beam of sodium atoms is slowed by counterpropagating laser light inside a solenoid with a parabolically increasing magnetic field. The slow atomic beam is collimated and deflected inside the slower by transverse two-dimensional optical molasses.

4. EXPERIMENTS AND RESULTS

In our experiments, we have used the increasing-field Zeeman slowing technique[25] to slow an effusive sodium beam (Fig.1). The maximum magnetic field in the slower magnet was 650 G, corresponding to a velocity capture range of 600 m/s. Atoms emerging from the oven are distributed among all hyperfine substates of the ground state, whereas only atoms in the $|F = 2, m_F = -2\rangle$ Zeeman sublevel can be slowed by our slower. In order to facilitate optical pumping of the atoms between the oven and the slower magnet the slowing light was focused down on the oven aperture and had sidebands at the ground state hyperfine splitting frequency of 1712 MHz. In a

conventional Zeeman slower, optical pumping is achieved without sidebands in the fringing field of the slower solenoid, whereas the fringing fields are negligible for an increasing-field Zeeman slower. Without sidebands, it was only by applying a small longitudinal magnetic field in the 40 cm region between the oven and the slowing magnet, that we found effective transfer of atoms into the $|F = 2, m_F = -2\rangle$ state. Since the sideband technique gave a slightly higher flux of slow atoms (10-20%) and required less precise alignment, it was used for the experiments described below.

The velocity distribution of the atoms emerging from the slower was determined by sweeping a probe laser through the Na resonance and recording the fluorescence spectrum with a photomultiplier. The probe laser beam intersected the atomic beam at 45 degrees, 21 cm downstream from the magnetic field maximum. The zero-velocity point of the distribution was determined using a second probe beam perpendicular to the atomic beam, or by retroreflecting the 45°-laser beam, which led to two slow atom peaks in the resulting spectra separated in frequency by $2kv \cdot \cos(45°)$.

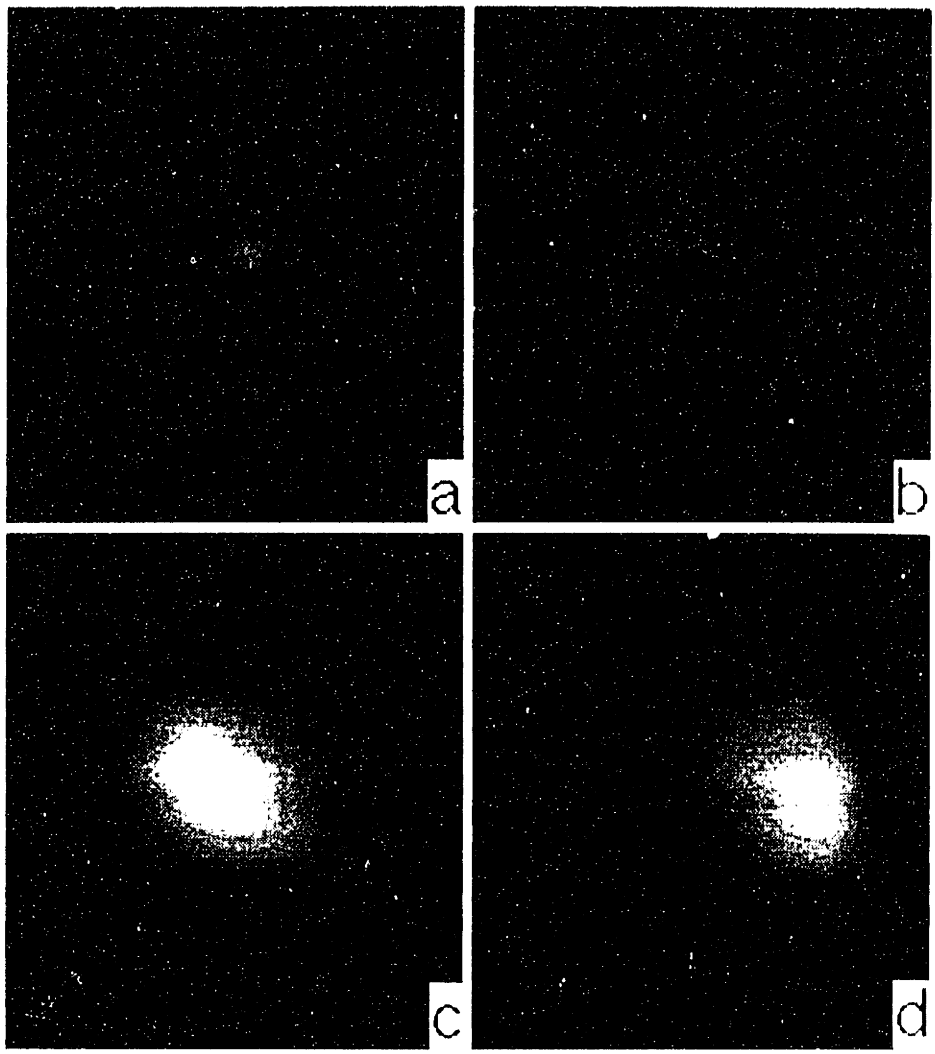

Figure 2 Atomic beam cross sections: (a) Thermal beam, (b) Xe atomic beam focused to a final velocity of 50 m/s, (c) The same atomic beam collimated by transverse cooling, (d) The same atomic beam collimated and deflected by an inhomogeneous magnetic field. The digitized images have been rescaled to correct for the observation angle ($45°$). The flux of slowed atoms is $\sim 10^{10}$ atoms/s.

To date, spatial profiles of slow atomic beams have been recorded using two-dimensional hot wire detectors[17]. In the present work, we used two-dimensional imaging of laser excited fluorescence. This diagnostic technique, common in other fields (e.g. combustion research[17]), has so far been applied only to thermal atomic beams[18]. In this method the probe laser is shaped into a light sheet and the fluorescence is observed

laterally using a CCD camera providing on-line two-dimensional images of the beam cross-section on a TV monitor (Fig.2). The images were digitized and stored for later analysis. Tuning the single-mode probe laser allowed us to obtain images of different velocity groups of the atomic beam. To obtain maximum fluorescence from the atoms, and hence maximum sensitivity, the probe beam had sidebands separated by the Na hyperfine splitting (1712 MHz) to avoid optical pumping.

Initial measurements were performed with a thermal beam collimated by apertures after the oven to ± 5 mrad. We obtained intense slow beams in the velocity range 25-100 m/s, with up to 10^{12} atoms/s at 100 m/s, a value which we determined using probe-laser absorption (Fig.3). The velocity distribution shows that about 20% of the thermal atoms are captured by the slower, which had a velocity capture range of ~600 m/s. It is possible in principle to achieve higher fluxes of atoms by increasing the temperature (and consequently atomic density) of the oven. However, as the temperature increases the thermal velocity distribution in the thermal beam (Fig.3) shifts to higher velocities and, even worse, the slow part of the distribution is depleted by collisions in the nozzle ("jetting"). Eventually this results in fewer atoms in the velocity capture range of the slower, which is determined by the maximum change of the magnetic field ΔB. For our slower and oven geometry, the optimal oven temperature was about 300°C.

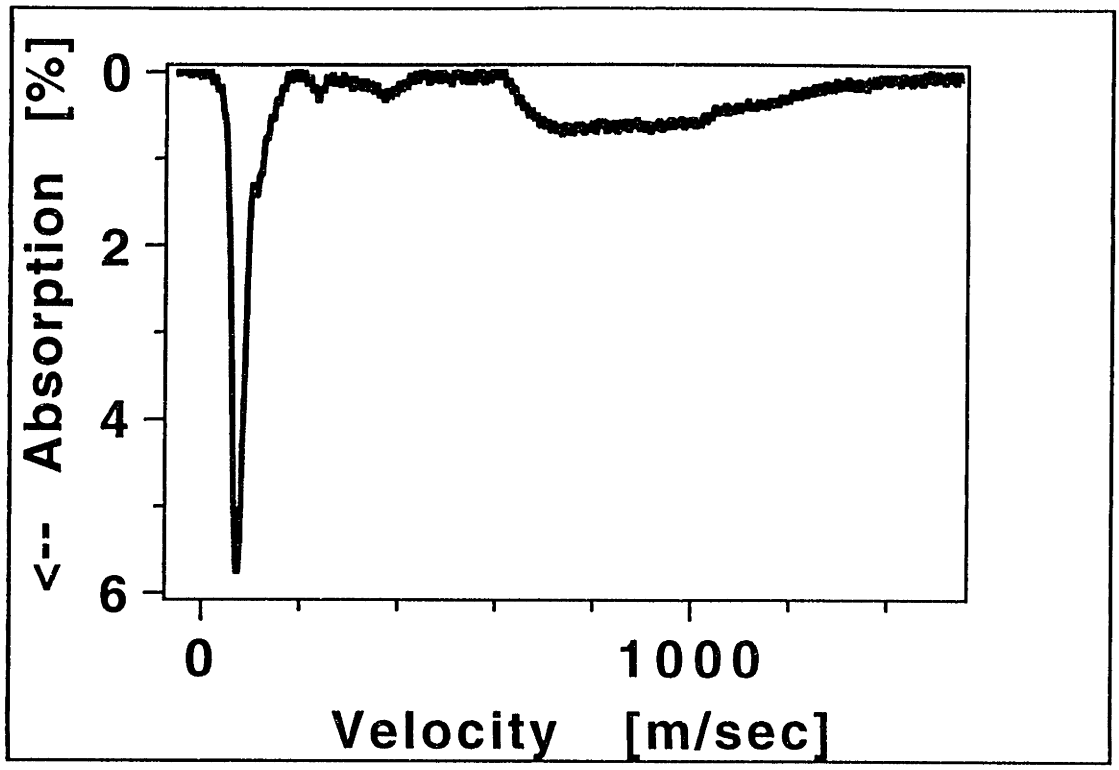

Figure 3. Absorption spectrum of a 70 m/s Na beam with $5 \cdot 10^{11}$ slow atoms/s.

One of the most important applications of intense beams of slow atoms is loading of atomic traps. In a recent experiment[29] with a magneto-optical trap (MOT), we obtained maximum loading rates of $\sim 10^{10}$ atoms/sec into a trap located downstream from the slower. It implies that only ~1% of the slow atom flux was captured by the trap. This loss of atoms is caused by the drastic increase of the beam diameter for smaller final velocities. For velocities below ~60 m/s the slow beam started to fill the observation region (22 mm i.d.) limited by the size of our vacuum chamber. The corresponding divergence and transverse velocity were ± 50 mrad and ± 3 m/s respectively. For 20 m/s atoms one would expect a beam diameter of ~10 cm, which clearly shows the need for transverse cooling.

The density of the slowed atomic beam showed an approximately linear decrease with final velocity (Fig.4), as expected for a constant flux of atoms with the transverse velocity independent of the final longitudinal velocity and in agreement with the model described in Section 2. In order to quantitatively study this effect, and the improved brightnessachieved with transverse molasses (Fig.2), further measurements were carried out with a more tightly collimated (± 1 mrad) effusive beam.

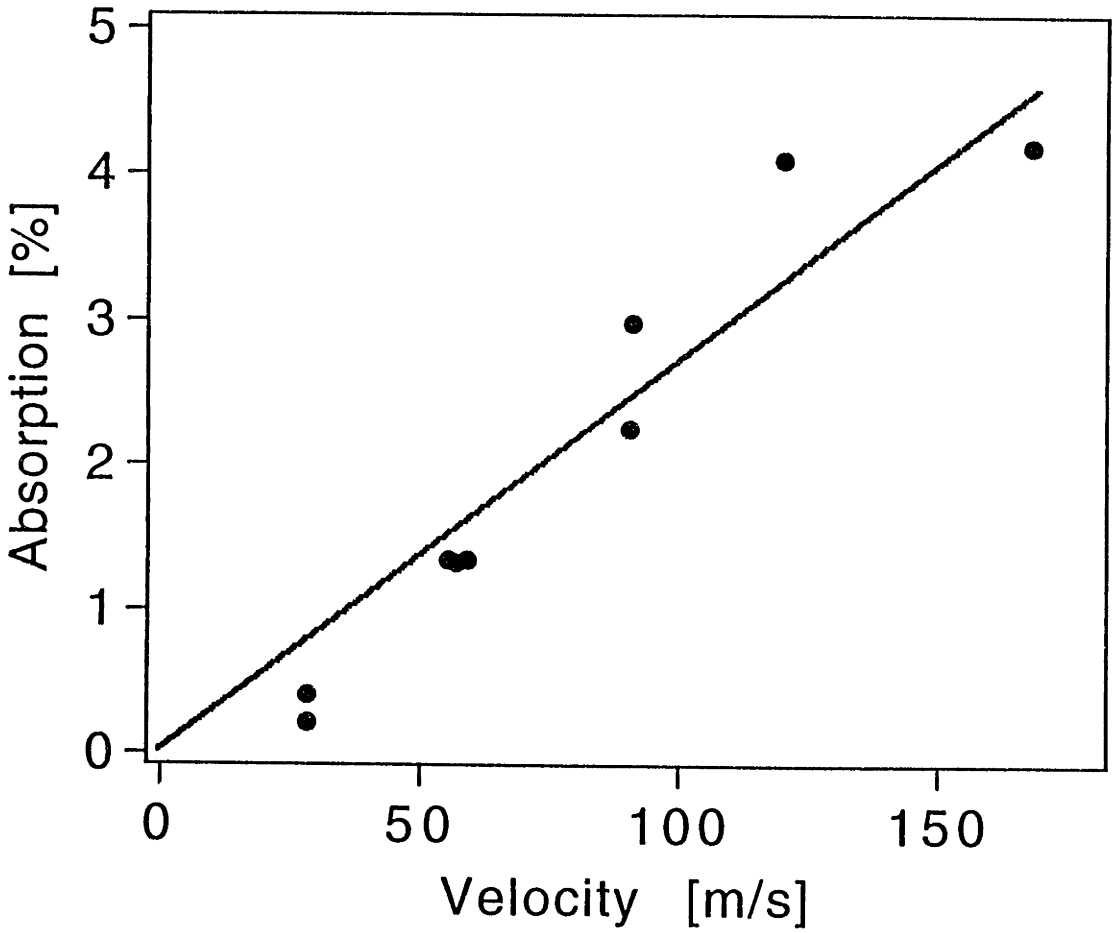

Figure 4. Maximum fractional absorption of a 1 μW probe laser beam as a function of the velocity of the slow atoms. A linear dependence is expected if the transverse velocity spread is independent of the longitudinal velocity.

For these experiments, the diameter of the slow beam in the molasses region was about 3 mm, so the transverse dimension of our windows (20 mm) allowed full optical access. The windows were located 4 cm from the end of the magnet and were 8 mm long in the atomic beam direction. Thus, atoms with a typical velocity of 50 m/s spent approximately 150 μs in the collimating light, much longer than the damping time of ~25 μs in two-dimensional molasses[26]. With the magnetic field curvature of 4 G/cm^2 longitudinally and 2 G/cm^2 radially at the field maximum, the magnetic field variation throughout the molasses region was only a few Gauss, limiting the Zeeman shifts to less than a quarter of the natural linewidth of 10 MHz.

The light beams for slowing and transverse cooling were produced by the same frequency-stabilized dye laser. The slowing light was frequency-shifted by 100 to 300 MHz using acousto-optic modulators, depending on the desired final velocity of atoms. For cooling, two pairs of molasses beams were sent through the windows inside the slower. The counterpropagating beams were obtained either by retroreflection or by using a separate laser beam. The latter setup was more advantageous, since it allowed arbitrary intensity imbalances.

The optical molasses was optimized for best performance using real-time diagnostics. The effectiveness of the transverse cooling was found to depend very weakly on laser intensity in the range of 1-10 mW/cm^2 per beam. This is presumably because the atoms pass through a region of decreasing light intensity as they leave the molasses. It is this final region of low intensity that probably determines the final transverse temperature, since the ultimate temperature of molasses and, therefore, the overall collimation achieved depend on laser intensity[26]. When the frequency of the molasses light was tuned from red to blue through resonance, a sudden transition from collimation to beam explosion due to transverse heating was observed; the optimal detuning was found to be a few MHz to the red of the resonance. The transverse cooling

process was also found not to be sensitive to the accuracy of alignment of the linear polarization of the cooling light beams perpendicular to the magnetic field.

Two-dimensional images of the atomic beam cross-sections were obtained for various velocities and parameters of the transverse molasses and are shown in Figure 2. In these images, the off-resonant fluorescence in the observation region due to the intense slowing laser has been subtracted.

The images were digitized and the rms values $v_{\perp}$ of the transverse velocities $v_{x,y}$ were determined from the measured atomic beam diameters D using the relation

$$D = \sqrt{d_0^2 + \left(2v_{\perp} \, l/v_f\right)^2}, \qquad (5)$$

where d_0 is the diameter of the slow beam at the transverse cooling point, v_f is the final longitudinal velocity, and l is the distance between the molasses and the observation region. Note, that d_0 is determined by both the diameter of the original thermal beam (1.5 mm) and the spreading of the beam during the slowing process. Sufficiently far away from the slower, the beam diameter will depend only weakly on the initial diameter d_0. The measured values of $v_{\perp}$ for the slowed, but not transversely cooled beam of 2.5 m/s are in good agreement with Eq.2. With transverse cooling, typical values of 0.9 m/sec for $v_{\perp}$ were obtained, consistent with the observed sixfold increase in density (Fig.5).

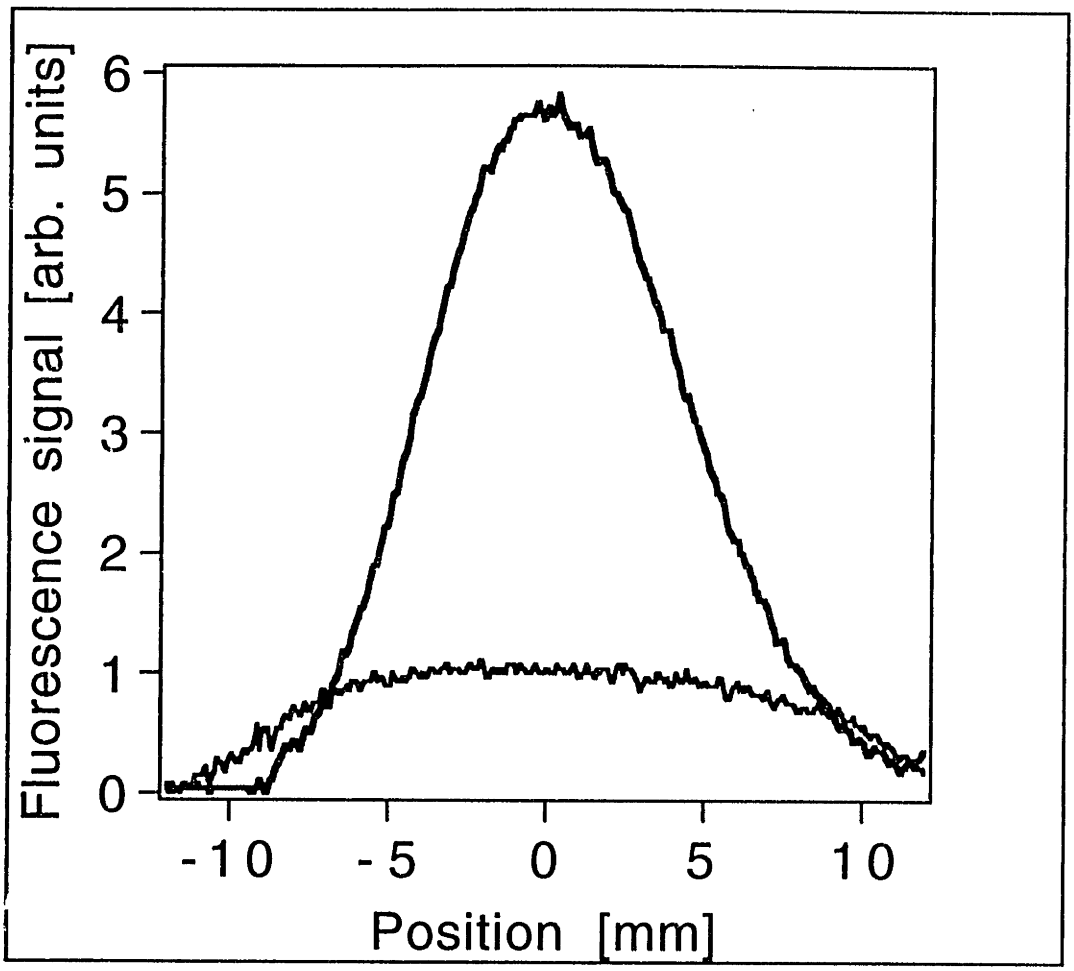

Figure 5. Cross-sectional profiles of uncollimated and collimated 40 m/s Na beams. The uncollimated beam is partially cut off by a 22 mm aperture in the experiment. The apparent "non-conservation" of atoms is due in part to this cut off, and in part to the fact that the profiles are one-dimensional representations of a two-dimensional density distribution. Proper comparison requires integration not along a line, but over the area.

This transverse velocity is approximately three times higher than the Doppler limit[26], probably due in part to residual off-resonant slowing after the cooling, and, to a smaller degree, due to defocusing forces arising from the inhomogeneous magnetic fields at the end of the slower.

For many experiments, one would like to separate the slow atomic beam from the strongly perturbing intense slowing light[30,17]. With an increasing-field Zeeman slower, such as in the present experiments, this problem is already mitigated compared to a conventional Zeeman slower since the slowing laser is detuned 1 GHz from the zero-field atomic transition. In addition, the transverse molasses not only allowed us to increase the brightness of the atomic beam, but also to deflect it by introducing a small intensity imbalance into one pair of the molasses beams, while still preserving the collimation. Deflection angles exceeding 6° were achieved, limited only by the geometry of our vacuum chamber (Fig.2). Furthermore, by varying the imbalance in each of the two arms we were able to steer the slow beam arbitrarily in the x-y plane. In our experiments the molasses beams had the same frequency. The use of "moving molasses"[31] with counterpropagating beams of different frequencies should give similar results, but has no obvious advantage for small deflection angles since polarization-gradient cooling is not present for a two-level system.

5. CONCLUSIONS

In summary, we demonstrate an efficient way to collimate an atomic beam with transverse light while simultaneously slowing with counterpropagating light. Transverse cooling of a slow beam at this very early stage avoids unnecessary spreading and increases its brightness. Collimation preserving large-angle deflection allows the extraction of the slow atomic beam from the residual thermal beam, and appears to be a promising way of providing dense continuous beams of slow atoms for future applications.

Perhaps one of the most important applications of an intense beam of slow atoms is to load a mgneto-optical trap[32] or an atomic funnel[33,34] for further cooling and

compressing of the atoms. The key figure of merit for a slower is therefore the atom flux which is delivered into the capture area of such a trap, typically a few cm^2. In this work, we demonstrate that an increasing-field Zeeman slower can deliver more than 10^{12} atoms/s at a velocity of 100 m/s to within such an area, more than an order of magnitude more than previously reported[17,25]. The apparent loss of atoms when the final velocity is reduced to below the capture velocity of a trap (typically 20 to 30 m/s) is shown to be due to transverse spreading. We demonstrated a way of reducing this spreading at the earliest stage possible. If off-resonant slowing after the collimation can be avoided by an improved geometry and a steeper magnetic beam profile, the divergence of a 30 m/s beam transversely cooled to the Doppler limit will be only ± 10 mrad, sufficiently small to transfer all slow atoms to the optical trap. Further improvements should be possible from a reduction of the distance between the slower and the trap, but careful consideration of stray fields of the slower solenoid would be required.

At present, the highest loading rate of an optical trap of $2 \cdot 10^{11}$ atoms/s has been achieved in a vapor cell trap[35]. We expect that with an improved increasing-field Zeeman slower which has a slightly larger velocity capture range and a smaller separation from the trap, loading rates of at least $5 \cdot 10^{12}$ atoms/s are possible. Such a slower will be extremely useful for obtaining a large number of atoms at high density for the study of cold collisions and collective effects.

6. ACKNOWLEDGMENTS

We would like to acknowledge technical assistance from K. Davis. This work was supported by Office of Naval Research and U.S. Air Force Office of Scientific Research under grant #N00014-90-J-1642 and the National Science Foundation under grant #8921769-PHY. W.K. would like to acknowledge a fellowship from the NATO Science

Committee and DAAD. A.M. would like to acknowledge a fellowship from the D.G.I.C.Y.T., Spain during part of this work.

* On leave from: Instituto de Optica, C.S.I.C., Madrid

References

1. D.E. Pritchard, K. Helmerson, and A. Martin, "Atom traps", in *Atomic Physics* XI, S. Haroche, J.C. Gay, G. Grinberg, eds. (World Scientific, Singapore, 1989), p.179-197.

D.E. Pritchard and W. Ketterle, in Proceedings of the Varenna Summer School on Laser Manipulation of Atoms and Ions, edited by E. Arimondo and W. P. Phillips (North-Holland, Amsterdam, to be published).

2. Special issue on atom optics and interferometry, J. Mlynek, V. Balykin, P. Meystre, eds., Appl. Phys. B 54, No.5 (1992).

3. H.R. Thorsheim, Y. Wang, and J. Weiner, "Cold collisions in an atomic beam", Phys. Rev. A **41**, 2873-2876 (1990).

4. W.D. Phillips, J.V. Prodan, H.J. Metcalf, "Laser cooling and electromagnetic trapping of neutral atoms", J. Opt. Soc. Am. B **2**,1751-1767 (1985).

5. J. Liang and C. Fabre, "Modifications of the velocity of atoms submitted to a resonant multimode laser: an experimental study", Opt. Comm. **59**, 31-35 (1986).

6. P. Strohmeier, T. Kersebom, E. Krüger, H. Nölle, B. Steuter, J. Schmand and J. Andrä, "Na-atom beam deceleration by a mode-locked laser", Opt. Comm. **73**, 451-454 (1989).

7. L. Moi, "Application of a very long cavity laser to atom slowing down and optical pumping", Opt. Comm. **50**, 349-352 (1984).

8. M. Zhu, C.W. Oates, J.L. Hall, "Continuous high-flux monovelocity atomic beam based on a broadband laser-cooling technique", Phys. Rev. Lett. **67**, 46-49 (1991).

9. W. Ertmer, R. Blatt, J.L. Hall, M. Zhu, "Laser manipulation of atomic beam velocities: demonstration of stopped atoms and velocity reversal", Phys. Rev. Lett. **54**, 996-999 (1985).

10. V.I. Balykin, V.S. Letokhov, V.I. Mishin, "Cooling of sodium atoms by resonant laser emission", Sov. Phys. JETP **51**, 692-696 (1980).

11. I.C.M. Littler, H.-M. Keller, U. Gaubatz, K. Bergmann, "Velocity control and cooling of an atomic beam using a modeless laser", Z. Phys. D 18, 307-308 (1991).

12. W. Ketterle, A. Martin, M. A. Joffe and D.E. Pritchard, "Slowing and cooling atoms in isotropic laser light", Phys. Rev. Lett, **69**, 2483-2486 (1992).

13. M. Prentiss, A. Cable, "Slowing and cooling an atomic beam using an intense optical standing wave", Phys. Rev. Lett. **62**, 1354-1357 (1989).

14. V. S. Letokhov and V. G. Minogin, "Laser radiation pressure on free atoms", Phys. Rep. **73**, 1-65 (1981).

15. M. Prentiss, A. Cable, N. Bigelow, "Effect of transverse guiding on the velocity distribution of an atomic beam", J. Opt. Soc. Am. B **6**, 2155-2158 (1989).

16. M. A. Joffe, A. Martin, W. Ketterle, and D.E. Pritchard, "Diffuse light slowing of atoms", (to be published).

17. A. Witte, Th. Kisters, F. Riehle, and J. Helmcke, "Laser cooling and deflection of a calcium atomic beam", J. Opt. Soc. Am. B **9**, 1030-1037 (1992).

18. B. Sheehy, S.-Q. Shang, R. Watts, S. Hatamian, H. Metcalf, "Diode-laser deceleration and collimation of a rubidium beam", J. Opt. Soc. Am. B **6**, 2165-2170 (1989).

19. V.I. Balykin and A.I. Sidorov, "Collimation and decollimation of atomic beams by laser radiation", Appl. Phys. B **42**, 51-54 (1987).

20. C.E. Tanner, B.P. Masterson, and C.E. Wieman, "Atomic beam collimation using a laser diode with a self-locking power-buildup cavity", Opt.Lett. **13**, 357-359 (1988).

21. J. Chen, J.G. Story, J.J. Tollett, and R.G. Hulet, "Adiabatic cooling of atoms by an intense standing wave", Phys. Rev. Lett. **69**, 1344-1347 (1992).

22. E. Riis, D.S. Weiss, K.A. Moler. and S. Chu, "Atom funnel for the production of a slow, high-density atomic beam", Phys. Rev. Lett. **64**, 1658-1661 (1990).

23. J. Nellessen, J. Werner and W. Ertmer, "Magneto-optical compression of a monoenergetic sodium atomic beam", Opt. Comm. **78**, 300-308 (1990).

24. V.S. Bagnato, C. Salomon, E. Marega, Jr., and S.C. Zilio, "Influence of adiabatic following and optical pumping in the production of an intense steady flux of slow atoms", J. Opt. Soc. Am. B **8**, 497-501 (1991).

25. T.E. Barrett, S.W. Dapore-Schwartz, M.D. Ray and G.P. Lafyatis, "Slowing Atoms with σ^- Polarized Light", Phys. Rev. Lett. **67**, 3483-3486 (1991).

26. P.D. Lett, W.D. Phillips, S.L. Rolston, C.E. Tanner, R.N. Watts, C. I. Westbrook, "Optical molasses", J. Opt. Soc. Am. B **6**, 2084-2107 (1989).

27. A. Arnold, W. Ketterle, H. Becker, and J. Wolfrum, "Simultaneous single-shot imaging of OH and O_2 using a two-wavelength excimer laser", Appl. Phys B **51**, 99-102 (1990).

28. T. Esslinger, A. Hemmerich and T.W. Hänsch, "Imaging an atomic beam in two-dimensions", Opt. Comm. **93**, 49-53 (1992).

29. W. Ketterle, K.B. Davis, M. A. Joffe, A. Martin, and D.E. Pritchard, "High densities of cold atoms in a *dark* spontaneous-force optical trap", Phys. Rev. Lett., **70**, 2253-2256 (1993).

30. J. Nellessen, J.H. Müller, K. Sengstock and W. Ertmer, "Large-angle beam deflection of a laser-cooled sodium beam", J. Opt. Soc. Am. B **6**, 2149-2154 (1989).

31. M. Kasevich, D.S. Weiss, E. Riis, K. Moler, S. Kasapi, and S. Chu, "Atom velocity selection using stimulated Raman transitions", Phys. Rev. Lett. **66**, 2297-2300 (1991); A. Clairon, C. Salomon, S. Guellati and W.D. Phillips, "Ramsey Resonance in a Zacharias Fountain", Europhys. Lett. **16**, 165-170 (1991).

32. E.L. Raab, M. Prentiss, A. Cable, S. Chu and D.E. Pritchard, "Trapping of neutral sodium atoms with radiation pressure", Phys. Rev. Lett., **59**, 2631-2634 (1987).

33. E.Riis, D.S. Weiss, K.A. Moler, and S.Chu,"Atom funnel for the production of a slow, high-density atomic beam", Phys. Rev. Lett. **64**, 1658-1961 (1990).

34. J. Nellessen, J. Werner and W. Ertmer,"Magneto-optical compression of a monoenergetic sodium atomic beam", Opt.Comm. **78**, 300 (1990).

35. K.E. Gibble, S. Kasapi, and S. Chu, "Improved magneto-optic trapping in a vapor cell", Opt. Lett. **17**, 526 (1992).

Each one sees what he carries in his heart.
— Johann Wolfgang von Goethe

3. EXPERIMENT

3.1. EXPERIMENTAL APPARATUS

A schematic of the experimental apparatus (Fig. 3-1) shows the key parts of the machine.

The effusive sodium beam comes from the *oven* , is collimated by *apertures* and slowed by the counterpropagating *slowing laser* beam. The increasing-field *solenoid* is the crucial part of the Zeeman slower described in the previous Chapter. Slow atoms are directly loaded into the magneto-optical *trap* created downstream from the slower in the ultra-high vacuum chamber. The trap consists of a pair of magnetic coils and three pairs of retroreflected *trapping laser beams.* Once the atoms are trapped they are probed by the weak *probe laser.* The intensity of the probe light is measured up by a *photodiode*. At the same time the trap images can be captured by the *video camera* , digitized and

stored on a computer. In this Chapter I will discuss in detail the technological aspects of important elements of the experiment.

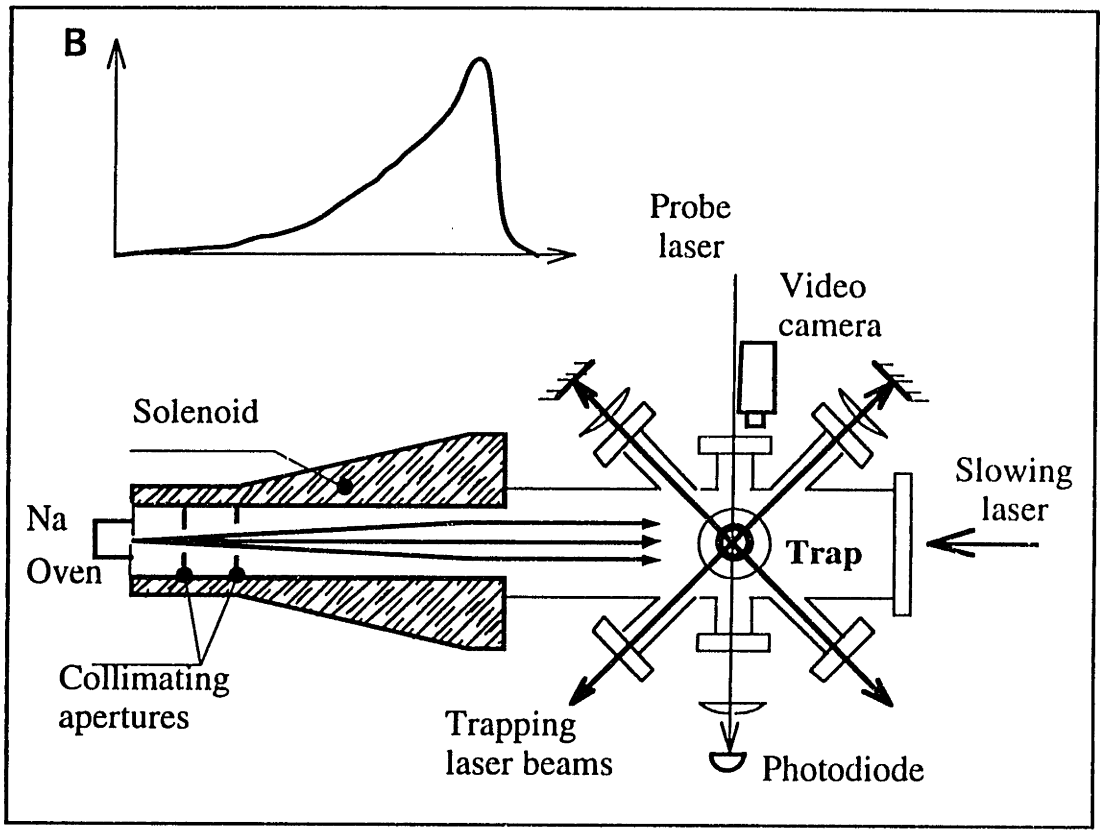

Fig. 3-1: Experimental Setup

3.2. VACUUM SYSTEM

Cold trapped atoms can be easily knocked out of the relatively shallow potential well by the residual atoms and molecules in the vacuum system. These background collisions are responsible for the dominant loss mechanism in most of our experiments. So it is extremely important to achieve a very low pressure in the trap chamber. At the same time, the intense atomic beam passing through the chamber constitutes a very large gas load. Furthermore, to achieve high loading rates the intensity of this beam can not be compromised. So the vacuum system has been developed that satisfies both of these

conflicting requirements without sacrificing performance. All the home-made parts operate on the level of the best commercially available ultra-high vacuum technology.

3.2.1 Chamber

The major part of the machine is the custom-designed stainless steel vacuum chamber*. To avoid vibrations the chamber is supported by a frame which is in its turn bolted down to the surface of an optical table. The chamber has a total of 18 ports and is basically a large six-way cross with 12 additional smaller 45-degree ports added between the large ones (Fig. 3-2).

All the ports had ConFlat® flanges with copper seals that provided ultra-high vacuum seals, bakeability, and allowed (relatively!) easy rearrangement of modular mating components to meet new and ever-changing needs. The large ports had 8" CF flanges and the smaller ones were 4.5" CF ones.The large ports allowed for convenient optical access to the geometrical center of the chamber where the trap was. The size of the larger ports has been chosen so that several laser beams can be sent through a large viewport. The smaller ports allowed using the 5-cm diameter trapping beams to collect the maximum number of atoms into the MOT. In order to improve the optical qualities of commercial viewports the glass has broadband-AR coating on both surfaces. This definitely improved the transparency of the glass and had no negative effect on the vacuum. The coating turned out to be sturdy enough to survive multiple bakeouts without visible deterioration.

To reach a higher loading rate the spreading slow atomic beam has to be brought as close to the trap as possible. For that purpose, the "slower" port has a tapped flange of reduced size (4 1/2" instead of 8" o.d.) recessed closer to the center of the chamber.

---

* The chamber has been manufactured by Nor-Cal, Inc. As a rule of thumb this vendor should be avoided.

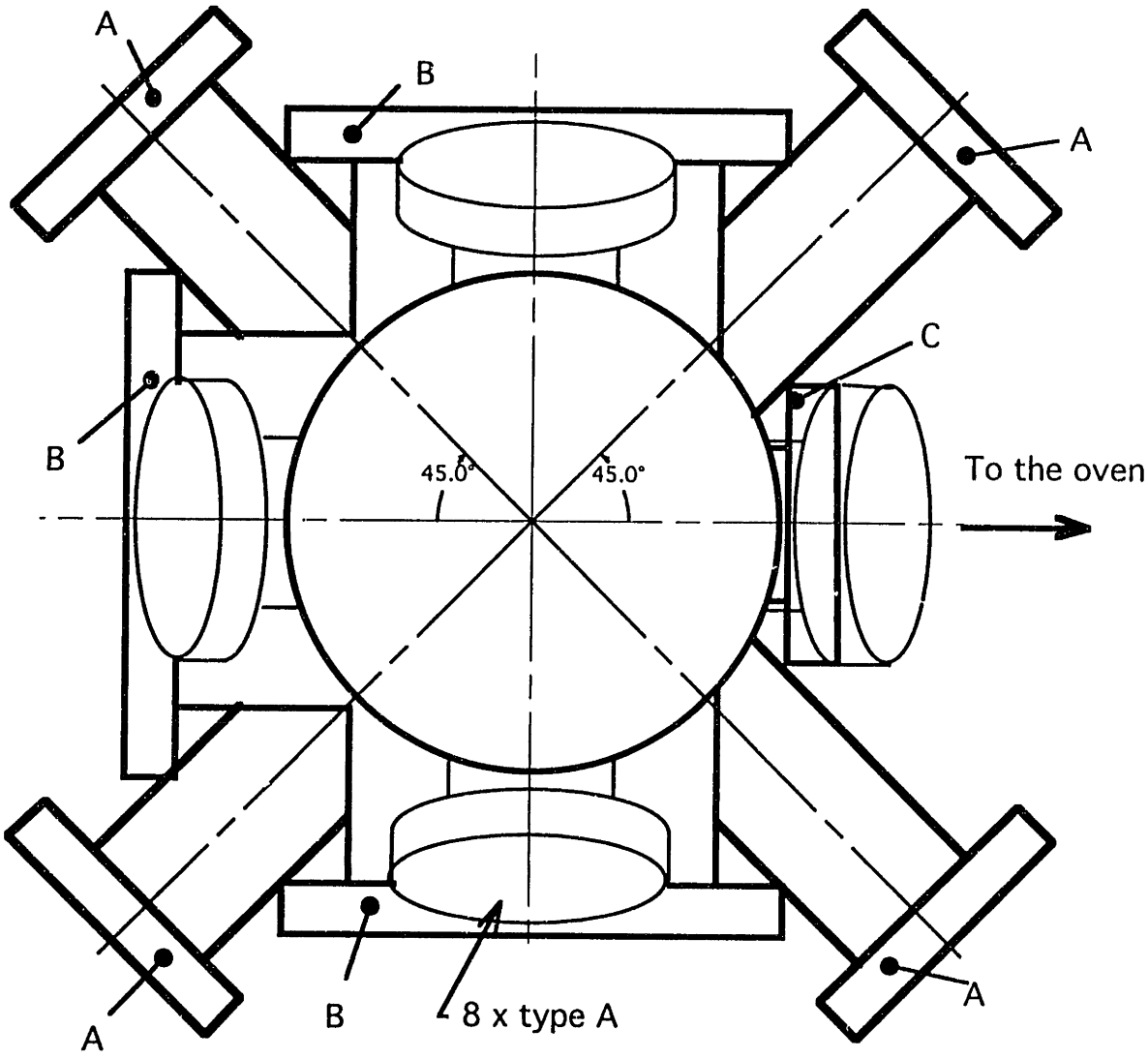

A - 4 1/2" Rotatable ConFlat Flanges; 2 1/2" Tubing
B - 8" Tapped Rotatable ConFlat Flanges;6" Tubing
C - 4 1/2" Nonrotatable-Tapped ConFlat Flanges;2 1/2" Tubing

Fig. 3-2: The Main Chamber

3.2.2 Pumps and gauges

The main chamber has been pumped by a total of four different pumps which makes it a good illustration of modern vacuum technology. Initially the chamber is pumped out by a turbo-molecular pump to a pressure below 10^{-7} Torr. At these pressures a 60-l/s ion

pump can be turned on and even take over. At this point, the turbo pump can be valved off and shut down to save wear of the bearings. During the bakeout, however, both pumps are usually run together. The pressure is measured by the nude UHV ionization gauge with a low x-ray limit. Furthermore, the composition of the residual gases is continuously monitored with the very useful on-line Residual Gas Analyzer.

The chamber is baked out at ~300 °C for a few days, depending on how clean it was. To cut down on bakeout time the provision has been made to vent the chamber with dry nitrogen before opening. To ensure uniform heating of the parts during bakeout the chamber is wrapped with aluminum foil.

These efforts typically bring the pressure below 10^{-9} Torr. To make the final leap to the 10^{-11}-Torr range we used the Ti sublimation pump. The commercial unit has been modified: the filament is bent and put into a shorter holder, so that sprayed titanium uniformly covers a large area while not obstructing the atomic beam. The filament is heated in a standby mode with 30-A DC current to ensure proper outgassing. Before the experiment it is heated with 50 A current for ~ 1 min, after which it is switched off. After the titanium is sprayed, the pressure in the chamber decays to its final value of ~10^{-11} Torr in the course of an hour or so. To gain maximum pumping speed titanium was sprayed on the inner surface of the large copper cylinder (5.3" i.d.) that was cooled with liquid nitrogen. The mouth of the cylinder is only a few centimeters away from the trap and the calculated pumping speed of the setup is ~1000 l/s.

3.2.3 Na Oven

The oven region of the machine consists of the commercial six-way cross with 4 1/2" flanges that accommodates all the necessary parts and is attached to the entrance of the slower. A dedicated turbo pump shielded from the sodium vapor with a water-cooled baffle pumps this cross to the pressure of ~10^{-8} Torr. The oven region can be valved off

from the slower (and the main chamber, to which the slower is attached) with pneumatically operated gate valve. The remaining ports are taken by the Na beam shutter, liquid nitrogen feedthrough, an ion gauge and a viewport. The latter is useful for focusing the slowing laser beam exactly on the oven aperture. The beam shutter is a modified electromechanical relay that is mounted in the vacuum and has a long moving "arm" protruding into the beam path. The arm ends with a blade that actually interrupts the atomic beam.

The oven itself consists of a short ConFlat Nipple with one end attached to the 4 1/2" cross and blanked-off on the other end (Fig. 3-3). The nozzle is a 4 mm diameter hole in a solid copper gasket. To prevent jetting of the beam the ~3 mm thick gasket is thinned around the hole. The oven is heated with external heaters, so the good thermal conductivity of copper prevents the nozzle from clogging. Alignment of the nozzle with the rest of the machine is determined with a telescope that views from the main chamber side. The main chamber had to be vented for this purpose, since the gate valve must be open. With the exception of this small nuisance, the procedure permitted perfect alignment. Positioning of the nozzle hole was achieved by carefully drilling the gasket in exactly the right place. Using a saphire viewport instead of the oven blank-off allowed to at least check the alignment and the condition of the nozzle without breaking the vacuum.

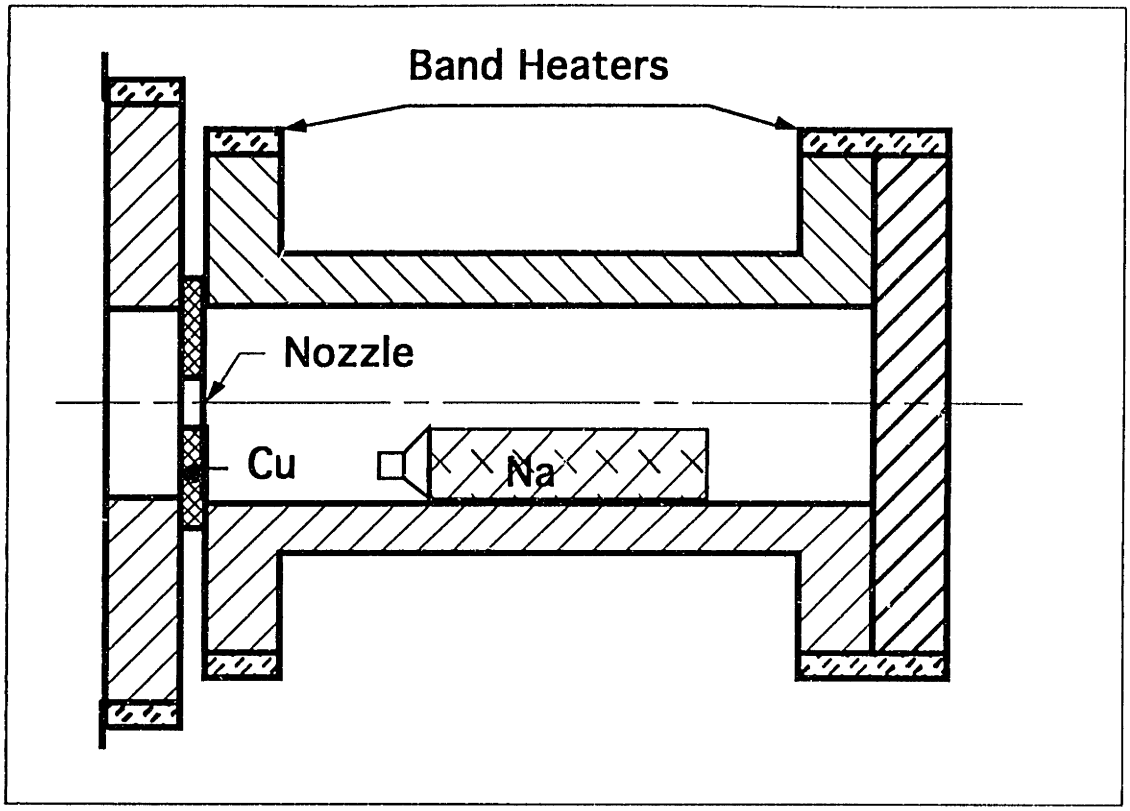

Fig. 3-3: A simple oven consisted of an externally heated stainless steel enclosure with a pre-scored vile with sodium metal inside. The 4 mm hole in the solid copper gasket worked as a nozzle.

This simple and cost-effective design allows fast reloading, which is important since the oven uses ~ 1 g/day of sodium. For reloading, the oven region is valved off and vented with dry nitrogen. The blank-off flange is then removed and a new clean vile with sodium metal is added. A stream of dry nitrogen through and out of the oven ensures that neither oxidation of sodium nor contamination occurs meanwhile. The oven is then closed and pumped out. The whole operation takes a trained person about 1 hour and in case of emergency (desperation) can be carried out in real time during the run. The temperature of the oven is maintained at a set level by temperature controllers. The operating temperature of the oven is ~300 °C. To avoid nozzle clogging, care has to be taken that the nozzle is always ~50 °C hotter than the rest of the oven. While the current design works fine, it could be improved by moving the reservoir further away to decrease

thermal coupling between the nozzle and the Na reservoir on the one side and the nozzle and the oven chamber on the other.

3.2.4 Combining UHV with an Intense Beam

Shooting an intense thermal beam through an ultra-high vacuum chamber while maintaining a pressure of ~10^{-11} Torr posed a challenging engineering problem. The solution of the problem consisted of two parts of the machine: one allows the sodium beam and only the sodium beam enter the chamber (beam pitcher), while the other captures the beam after it has passed through the trap and prevents sodium atoms from rattling around the UHV chamber (beam catcher).

Beam Catcher

A flux of 10^{13} atoms/s injected in our vacuum chamber is equivalent to a substantial leak rate of ~10^{-6} Torr·l/s. Fortunately, the dense atomic beam itself does not constitute much of a problem as long as atoms follow straight trajectories and do not scatter much away from the beam. The Na beam in our experiments is so intense however that in a couple of minutes it turns the viewport on the opposite side of the machine into a mirror. Since counterpropagating slowing light has to enter the chamber through this viewport, this can not be tolerated. To continuously clear itself from the deposited sodium the viewport is constantly heated to ~250 °C. These sodium atoms scattered away from the hot surface constitute a gas load to the chamber and limit the ultimate pressure in it. To prevent these atoms from getting back into the chamber the viewport is shielded from the chamber by a cold plate: sodium atoms stick well to the surface kept at liquid-nitrogen temperature. To let the directed beam get through but not the scattered atoms the shield is a long tube which is an integral part of the Ti sublimation pump setup (Fig. 3-4).

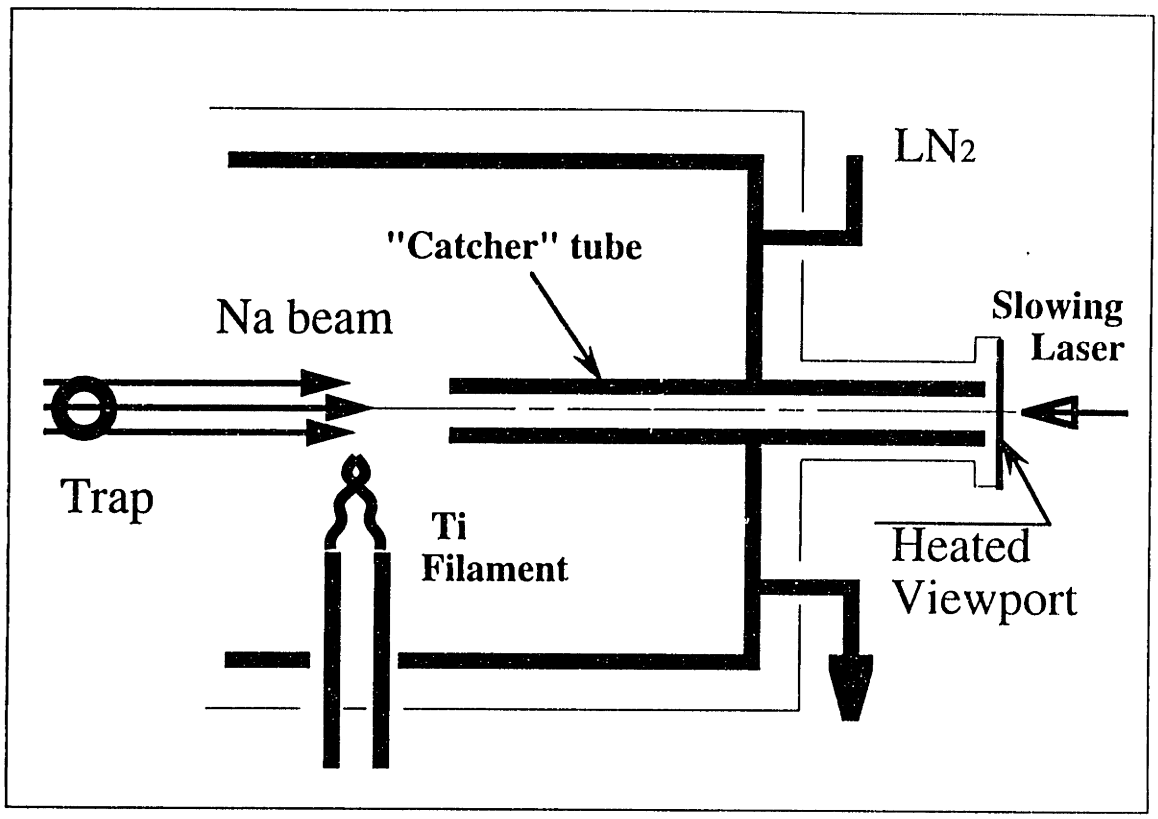

Fig. 3-4: Beam "catcher" setup.

Beam "Pitcher" - Differential Pumping setup

The thermal atomic beam is 4 mm in diameter so the hole between the oven region and the main UHV chamber should be at least that large. At the same time the oven region is at a vacuum $\geq 10^{-8}$ Torr so, if no provisions are made the gas load through the hole would increase the ultimate pressure in the trapping chamber. One effort was to minimize the pressure in the oven region. For that purpose the sodium beam there is collimated by a liquid-nitrogen cooled aperture, so that the part of the broad effusive that misses the aperture is efficiently captured. To increase the capturing efficiency the cold shield has a shape of a cylinder protruding very close to the nozzle (Fig. 3-5). Also, a 15-cm long 1/4" o.d. copper tube provided differential pumping between the HV and UHV chambers. Further increase of the length of the differential pumping tube was not possible, since it would limit the intensity of an atomic beam. Initially, the tube gave a differential

pumping factor of ~300. To further boost this factor, one end of the tube is attached to the cold plate. This resulted in the differential pumping factor of ~1000 which is enough to achieve pressures of ~10^{-11} Torr in the main chamber with the atomic beam on. The design was complicated by two other constraints: (a) the position of the tube had to be adjustable to allow its alignment along the beam axis and (b) the tube could not be directly attached to the cold plate because of the moving blade of a beam shutter. The sketch of the assembly is shown on the Fig. 3-5.

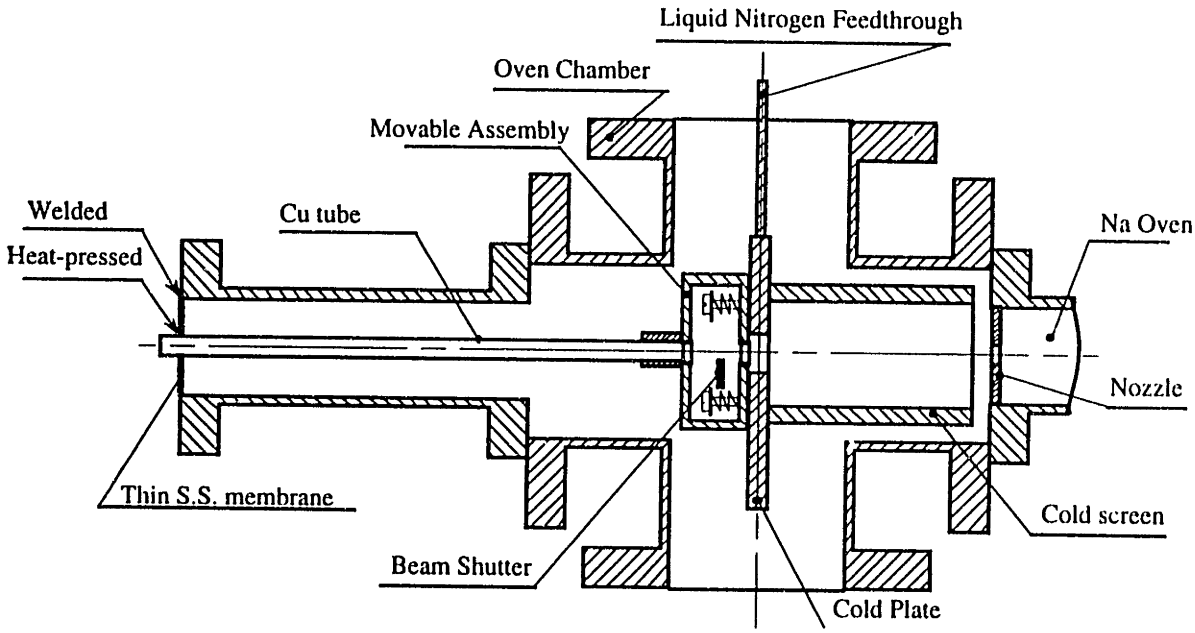

Fig. 3-5: The oven chamber with differential pumping assembly.

3.3. MAGNETIC COILS

To avoid unavoidable losses during the transfer from the light trap to the magnetic trap we chose to keep atoms in the same place while changing the trap, using the same spherical quadrupole magnetic field for both magneto-optical and magnetic trapping. Since the design is pretty crowded altogether, it is advantageous to use the *same* pair of anti-Helmholtz magnetic coils for both traps. This solution saves room in the center of the vacuum chamber but imposes stricter requirements of the coils. For the MOT the

field gradient requirements are moderate (~10 G/cm) but the coils have to be large enough to allow optical access for large trapping beams (Fig. 1-3). For magnetic confinement one would like to have the highest gradient possible, since it increases the depth of the trap and permits compression of trapped samples to higher densities. Since field gradients decrease rapidly with increasing size, the coils must carry large currents and have many turns. To make things more challenging, the coils have to be compatible with the ultra-high vacuum: they have be bakeable, must not outgas, and should not overheat.

The coils are wound with 1/8" refrigerator tubing and are mounted on a 8" ConFlat flange. The inner diameter of the coils is ~5 cm and the turns are arranged in 5 layers of 5 turns each, so the coils look like ~2.5 cm thick toroids. The individual turns are separated by alumina beads (ISI Inc.) and isolated from the support structure with kapton film (DuPont). This UHV-compatible insulator limits the bakeout temperature to high enough value of ~250 °C.* The tubing ends are brazed to four water cooled high-current feedthroughs welded into the flange. All electrical connections between the coils are made outside the vacuum chamber which allows us to manipulate currents through the coils individually. The coils are cooled by tap water (~40 psi) flowing through the tubing. No noticable heating has been observed with 100 A current running through the coils. Each of the coils creates a 3.7 G/A field in its center and in anti-Helmholtz configuration the pair of coils creates a field gradient of 0.94 G/cm·A along the z-axis.

The coils are energized with a 100 A power supply (Kepco Model ATE 6-100DM). This fast-switching model has been chosen to rapidly change current settings between the MOT (~7A), molasses (no current) and magnetic trap (up to 100 A). However, in the

---

* An attempt to electrically insulate coils with fiberglass (Omega Inc.) sleeves failed due to tremendous outgassing of the insulation material. Perhaps, this could be improved by very thourough cleaning of the fiberglass in agressive solvents.

remote voltage-control mode that allows for fast changing of the current produced by the power supply, even ~10 mV pick-up noise would result in currents ~ 0.1 A when the control voltage is set to zero. This is critical, however, since even small currents flowing through the coils create enough magnetic field to impair the performance of polarization-gradient molasses. To avoid this, the current produced by the regulated power supply can be switched on and off with fast high-current TTL-controlled solid-state relays (Crydom, Model D1D40). The relays are rated for 40 A each, so three units are hooked up in parallel. Since the coils have significant inductance (~50 μH) they are shunted with a diode to limit the voltage spikes during switching. The electric connections are shown in Fig. 3-6. The setup allowed us to switch up to 100 A currents on and off in less than ~100 μs (Fig. 3-7).

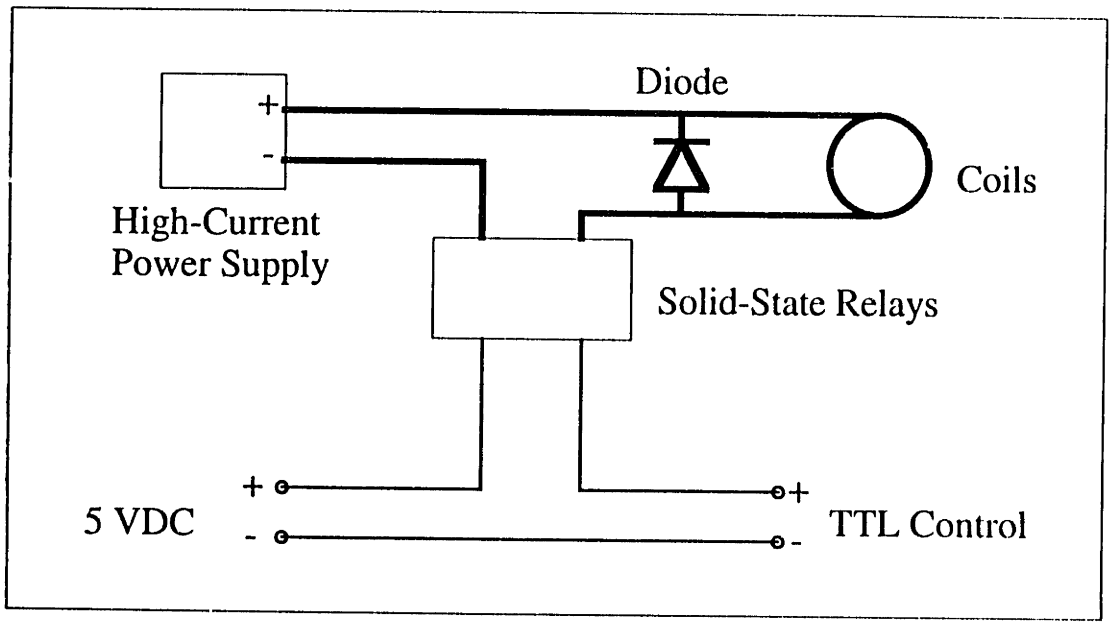

Fig. 3-6: Electric connections of the trap coils.

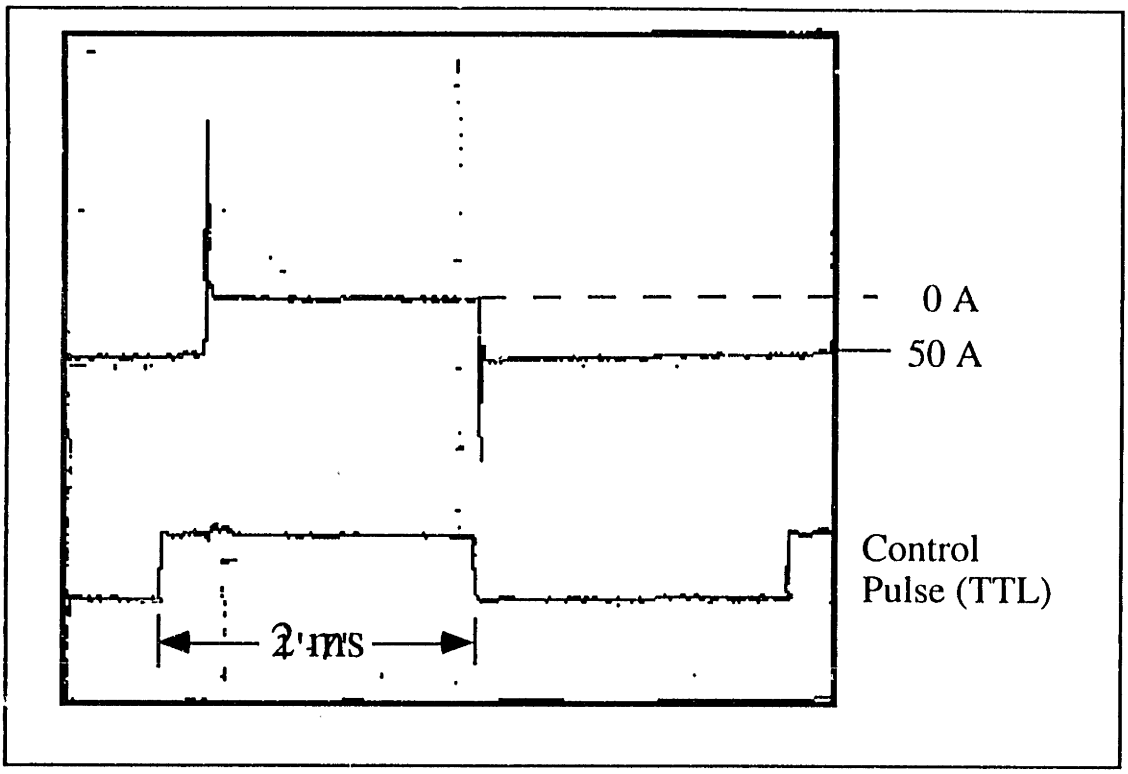

Fig. 3-7: Fast switching of currents through the trap coils.

In a spherical quadrupole magnetic trap the center of the trap is at zero magnetic field, while the center of the MOT may be somewhere nearby depending on the small imbalances in the trapping laser beams. For efficient reloading from a light trap to a magnetic trap these points have to be well overlapped. Furthermore, polarization-gradient molasses requires careful nulling of external magnetic fields (the Earth magnetic field, scattered fields from magnetic bases, slower solenoid, etc.). For these purposes, we use three-pairs of large orthogonal Helmholtz coils and an additional coil to cancel out the gradient field from the slower. All these coils were made of high-temperature wire wrapped outside the vacuum chamber. The current settings are finally adjusted during the experiment.

3.4. OPTICAL SETUP

The elaborate optical part of the experiment has been primarily taken care of by Ken Davis and will be described in greater detail in his thesis [DAV95], so I will only briefly describe it here.

Light for trapping, repumping and probing (~1.2 W) has been generated by a cw single-frequency tunable dye laser (Coherent CR-699). The laser has been frequency-locked to the sodium transition by using Doppler-free saturation spectroscopy. Sidebands at the sodium hyperfine splitting (1712 MHz) have been generated with electro-optical modulators (EOM). The rf power coupled to the EOMs could be varied with attenuators, so the intensity of the sidebands could be changed up to ~30% of the carrier. The trapping laser beam is split into three circularly polarized beams that are sent through the chamber from orthogonal directions and retroreflected onto themselves. Special care has been taken to maintain near-gaussian beam profiles because deviations dramatically affect the performance of the MOT. The repumping and probing light has been split from the trapping laser beam and frequency-shifted by a 1.7-GHz acousto-optical modulator (AOM). Light for slowing (~100 mW) has (in most experiments) come from a second laser (Coherent CR-599) or from a beam split from the main laser and frequency-shifted by ~1000 MHz to the red with a double-pass 500-MHz AOM. All laser beams could be quickly turned off with fast AOMs and/or mechanical shutters.

3.5. OPTICAL DENSITY MEASUREMENT

3.5.1 Absorption Spectroscopy

The density of atoms in the trap can be derived from the optical density of the cloud using the known cross section and the size of the cloud. The optical density has been measured by resonant absorption of light. The frequency of the probing light could be scanned around resonance in a 240 MHz range with two 200-MHz AOMs arranged in series to produce twice the frequency shift with no angular deviation of the beam. The weak absorption probe (typically ~0.5 $\mu W/cm^2$) is sent through the trapped cloud and onto the photodiode. For the reasons explained below in Sections 3.6 and 3.7 the diameter of the beam (~1 cm) is larger than the size of the cloud (~5 mm). The required spacial resolution of the method is determined by a ~0.5-mm diameter pinhole in front of the photodiode. The diameter of the pinhole is chosen to be a compromise between the signal amplitude and spectral resolution. In addition, another pinhole in the waist of the telescope improved the signal-to-noise ratio by shielding the photodetector from bright fluorescence of the trap. The signal from the photodiode is then amplified and recorded on a digital oscilloscope or on a computer. The spectrum is then fitted to a model to derive the optical density (Fig. 3-8).

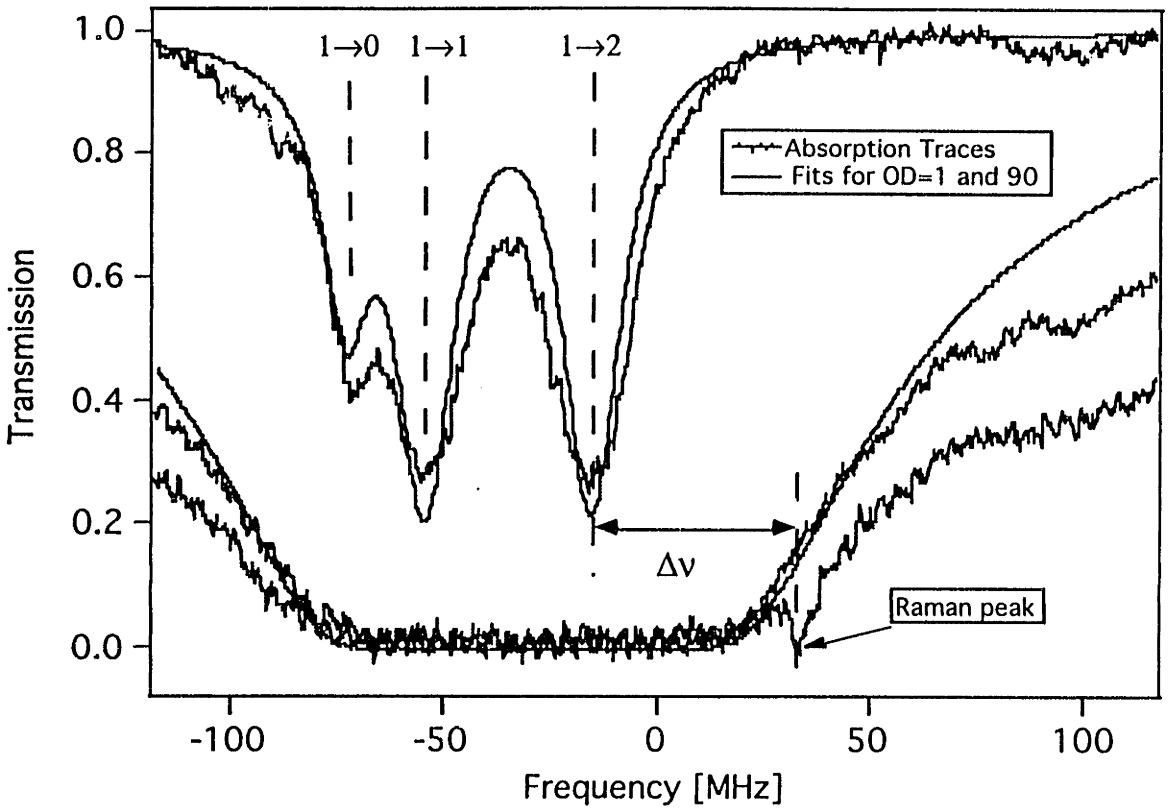

Fig. 3-8: Absorption spectra of sodium atoms in (F=1) ground state. The frequency interval $\Delta\nu$ is used for absolute calibration of the laser detuning as explained in Section 3.5.3.

3.5.2 Intensity Stabilization of the Absorption Probe

In order to fit the recorded spectrum accurately, a flat background is required. Unfortunately, the efficiency of AOMs is frequency dependent (Fig. 3-9), so we actively stabilized the intensity of the probe light.

Since the intensity of the AOM-shifted beam is dependent on the rf power input to the device it was natural to choose one of the 240-MHz AOMs used to frequency sweep the probe as the active element of the stabilization scheme (Fig. 3-10). The intensity of the probe light was monitored with a fast photodiode. This signal is then compared with a pre-set control voltage, the difference is amplified and sent to a voltage-controlled rf-power attenuator. The latter changes the rf power fed into the acousto-optical modulator - the active element in the closed negative-feedback loop.

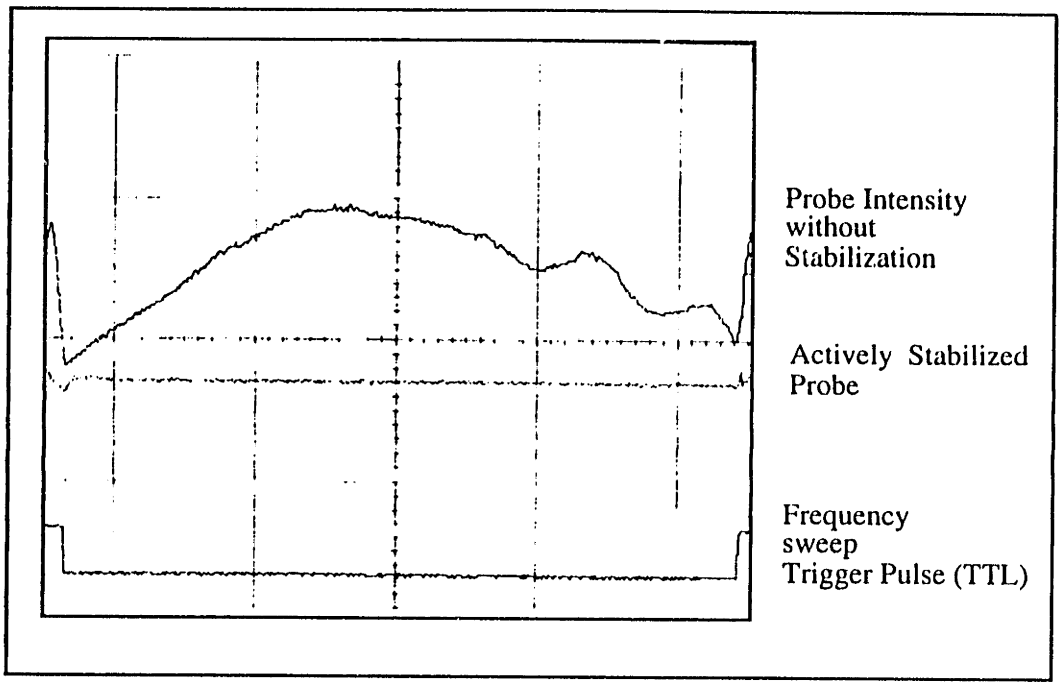

Fig. 3-9: Traces of probe intensity picked up with a fast photodiode . 240 MHz frequency range is swept in ~10 ms.

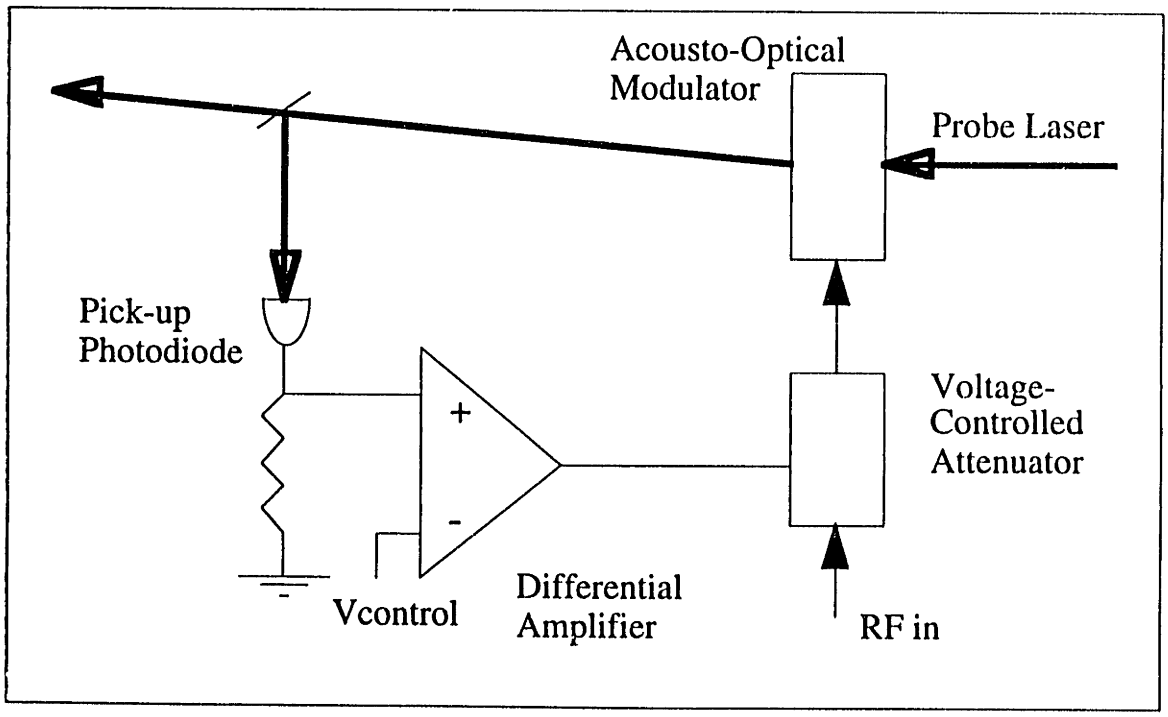

Fig. 3-10: Principle of the "Noise eater" - a device for active stabilization of the absorption probe intensity.

In addition to the intensity variations of AOMs additional noise can be picked up by the probe light by the time it reaches the apparatus. A few sources of such noise are beam steering due to air currents, scattering on dust particles, and the far-field spatial variations of the beam profile produced by the AOM crystals. To let the intensity stabilization correct for these fluctuations as well, the pick-up photodiode has been placed very close to the apparatus, right before the probe was sent through the vacuum chamber. The present setup works well up to sweep frequencies of ~3 kHz, which allowed us to take a full absorption spectrum in less then a millisecond.

3.5.3 Calibration of Trap Laser Detuning

To quantify the behavior of the optical trap and molasses it is important to know the absolute detuning of the trapping light with an accuracy of ~1 MHz. Absorption spectroscopy has turned out to be an effective tool for on-line measurement the absolute laser frequency. At high optical densities of trapped atoms, an absorption spectrum features a well-resolved peak arising from a stimulated Raman transition excited by a probe laser and a red-detuned trapping light (Fig. 3-11). The laser detuning δ can then be derived from the known hyperfine splitting for sodium and the measured frequency interval $\Delta\nu$ as shown in Fig. 3-8.

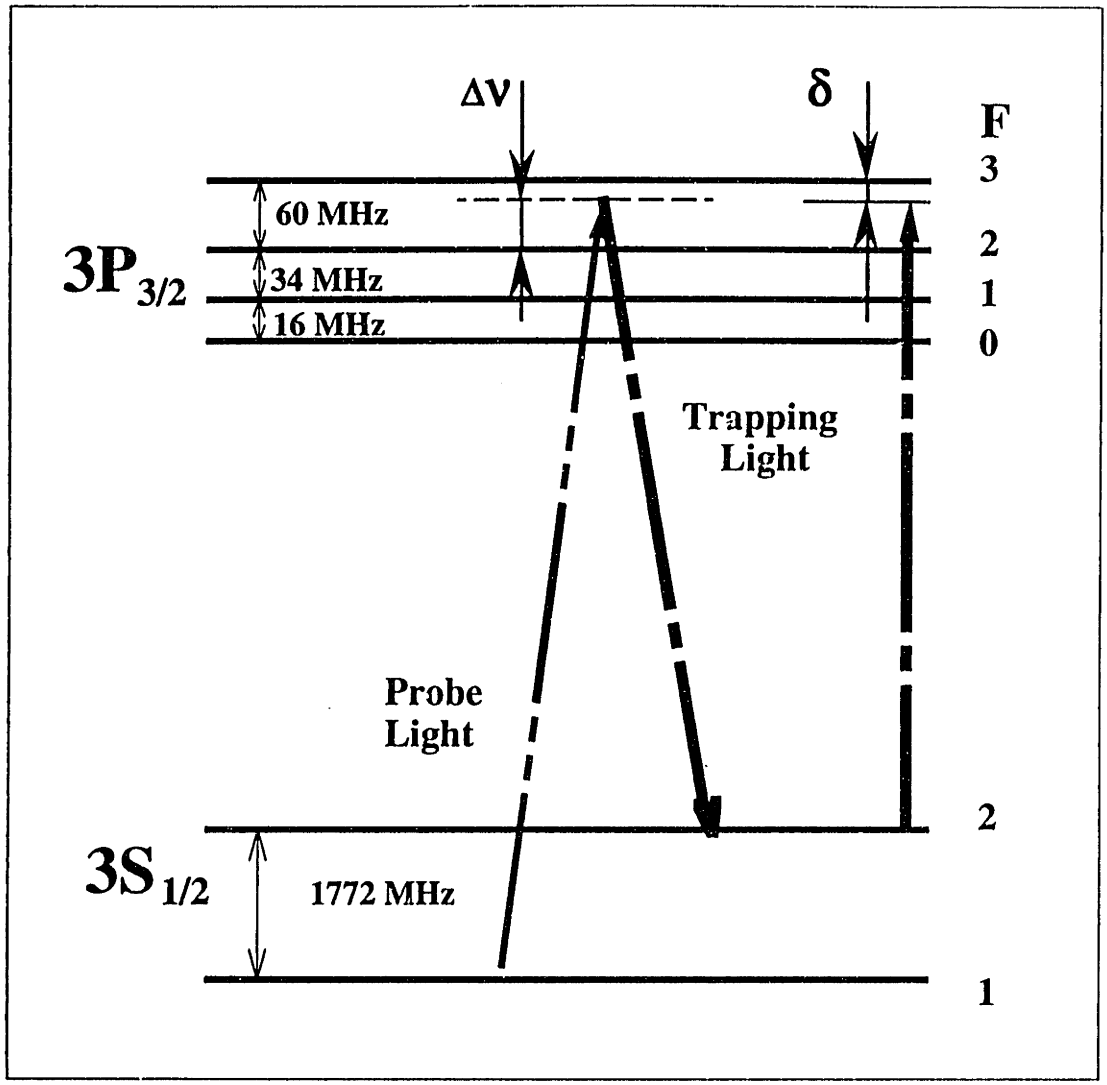

Fig. 3-11: The stimulated Raman transition used for absolute measurement of the laser detuning δ.

3.6. TRAP IMAGING

In this section I will discuss the ways of obtaining images of the trapped atoms. In addition to being a useful on-line diagnostic tool, images are a source of important quantitative information. For example, in order to derive the atomic density in a trap from the optical density measurement it is necessary to know the optical path length for the probe, which is the size of the trapped sample. Also, the volume of the cloud combined with the determination of the total number of atoms (Section 3.7) yields an

independent measurement of the density. Furthermore, the spatial distribution of atoms in a known potential provides a value of the temperature of the trapped sample. All this information can be obtained from video images of the trap.

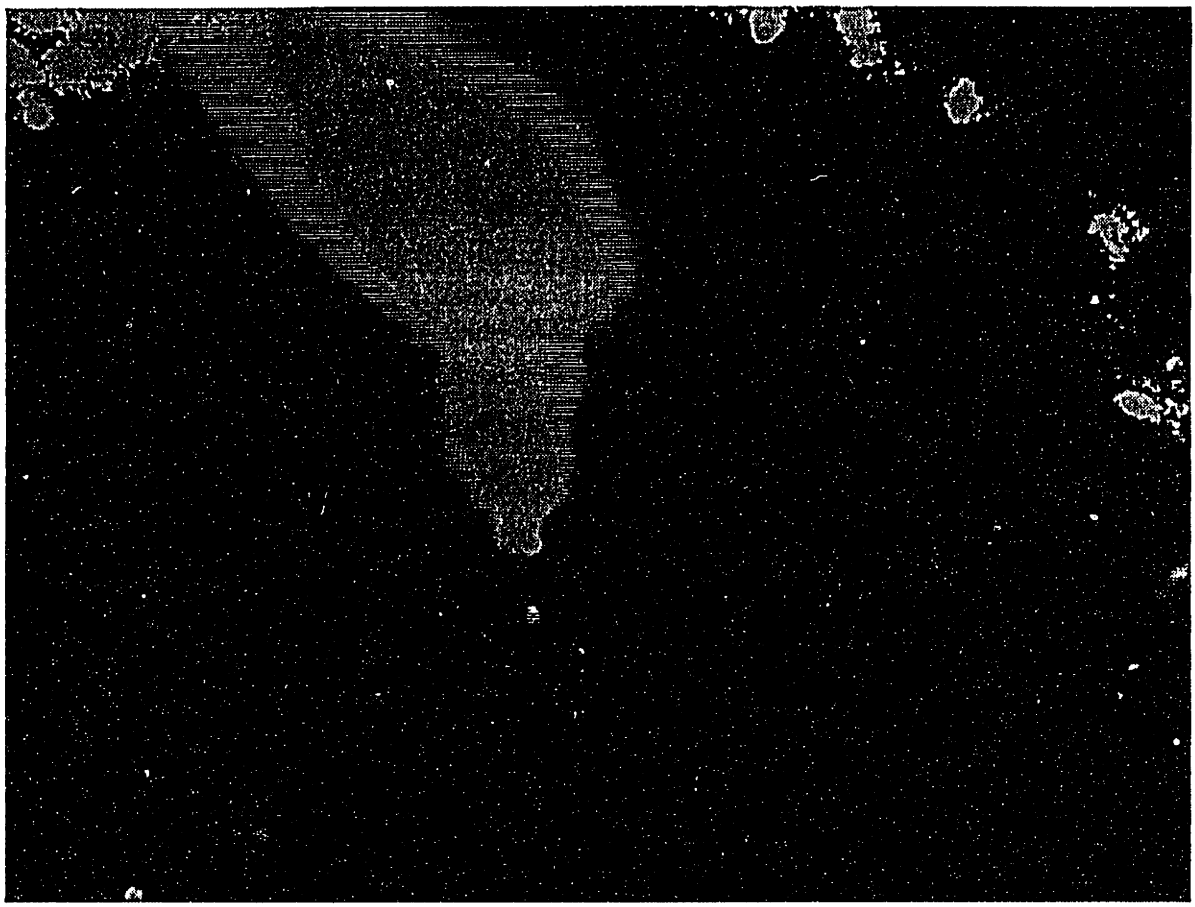

Fig. 3-12: Fluorescence of atoms in a magneto-optical trap. The speckle around the circle is scattering from the magnetic coils.

Images of the trap can be obtained using fluorescence or absorption techniques. In the former method, fluorescence is excited by a resonant laser beam and is picked up with a videocamera (COHU, Model 6515) (Fig. 3-12). In the absorption method, a large diameter probe beam is sent through the trap and the optically dense cloud casts a shadow that serves as a "negative" image (Fig. 3-13). In both cases the video signal from the camera is captured by a frame grabber card and stored in the computer for later processing. The frame grabber is externally triggered (Section 3.9), so the imaging

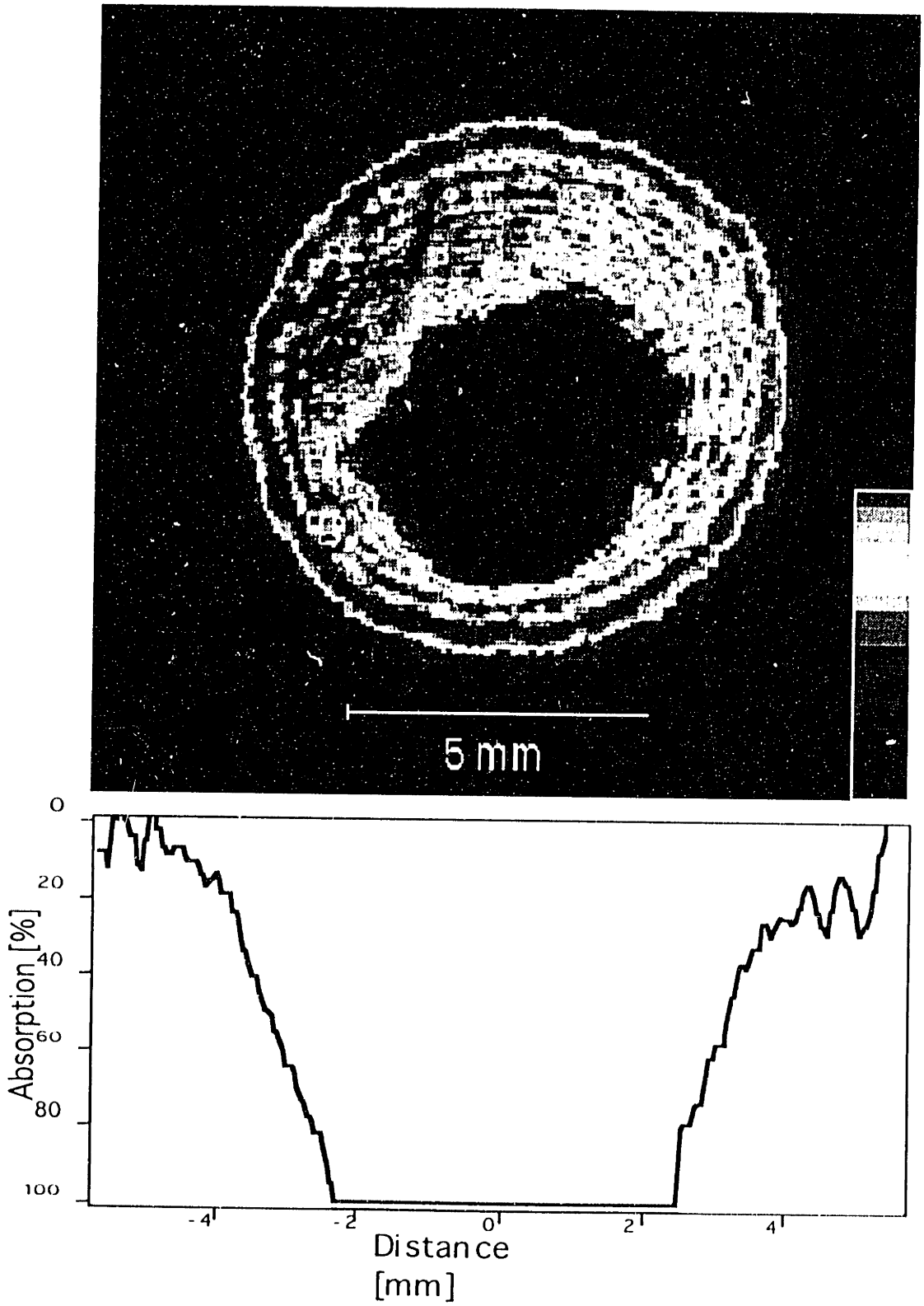

Fig. 3-13: Absorption imaging of the trap: The bright circle is a probe laser beam shining into the camera; the "black hole" in the center is a shadow from an optically dense trapped atom cloud.

technique is also time resolved. Computer-generated false coloring makes imaging more sensitive and is very useful for on-line diagnostics of the trap.

The two imaging techniques are in some sense complementary and we have used both in our experiments. Fluorescence imaging is somewhat easier to implement, is less sensitive to noise and gives crisper images. Also, for a dense cloud, the fluorescence signal can be easily attenuated (optically or electronically) so that the camera is not saturated. This is important, for example, for accurate measurement of the FWHM size of the cloud. In absorption, extraction of a FWHM value is harder because the profile of the cloud often has a top hat rather than bell shape (Fig. 3-13). Fluorescence also has the advantage of being able to probe all atoms irrespective of the state they are in. For that purpose the exciting laser light carries sidebands at the frequency of ground-state hyperfine splitting, so that the probe "talks" to both atoms in (F=1) and (F=2) states.

As will be discussed later in Chapter 4, it is often undesirable to have light with sidebands shining through the trap. Furthermore, even probing light with a "right" frequency, if it is intense enough, can optically pump atoms to the "wrong" hyperfine state and destroy the trap. So, it is important to keep the probe intensity as low as possible. Unfortunately the sensitivity of fluorescence detection is severely limited by the poor collection efficiency of the imaging optics (typically $\sim 10^{-2}$), and therefore demands a relatively high intensity probe. That is where the absorption technique has the big advantage. Since in this method the probe is shining right into the camera and the quantum efficiency of CCD detectors approaches unity, ultra weak probes can be employed. We can continuously record absorption images with a probe as weak as ~ 1 nW/cm^2. The optical pumping rate at this power is ~ 1 s^{-1}, so with this method we can capture about 60 frames (16 ms per frame) during the trap lifetime without serious perturbation of the atoms.

3.7. N - MEASUREMENT: TITRATING ATOMS WITH PHOTONS

Another important parameter of the trap that requires careful quantification is the total number of atoms. It can be measured directly, which provides a consistency check of the atomic density value obtained from optical density.

The idea behind atom titration is to optically pump atoms from one hyperfine ground state to the other and measure how many photons it takes. When an intense resonant laser beam is shone at an optically dense cloud no light gets through initially, so attenuation of the light can be measured using the previously described absorption setup. As time goes by and more and more atoms are optically pumped to a state that is not excited by the monochromatic light, the sample becomes optically thin and the absorption signal decreases (Fig. 3-14).

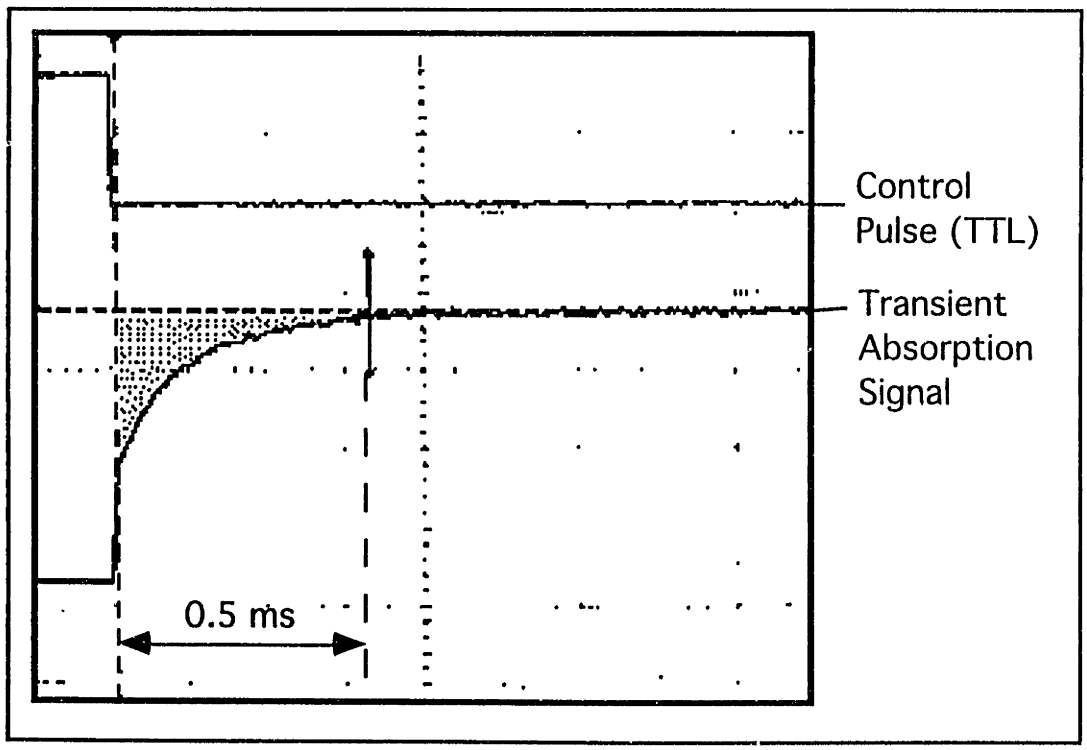

Fig. 3-14: Transient absorption trace. The shaded area is a measure of "missing" photons.

When all atoms have been pumped, all the light goes through and the absorption signal goes to zero. The area under the curve then is a measure of missing photons. The actual number can be obtained from the known quantum efficiency of the photodetector (in electrons per photon) and the gain of the detection electronics. In order to count all atoms we use an intense probe beam with the diameter larger than the size of the trapped sample.

The question remains however: how many photons does it take to optically pump one atom? Since the branching ratio for the upper level is less than unity an atom can fall back to the original ground state and be re-excited several times before it is optically pumped to another ground state. Exact calculation of the average branching ratio for the multilevel sodium atom is complicated, but for individual transitions it can be calculated from known matrix elements [WRS89]. For the $1 \rightarrow 2$ transition the branching ratio is 1:1, so it takes two photons to optically pumped one atom; for the $1 \rightarrow 1$ transition the branching ratio is 1:5, so it takes 6 photons to optically pumped one atom. The case of $1 \rightarrow 0$ transition is more complicated, since the transition is cycling but the sample can become transparent due to formation of quantum dark states. Furthermore, the F = 0,1,2 levels are close to each other, so that the probe can off-resonantly excite several transitions. Based on these estimations, we assume an average branching ratio ~5 accurate to about a factor of 2.

The picture is more complicated in case of an optically thick sample. In a crude one-dimensional picture, a probe beam "eats" its way through the optically dense sample, leaving behind optically pumped atoms. In this simple picture the forward scattered laser photons are reabsorbed and "recycled", whereas the ones scattered back escape through the transparent region of optically pumped atoms. The recycling of photons in the optically thick would effectively change the number of photons required to optically pump one atom. This process is compensated (in the assumption of equal pumping rates)

by the reabsorption of back-scattered Raman photons which brings atoms in the optically thick "repumped" region back into their original state, thus recovering the original photons-per-atom ratio. According to this model the number of photons required to optically pump one atom is the same for optically thick or thin samples.

To experimentally verify this model we varied the frequency of the pumping light and sent it through the trap with the same number of atoms. The result was practically independent from the frequency (Fig. 3-15) with variations expected for different branching ratios and detunings.

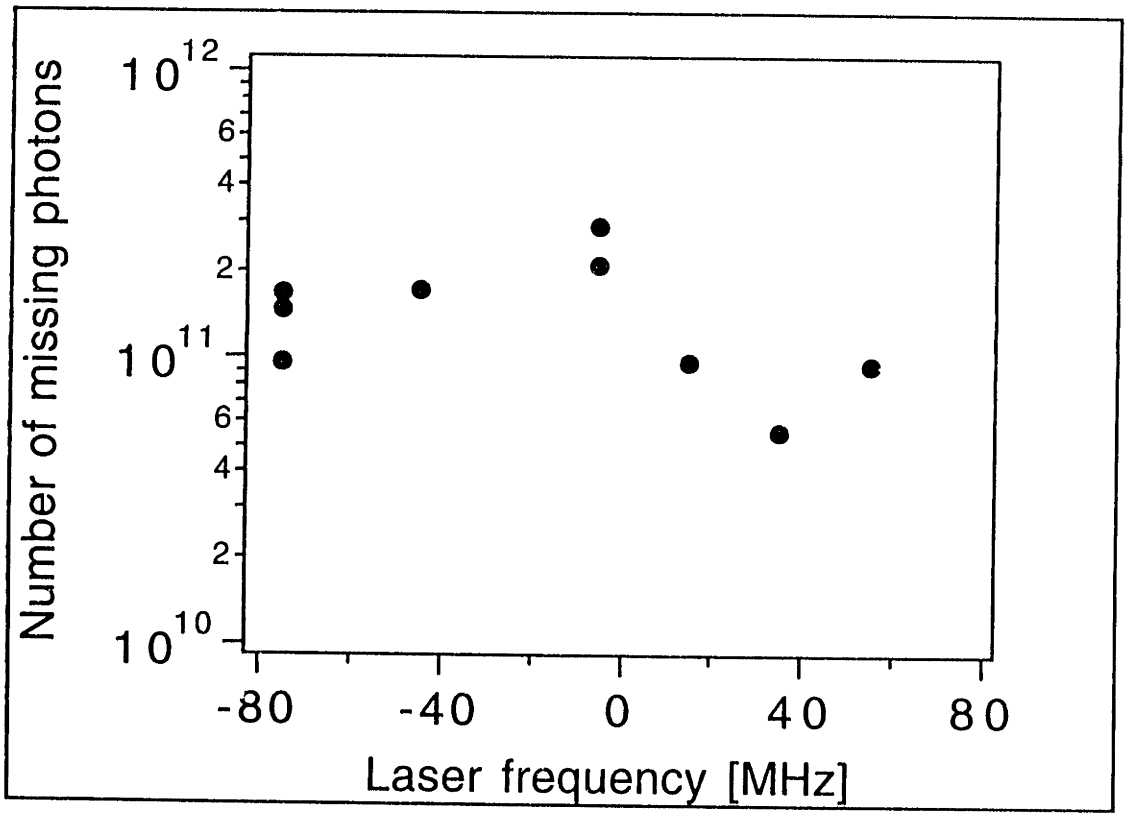

Fig. 3-15: N-count vs. frequency of the probe.

3.8. Temperature Measurement by Ballistic Expansion

To measure temperatures of atomic samples we use a modification of the time-of-flight method. When a trap is rapidly switched off the cold cloud starts falling down like a

rock. In addition the cloud expands since some freed atoms are ballistically flying away from the origin. The rate of this expansion is a measure of the temperature (Fig. 3-16). In our method, atoms are permitted to fly in the dark and then after a variable delay t light is flashed on them. The bright fluorescence gives a strobe image of the falling cloud (Fig. 3-17). Assuming

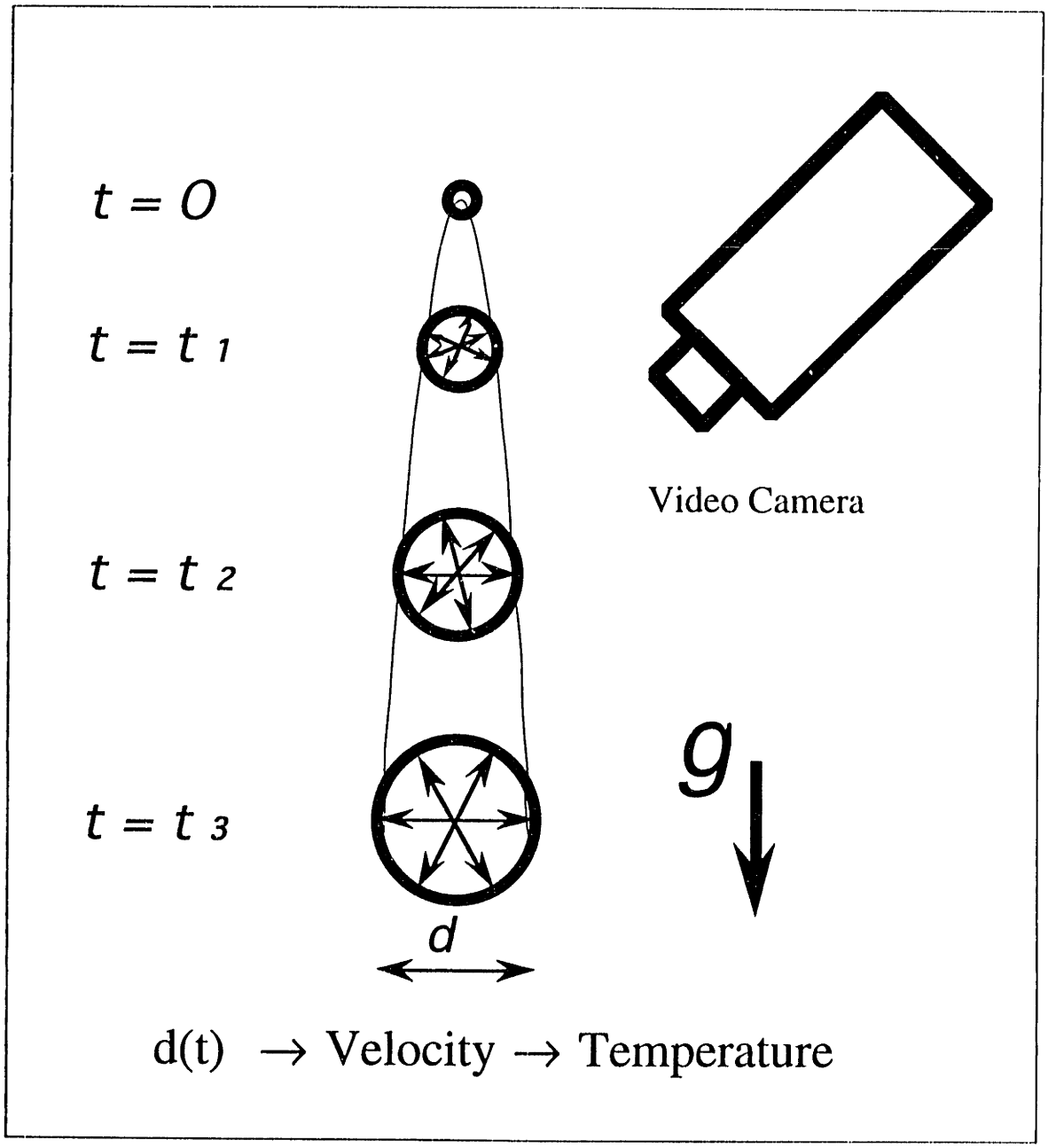

Fig. 3-16. Temperature measurement by fluorescence imaging

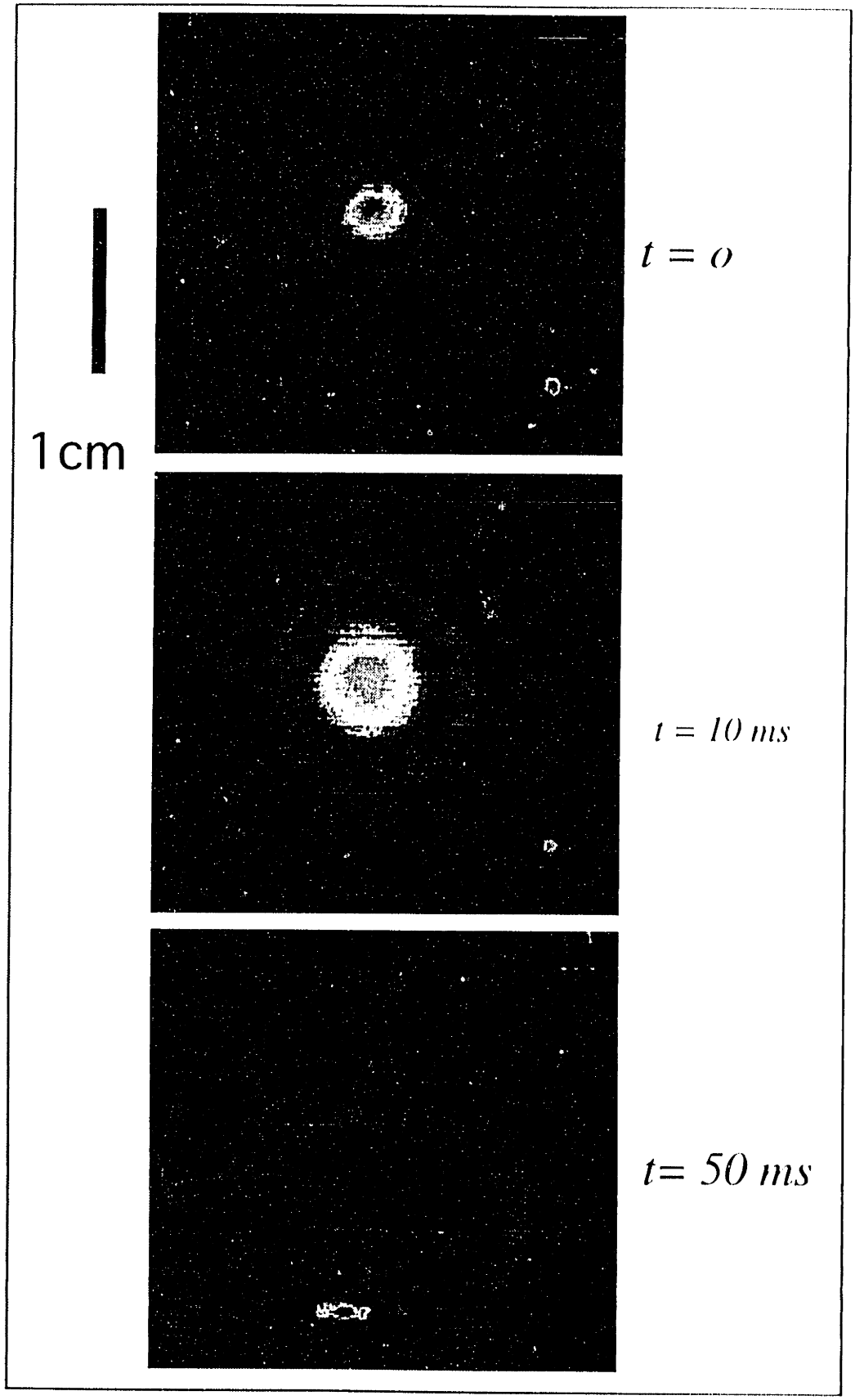

Fig. 3-17. Strobe images of falling atoms

Gaussian density distribution, from the diameter d of the cloud we extract the rms one-dimensional velocity of atoms v by the relation:

$$d^2 = d_0^2 + (2v \cdot t)^2, \tag{3.1}$$

where d_0 is the initial diameter of the cloud. The temperature T is then given by:

$$T = mv^2/k_B. \tag{3.2}$$

There is another way to derive temperature using absorption probing: from optical density. Optical density (OD) scales with diameter d of the cloud as d^{-2}:

$$OD = \sigma n d = \alpha \, 1/d^3 \, d = \alpha/d^2, \tag{3.3}$$

where σ is absorption cross section, n - density, and α is a constant. If at t = 0 the cloud has a diameter d_0 and optical density OD_0 then:

$$OD_o = \alpha/d_o{}^2. \tag{3.4}$$

If we define normalized optical density $y = OD/OD_o$, than (3.3) and (3.4) relate y and d as:

$$y = \left(\frac{d_o}{d}\right)^2. \tag{3.5}$$

As can be seen from (3.1), the OD-measurements linearize in coordinates $1/y$ vs. t^2. The slope of a straight line fit is then $\left(2v/d_o\right)^2$ and combined with the independent measurement of d_o gives the temperature via (3.2). The method is complementary to the first one. It is more complicated, since it requires both imaging and absorption measurement, but is somewhat faster which can be a virtue.

3.9. ELECTRONIC CONTROL OF THE EXPERIMENT

To control the experiment and to collect and store the acquired data we developed a Macintosh-based computer system. The Mac IIx computer has been chosen because it has 6 six NuBus slots that accomodate additional plug-in boards for adiitional functionality and flexibility.

Data Acquisition

The data-acquisition system consists of a data acquisition card NB-MIO-16X supported by a LabView for Mac software package, both from National Instruments. The data acquisition system emulated a three-channel digital oscilloscope. The multiple channel feature allows simultaneous recording of several signals, for example an absorption trace, a frequency sweep ramp, and a synchronization pulse. The board is configured to be externally triggered and allows expansion up to eight differential inputs. With addition of the direct memory access card (NB-DMA-2800) the collection speed reached ~0.1 ms per point. The DMA card also has a built-in controller that enables us to program stand-alone instruments, such as frequency synthesizer, via the GPIB bus.

Images are captured by an externally triggerable frame grabber card (Scion Corp.). The hardware is supported by a very good (and free) software package - Image - developed at NIH. Both traces and images are stored in a digital form for later analysis. Although the LabView package has extensive analysis capabilities we found that Igor data analysis software (Wavemetrics) is a better tool for the job.

Timing Control of the experiment

This experiment requires precise timing of several parameters. For example, once the trap is loaded it is advantageous to shut off the atomic beam and the slowing laser, so that no unnecessary losses are introduced. While intense laser light is indispensable for the MOT, once the high currents in the coils are turned on and the atoms are magnetically trapped, it is much better to keep them "in the dark," so the light has to be shut off. For temperature measurements it is crucial to flash the strobe light after a variable delay. As can be seen from these examples the timing issue is crucial and synchronization of different parts of the experiment requires a single controller.

The timing patterns in the earlier of these experiments have been generated by a 16-channel word generator in a timing simulator mode (Interface Technology, Model RS-660). Later a digital input/output computer card (NB-DIO-32F, National Instruments) was used. All peripheral devices (actuators, shutters, switches, modulators, etc.) were configured to understand standard TTL control pulses. A typical timing diagram is shown on Fig. 3- 18.

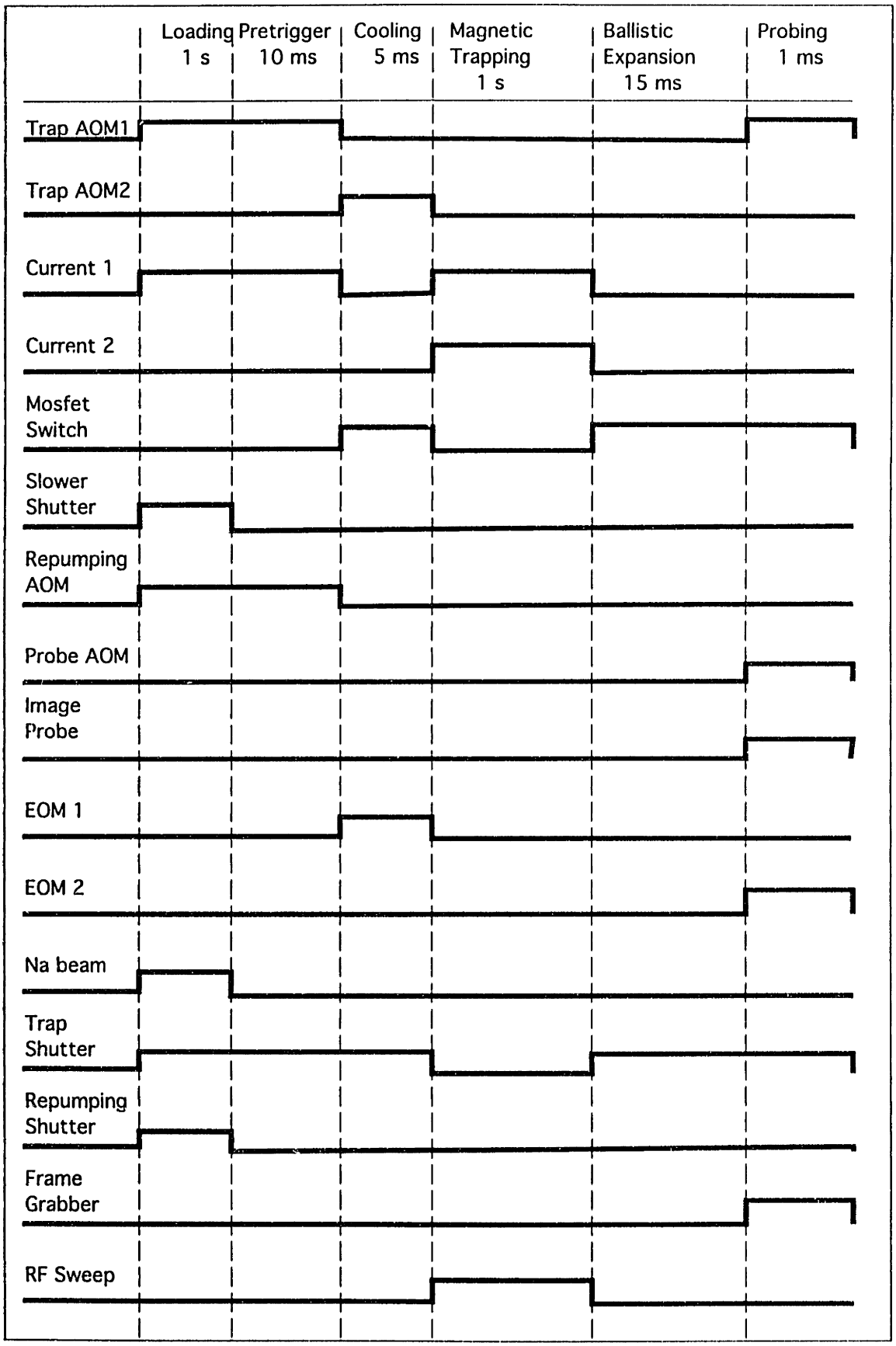

Fig. 3-18: Typical timing pattern of the experiment.

Videocamera Sinchronization

The only instrument used in our experiment that can not be controlled by external TTL pulses is the free-running videocamera. It has its own clock and complies with a TV frequency standard (16 ms per field or 32 ms per image). Meanwhile, the typical experiment consists of a continuously repeated loading-trapping-probing cycle with a period determined by the timing simulator. To ensure consistent capturing of images frequency beating between the two instruments has to be avoided, so the videocamera and the timing simulator have to be synchronized or phase-locked. To do so the timing simulator is programmed upon completion of a cycle to set a certain bit to "high", signaling that it is ready to start the new cycle and is waiting for a trigger pulse. Also, the sync pulse corresponding to beginning of a field of certain oddity (Odd Vert. Sync and Even Vert. Sync) is extracted from video signal with a special "sync stripper" chip. The "ready" signal from a timing simulator and an "even" sync pulse from the camera are sent to the "AND"-gate and the output of the gate triggers the timing simulator (Fig. 3-19). This ensures that each new experimental timing cycle started when the camera is exactly in the same state. A variable delay introduced into the video sync line allows us to shift the two timing patterns relative to each other, while maintaining phase lock between them.

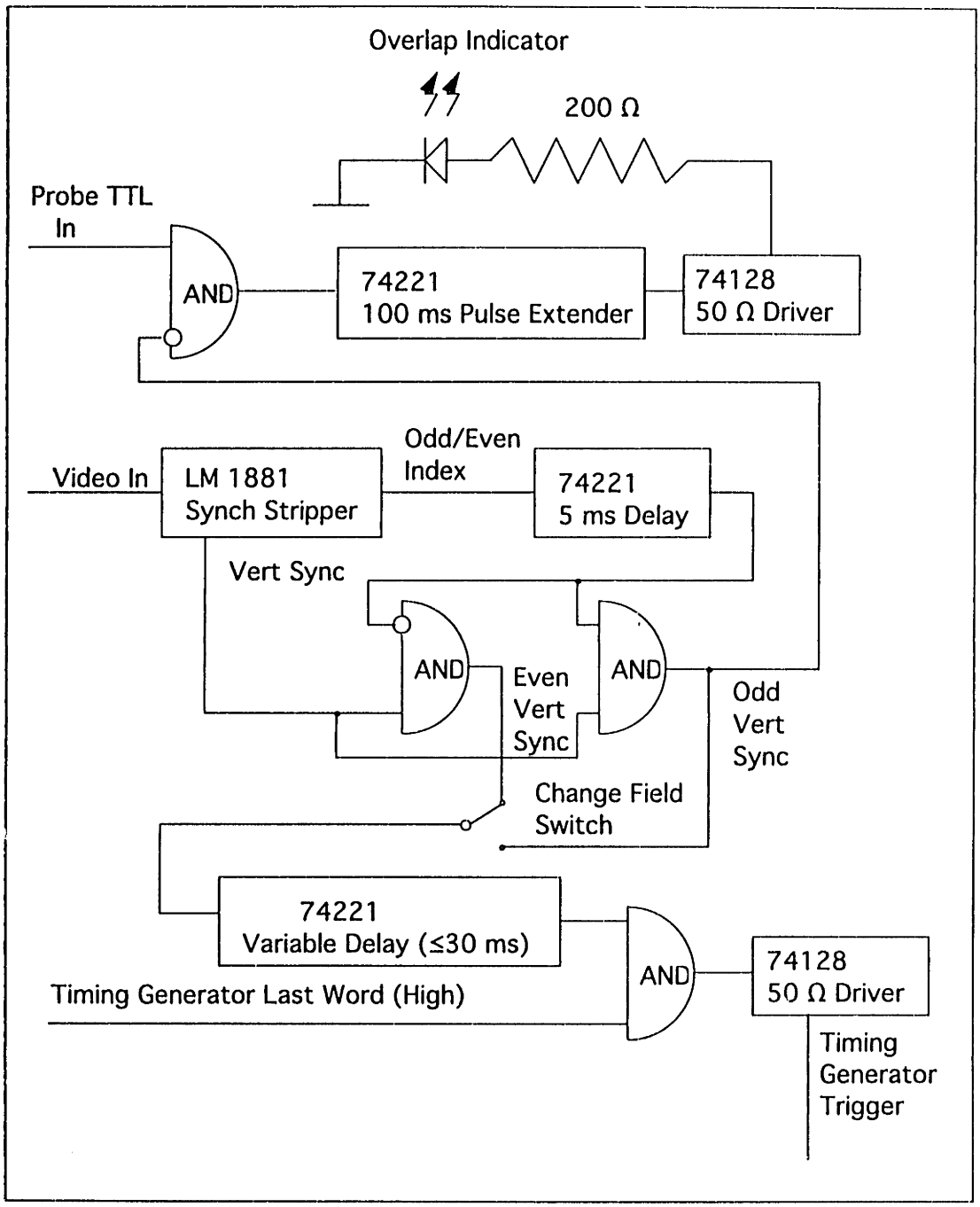

Fig. 3-19. Schematic of the videocamera synchronization setup. A 5 ms delay is introduced into the line to avoid glitch pulses. A 100 ms beam extender is installed to brighten the flickering LED, which indicates overlap of the probe pulse with the high-speed shutter of the CCD camera.

3.10. RF ANTENNA

To irradiate atoms with radio frequency electromagnetic waves a special antenna is installed in the vacuum chamber. The antenna has 10 turns of kapton insulated copper wire and is mounted on the inner side of one of the trap magnetic coils. The antenna is a ~3-mm thick toroid with 5.6 cm i.d. and 6.5 cm o.d. The distance from the antenna to the center of the trap is ~ 2.5 cm. To defeat parasitic resonances due probably to induced currents in the trapping coils both coils are shunted by 2-μF capacitors hooked up outside the vacuum chamber. The rf fields produced by the antenna have been measured in situ with a calibrated pick-up coil. The results are shown in Fig. 3-20.

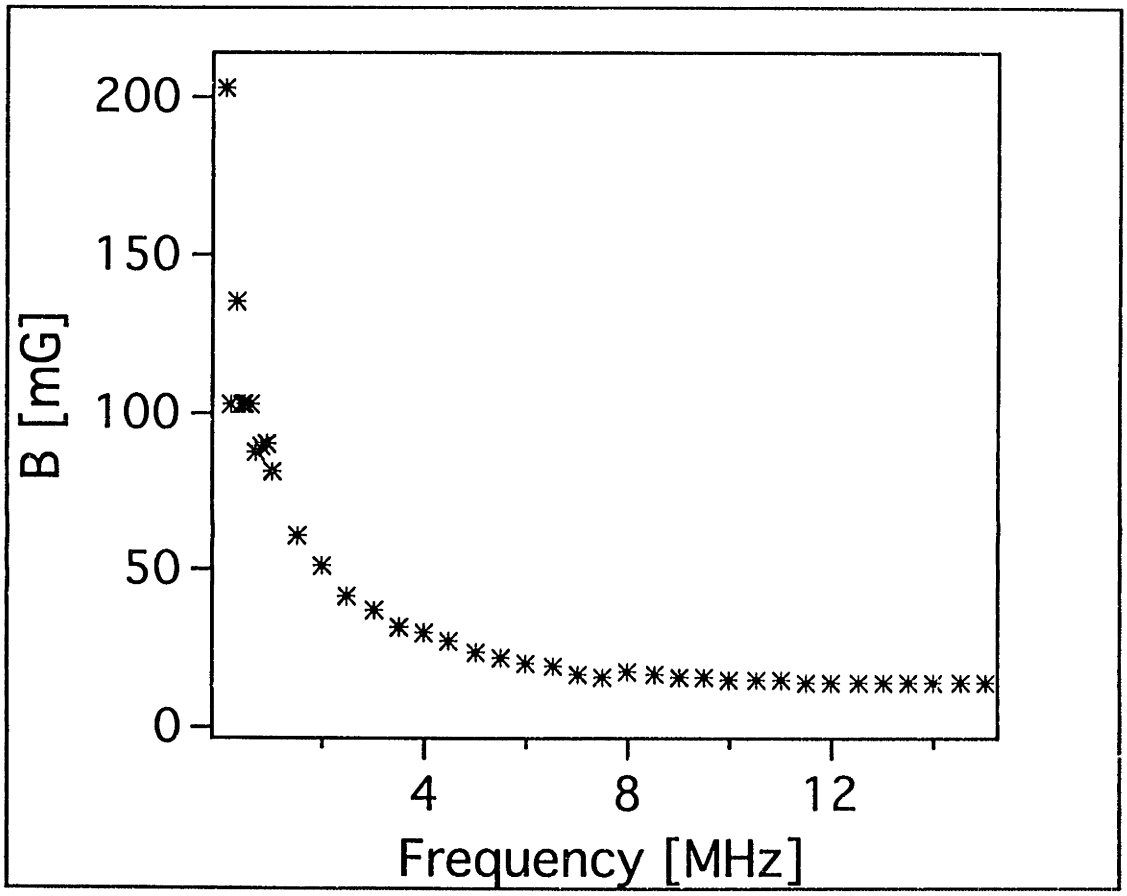

Fig. 3-20. The z-component of the rf magnetic field created by the antenna vs. the rf frequency.

There are two kinds of light—the glow that illuminates, and the glare that obscures.

— James Thurber

4. DARK SPOT

4.1. LIMITATIONS OF MAGNETO-OPTICAL TRAPS

One of the problems with optically trapped sodium is that a reasonably dense trapped atom cloud looks like a suspended wind-blown flame. In more physical terms, the cloud in a MOT does not look at all like an ideal-gas sample as one might expect for these densities ($< 10^{11}$ cm^{-3}). The trap exhibits pronounced dynamic behavior with all kinds of striations, rings, filaments, vortices, etc. as can be seen on the snap shot of the cloud in Fig. 3-12. The behavior has been observed by many groups and is due to processes posing a more severe problem than just instability: they restrict the maximum density achievable in a MOT. The problem has been carefully investigated by the Colorado group [SWW91] who have identified three different regimes of MOT operation. The discussion of the optical forces below follows the lines given in [WSW90].

When a trap contains only a small number of atoms (less than ~40 000 in the case of a Cs trap) the atomic sample does behave like an ideal gas of definite temperature. The volume of the trap is determined by the damped harmonic potential and the density is proportional to the number of atoms. As more atoms are added, photons from the

trapping laser beams absorbed and reemitted by one trapped atom can be reabsorbed by another neighboring atom. This gives rise to a long-range repulsive force between the trapped atoms which increases with the density of atoms in the trap. When this force becomes comparable to the confining spontaneous-light force the trap makes a transition into a different regime. As more atoms are added the density no longer increases. Instead, the volume of the cloud increases while its density and temperature remain constant. In this regime the local rescattering force exactly balances the trapping force in the interior of the sample. Therefore, the overall cloud shape becomes more sensitive to light intensity fluctuations and other imperfections, giving rise to the observed dynamic instability. Further increase of the total number of atoms leads to attenuation of the trapping light as the sample becomes optically dense [DAL88]. As a result the atomic density in the trap starts decreasing with additional increase of the number of atoms.

The above mentioned limits are static in a sense that they hold for a certain ensemble of atoms. There is another, dynamic limit on the highest achievable density in a magneto-optical trap: trap loss due to collisions between the excited- and ground state atoms. These resonant collisions are exothermic and when the excitation energy is transformed into kinetic energy the "hot" atoms may not be confined by the trap any more. The per-atom rate of this loss mechanism is βn with $\beta \approx (1-5)\cdot 10^{-11}$ cm^3/s for sodium atoms [PCB88]. For densities n ~10^{11} cm^{-3} this trap loss limits the lifetime of the trap to ~1 sec, so this high density can be sustained only by loading the trap at a very high rate.

Finally, there is a technological barrier to trapping high numbers of atoms in a MOT. 10^{11} atoms scatter ~100 mW of near-resonant laser light pushing the available laser resources to the limit.

4.2. TRAPPING ATOMS IN THE DARK STATE

Once the limits of the magneto-optical traps had been identified the next step was to find a way around them. The problems of the MOT arise from the interaction of atoms with the same resonant light that traps them. It is natural, then, to look for a way to hide trapped atoms from this light. We have demonstrated that the hyperfine structure of the atom ground state can be exploited to circumvent the severe limits on atomic density in a trap imposed by the light-atom interaction. The essential idea is that for sodium, transitions starting from the (F = 1) hyperfine state are ~170 linewidths away from the (2→3) cycling transition (Fig. 1-1) and atoms in this state are not often excited by the far-detuned trapping light. Thus, atoms can be hidden in the "dark" hyperfine state not accessible by the trapping light and, consequently, neither be affected by the repulsive forces nor be subjected to the trap-loss excited-ground state collisions. Since the atoms in this dark state do not experience any trapping force at all something has to be done to prevent them from escaping the trap. The idea is to keep atoms in the dark state only for some fraction of the time and periodically transfer them back and forth into the "bright" state in which they do feel the confining and cooling force.

This time sharing between the trapped and non-trapped states obviously makes the trap effectively shallower, but atoms can still be tightly confined even if the trapping spontaneous light force is orders of magnitude smaller than the maximum saturation value. Only 1% of the saturated spontaneous light force stops 1-mK sodium atoms moving with 1 m/s in 100 μm, which is much smaller than the typical trap size of ~1 mm. While the shallower trap potential would result in smaller density for the same number of atoms at a given temperature, the overall result, as will be shown below, is favorable because the negative effects of the trapping light are avoided. This "shelving" of atoms in the dark hyperfine state allows one to pile up more atoms in the trap and achieve densities orders of magnitude higher than in a conventional MOT.

The fraction of atoms that are in the dark hyperfine state is one more parameter of the trap (along with the total number of atoms and the trap volume) that can be varied in the experiment. Optimization of all parameters simultaneously allows achieving much better overall results: for large number of atoms, some sacrifice in the trap strength (due to shelving of atoms in the dark state) results in the volume increase but, at the same, in, fortunately, much more significant increase in atom density.

4.3. LIGHT FORCES IN A MAGNETO-OPTICAL TRAP

There are three kinds of forces acting on atoms in a magneto-optical trap: the trapping force, the attenuation force and the optical repulsion force. The first is the superposition of the spontaneous-light forces from the trapping laser beams. The combination of the magnetic fields with a circular polarizations makes atoms preferentially absorb photons from one beam compared to the other. As a result the atoms experience a restoring force towards the origin of the trap

$$\vec{F} = -k\vec{r}, \tag{4.1}$$

so the atoms are confined in a harmonic potential with the spring constant k. In addition the red-detuned trapping light provides damping such that the atomic motion is overdamped by a factor of ~10.

As the number of atoms in the trap increases the attenuation of the trapping light starts becoming important. The attenuation of light produces several effects. Since spontaneous light forces are intensity-dependent it leads to a reduction of the spring constant k. Also, in real experiments trapping beams are often retroreflected onto themselves. Consequently, the intensity of the retroreflected beams is smaller than the intencity of the incident beams that passed through the optically thick cloud. This can be corrected for, however, by appropriate focussing of the retroreflected beams. Lastly, the

more important efffect of the attenuation is that it gives rise to the second kind of optical force acting in a MOT: atttenuation force. When a light beam with intensity I_o propagates along the x axis through the absorbing sample of density n, its intensity is attenuated as a function of distance x as

$$I(x) = I_o e^{-\sigma_L n x}, \tag{4.2}$$

where σ_L is an absorption cross section. Two counterpropagating beams with respective intensities I_+, I_- are attenuated differently at each point and the resulting intensity imbalance results in the attenuation force along the x axis

$$F_{A,x} \propto \sigma_L (I_+ - I_-). \tag{4.3}$$

It has been shown [SWW91] that for the six-beam MOT the attenuation force obeys the relation

$$\vec{\nabla} \cdot \vec{F} = -6\sigma_L^2 I_o n / c \tag{4.4}$$

The minus sign indicates that the attenuation force is directed inward, i.e. it is a compression force.

Spontaneous light force arises from the repeating absorption-spontaneous emission cycle which means that every atom scatters many photons. These reemitted photons can be absorbed by other atoms in the optically dense sample, the effect known as radiation trapping. In course of every reemission-reabsorption act involving two atoms the relative momentum of the pair is increased by $2\hbar k$: the emitting atom experiences a recoil, while the other absorbes the photon momentum directed along the interatomic axis. Effectively it results in the third kind of optical forces: the long-range optical repulsion force between atoms.

If an atom is irradiated by laser light of intensity I it absorbes and reradiates light at rate $\sigma_L I$ in a random direction. Hence, another atom a distance d away is exposed to the reradiated light of intensity

$$I_{rad} = \sigma_L I / 4\pi d^2. \tag{4.5}$$

This atom then is experiencing a repulsive light-pressure force

$$F_R = \sigma_R \sigma_L I / 4\pi c d^2, \tag{4.6}$$

where σ_R is the absorption cross section for the scattered photons. This cross section is, in general, different from the cross section for the trapping laser photons σ_L, because the polarization and frequency distribution of the reemitted light is different from those of the incident light. Intense electro-magnetic fields (which is the case in a MOT) produce ac Stark shifts of atomic levels which lead to a modified fluorescence pattern known as Mollow triplet [MOL69]. Sesko et al. [SWW91] have shown that the absorption profile is peaked near the blue component of the Mollow triplet and, consequently, σ_R is larger than σ_L.

The expression (4.6) gives the repulsive force acting on an atom due to scattering from another atom. For a cloud of atoms with the density distribution $n(\vec{r})$ the expression for the force can be generalized to the form that allows easy comparison with the expression for the attenuation force (4.4):

$$\vec{\nabla} \cdot \vec{F}_R = 6\sigma_R \sigma_L I_o n(\vec{r}) / c. \tag{4.7}$$

Since $\sigma_R > \sigma_L$, the resulting density-dependent optical force is repulsive and when it counterbalances the confinement force (4.1) the trap reaches its maximum density. When the force is equal to zero its divergence is also equal to zero, so combining the divergence of the trapping force (4.1), $\vec{\nabla} \cdot (-k\vec{r}) = -3k$, with (4.4) and (4.7) we obtain for the maximum density of atoms in the MOT:

$$n_{\max,MOT} = \frac{ck}{2\sigma_L(\sigma_R - \sigma_L)I_o}. \qquad (4.7)$$

This fact explains why the cloud starts expanding, but its density stays constant when the total number of atoms reaches a certain threshold.

The described model is developed in the approximation that every atom behaves as a two-level system. This is pretty much the case in a sodium MOT operating on the cycling (2→3) transition. Leakage out of the two-level system occurs via optical pumping to the (F = 1) ground state. Since this state is far away from resonance, atoms ending in this dark state do not feel the confinement force and are lost. This loss is corrected by optically pumping atoms back with repumping light of a separate frequency (Fig. 1-1). This light is typically very intense, so that the leaking atoms are quickly repumped. However, the atoms do spend some time in the dark state and the average time an atom spends in this state is determined by the ratio of optical pumping and repumping rates. So, a trapped sample is actually a mixture of atoms in the "bright" (F = 2) and the "dark" (F = 1) states. The trap than can be conviniently characterized by a brightness parameter p which is the fraction of atoms in the bright state. For example, $p = 1$ would correspond to an ideal picture of a MOT with all the atoms trapped in (F = 2) state, and $p = 0$ would describe an empty "trap" in which all atoms are lost due to optical pumping. Up to now atom trappers tried to bring the brightness parameter of their traps as close to unity as possible by squeezing maximum power out of their repumping light sources. We have discovered, however, that it is to one's advantage to maintain p somewhere in between the limiting cases of zero and unity.

The higher the brightness of the trap p the stronger the trap is, because more atoms are cycled in the trapping transition and experience a "good" strong spontaneous light force. On the downside, the "bad" optical repulsion force increases also. Indeed, if the

brightness parameter of the trap p is taken into account, the expressions for the trapping and the repulsive forces can be rewritten respectively as

$$\vec{F}_T = -kp\vec{r} \tag{4.8}$$

and

$$\vec{F}_R = k(n / n_{\max,MOT})p^2\vec{r}, \tag{4.9}$$

where $n_{\max,MOT}$ is a constant given in (4.7). The density limit then becomes

$$n_{\max,p} = n_{\max,MOT} / p \tag{4.10}$$

or 100 times higher for p=0.01 than in conventional MOT (p = 1)! The key is that the confining and the repulsive force scale differently with p. It means that for the same number of atoms the atomic density would change depending on the value of p. In other words, depending on the number of atoms in a trap there is an optimal brightness parameter p which results in the maximum atomic density.

As has been previously discussed in Section 4.1, for different total numbers of atoms in the trap there are three distinct regimes of the trap operation. Each of these regimes asks for a different optimum value of p. The number of atoms in the trap is determined by the ratio of the loading and the loss rates; the brightness parameter can be varied by changing the intensity of the repumping light. The problem is that changes of the intensity of the repumping sidebands in the MOT affect its capturing properties and, hence, the number of atoms in it. Furthermore, the changed repumping rate changes the trap-loss rate and complicates the quantitative studies of the discussed effects. To overcome these problems, one would like to be able to vary the number of atoms in the trap and the brightness parameter in the trap independently. We have developed a way to do it and I will discuss it in the following section.

4.4. SEPARATE REPUMPING IDEA

As has been discussed above, the brightness has to be optimized in order to achieve maximum density in the trap. In other words the repumping light has to have certain (relatively small, as it turned out) intensity. However, in order to capture as many atoms into the trap as possible it is highly desirable to have intense repumping light to provide strong spontaneous-light force and increase the capture range of the trap. This Catch-22 situation can be solved by providing repumping light with a separate laser beam with a profile that looks like a donut rather that a circle (Fig. 4-1). We call this new kind of light trap a "dark SPOT" which may stand for dark **SP**ontaneous-force **O**ptical **T**rap. In the experiments a real dark spot was introduced into the separate repumping beam and imaged onto the zero-field point to avoid diffraction effects. After passing through the trap once, the repumping beam was sent is sent through it again at a different angle. As a result around an origin there is a shell of ~5-mm inner radius and ~2 cm outer radius which behaves like a conventional MOT: both trapping and repumping light are present. Inside this shell, however, atoms "see" only the trapping light. Actually, it turned out that even one passage of the repumping beam was sufficient, so the cylinder of darkness works almost as well as the dark ball. The improvement due to the second passage is on the order of a few percent and it was used in most of the experiments.

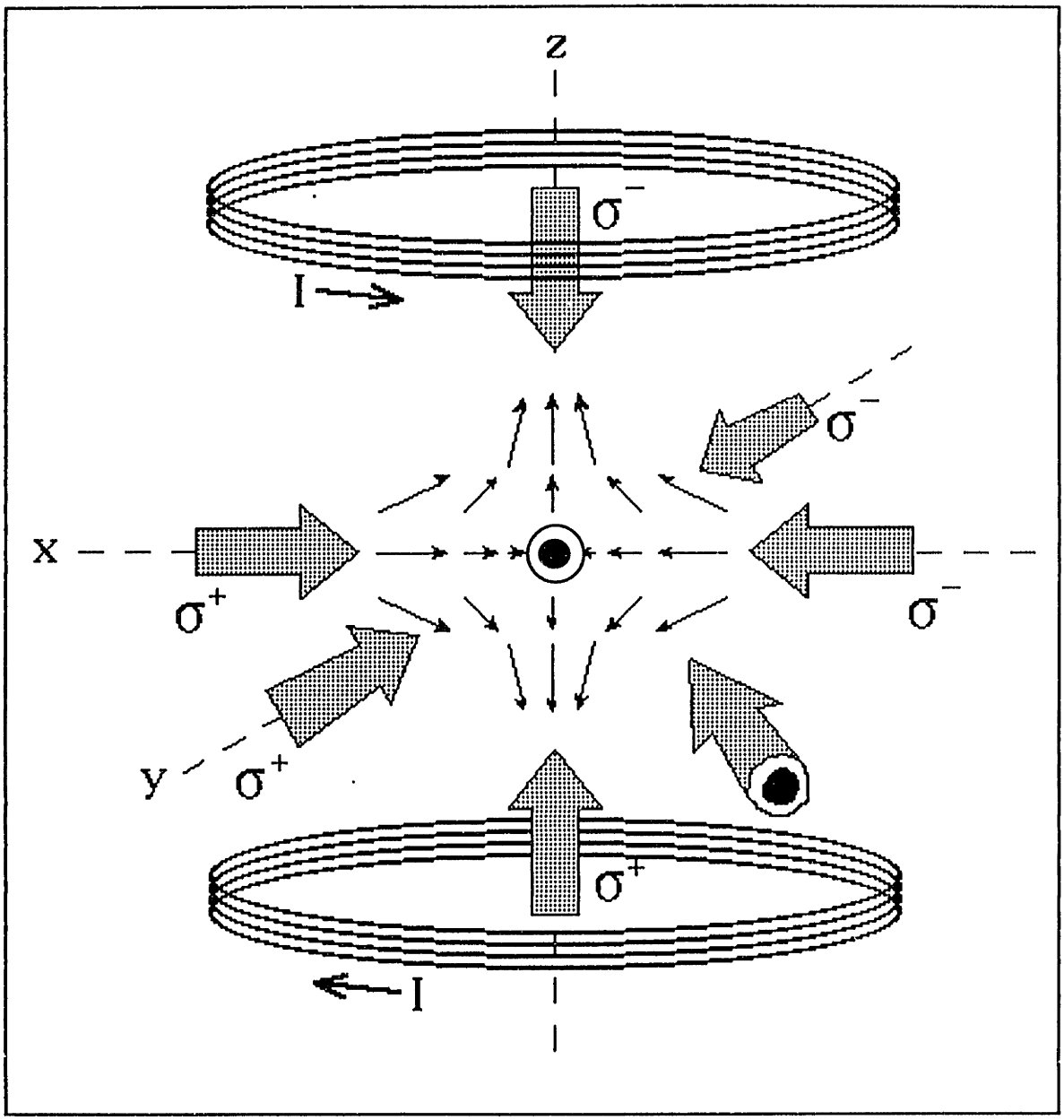

Fig. 4-1: The "dark SPOT" setup .

The repumping light in our experiments has been generated from part of the trapping laser beam by a 1.7 GHz acousto-optical frequency shifter (AOM). In addition, an electro-optical modulator (EOM) in the trapping light train added sidebands at the frequency of the hyperfine splitting of the ground state. The intensity of these sidebands could be varied by attenuating the rf power coupled to the EOM. As a result, this setup enabled us to vary the intensity of the repuming light in the trap without sacrificing the capturing efficiency of the shell that acted as a usual MOT.

4.5. RESULTS

When no dark spot is introduced into the separate repumping beam the trap operates, as expected, like a conventional MOT. The first striking result of sliding the spot in is the striking change of the cloud appearance. The very unstable cloud (Fig. 3-12) collapses to a much better behaved ellipsoidal ball (Fig. 4-2).

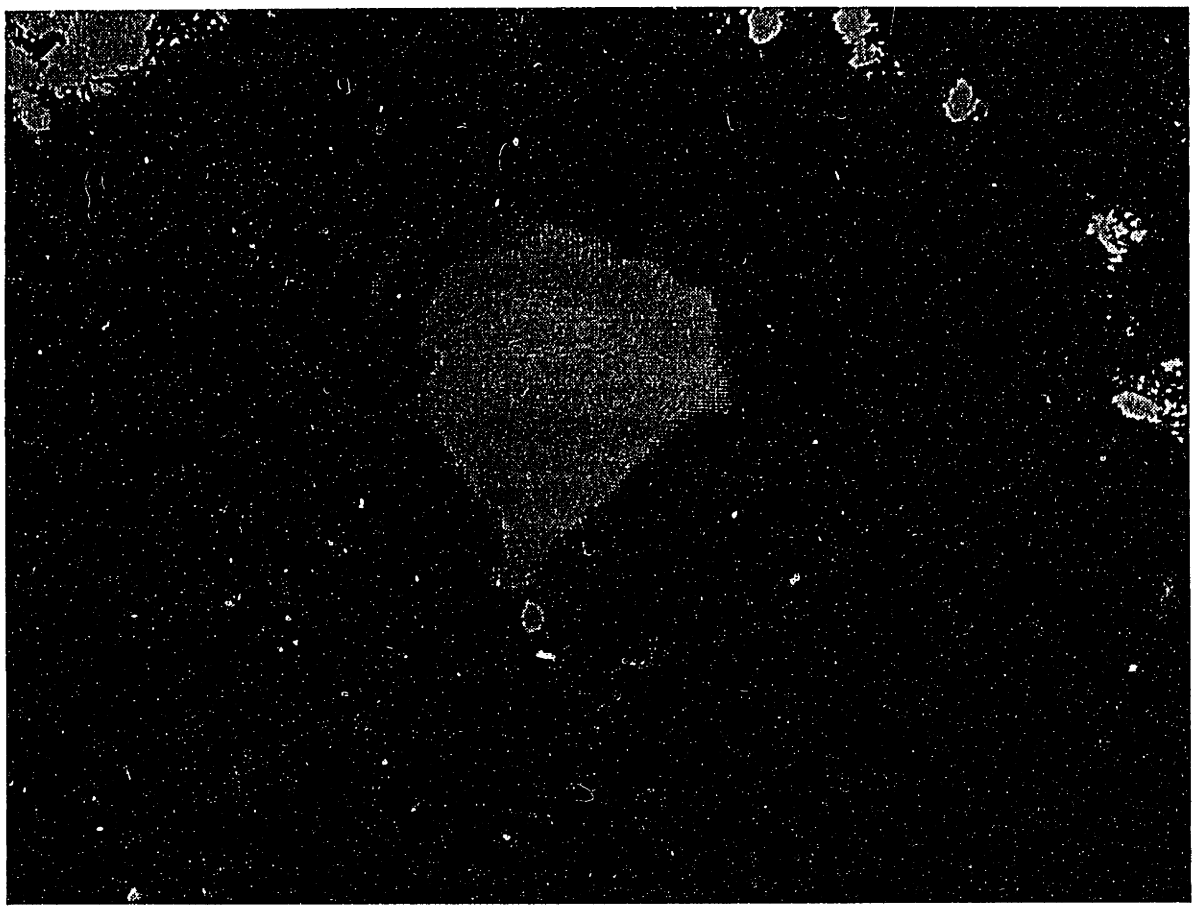

Fig. 4-2: Fluorescence image of atoms in the dark SPOT. The trapped cloud looks like a near-round bright ball. A shell around the very bright nucleus is the inner boundary of the "normally" repumped capturing region. The speckle near the edges of the picture is due to light scattering from the 5-cm diameter magnetic coils.

A more quantitative analysis of the absorption spectra showed that the difference is even more radical. The optical density of atoms in the (F = 1, reached 150! The traces are shown in Fig. 2 in Section 4.5. The loading efficiency, at the same time, is not

compromised. The counts of atoms show that ~10^{11} atoms have been confined in the dark SPOT (Fig. 3-15).

To check the model we varied the intensity of the repumping sidebands in the trapping light and measured the density of atoms. For a fair comparison the trap has to be loaded with the same number of atoms in each case. In order to do so we loaded the dark SPOT with the same number of atoms and then switched from separate repumping to repumping with an additional sideband of controlled intensity in the trapping light. The results are shown in Fig. 4-3. It is clearly seen that excessive repumping drastically reduces the atomic density due to the increased repulsion between atoms. The fact that the optimum is very close to zero sideband intensity indicates that near-optimum repumping is provided by some other source. The origin of this source, along with the other major results, is described in the Physical Review Letter appended in the Section 4.5.

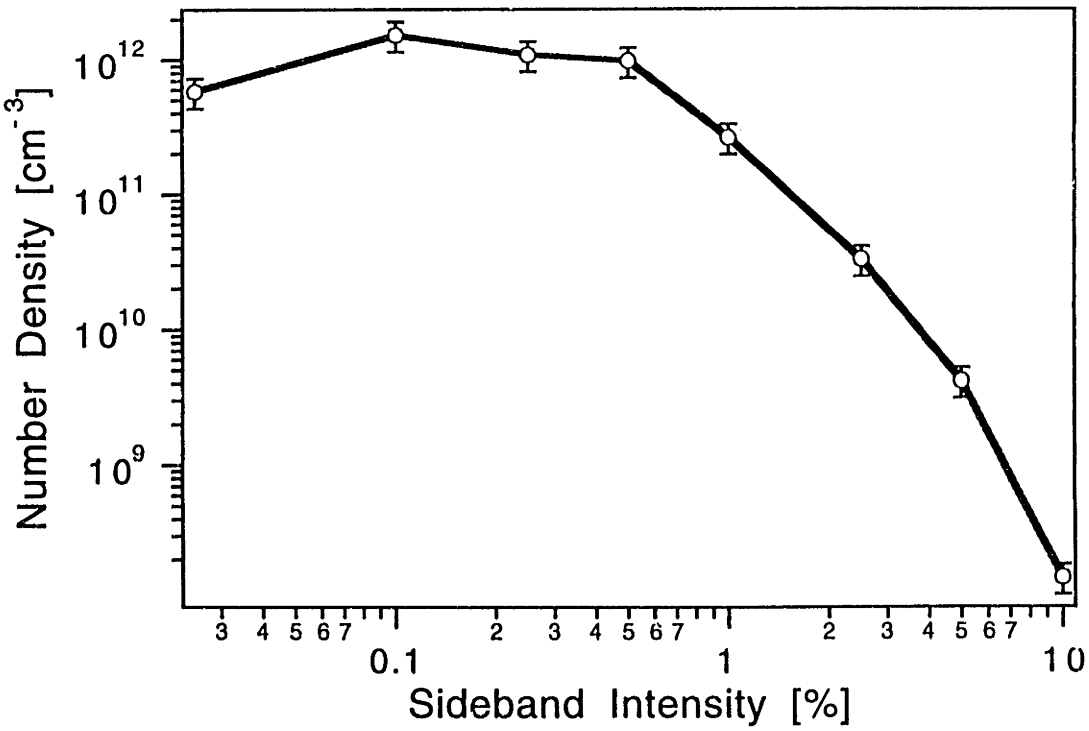

Fig. 4-3: Density of ~10^{10} atoms trapped in a dark SPOT as a function of the sidebands intensity in the trapping light.

An interesting experiment is to trap atoms in the dark SPOT at the high densities and the suddenly switch on the sideband. The switched on repumping thus turns on the repulsive forces and the cloud of atoms "explodes". The snap-shots of the "cold atomic explosion" are shown in Fig. 4-4.

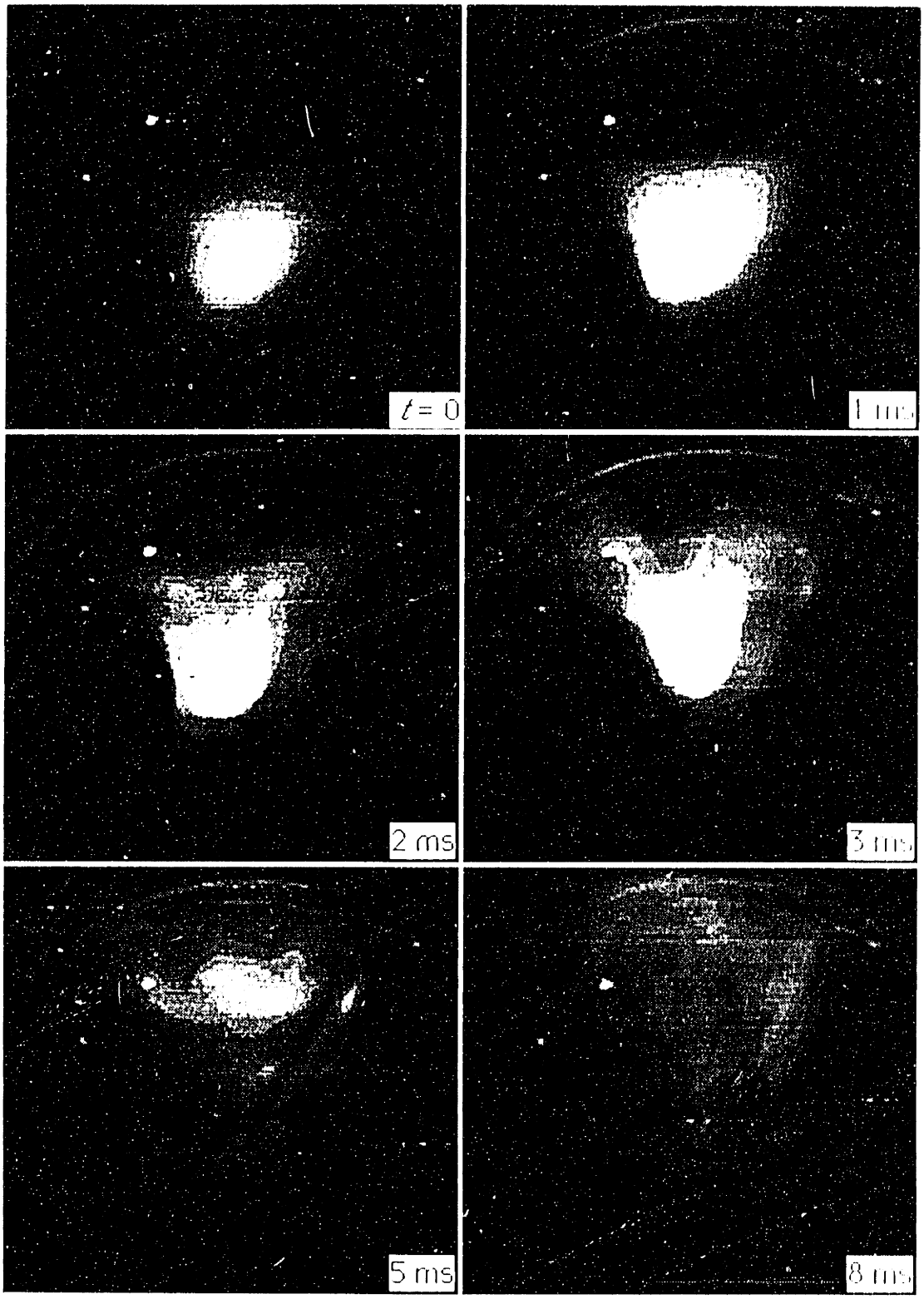

Fig. 4-4: The explosion of the cold atomic sample after the repulsive forces have been turned on. The atoms are trapped in a dark SPOT and at t=0 the repumping sideband in the trapping light is turned on. The images of the expanding cloud are taken after a variable time delay. Attenuation of the retroreflected laser beam results in the intensity imbalance and,consequently, a pushing force that makes the cloud expand in one direction.

Although the dark SPOT can confine sodium atoms at a density 100 times higher than the MOT, the same physical processes - light attenuation and optical repulsion - set the maximum limit on the atomic density. According to our model, the increase in the atomic density in the shallower trap is due to atoms hidden in the dark state. Furthermore, most of the atoms are trapped in the dark (F = 1) state with only a small fraction in the "bright" (F = 2) state: ~99% for the brightness parameter $p = 0.01$. However, as the number of atoms increases the density of atoms in the bright state increases too. Eventually, the repulsive forces become important again and start preventing the density from further increase. To verify this prediction of the model experimentally we took absorption spectra in the frequency range of transitions from this bright state (Fig. 4-5a). The optical density of atoms in this state is ~1 and is very close to the optical density of the usual MOT (Fig. 4-5b). The result indicates that the maximum density of atoms in a dark SPOT is reached when the density of the small "bright" fraction reaches the limit described in Section 4.3.

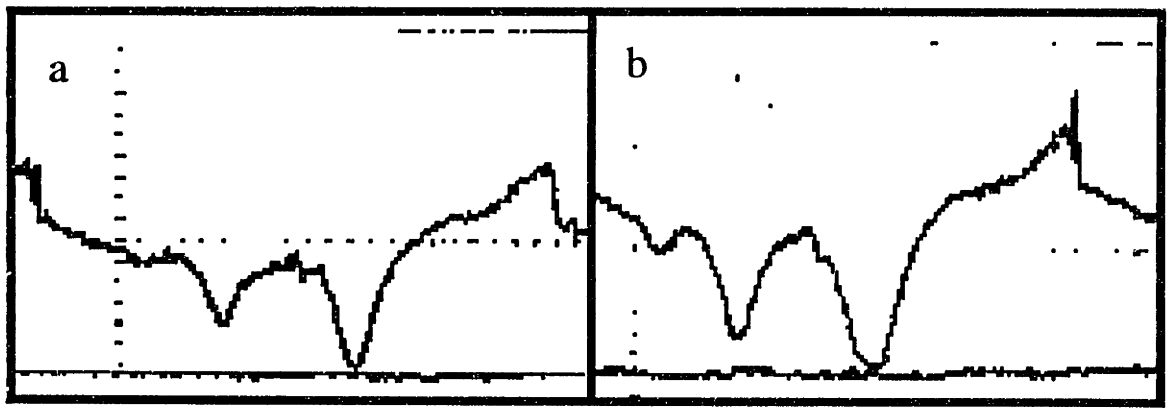

Fig. 4-5: Traces of absorption by atoms in (F=2) "bright" state. (a) "dark" trap ~2 mm in diameter; (b) "bright" MOT ~1 cm in diameter. The resolved peaks correspond to the transitions from F = 2 level to F' = 1, 2, 3 levels.

4.6. DARK SPOT PRL

Phys. Rev. Lett., **70**, 2253-2256 (1993).

High densities of cold atoms in a *dark* spontaneous-force optical trap

Wolfgang Ketterle, Kendall B. Davis, Michael A. Joffe, Alex Martin*,

and David E. Pritchard

Department of Physics and Research Laboratory of Electronics

Massachusetts Institute of Technology, Cambridge, MA 02139

Abstract

A new magneto-optical trap is demonstrated which confines atoms predominantly in a "dark" hyperfine level, that does not interact with the trapping light. This leads to much higher atomic densities as repulsive forces between atoms due to rescattered radiation are reduced and trap loss due to excited-state collisions is diminished. In such a trap, more than 10^{10} sodium atoms have been confined to densities approaching 10^{12} atoms cm^{-3}.

PACS number: 32.80.Pj

Although the original suggestion /1/ that spontaneous light forces could be used to trap atoms included several general ways to do this, the development of the magneto-optical trap (MOT) /2-4/ opened the way to the practical use of slow atoms in several different types of experiments involving cold collisions, quantum optics and atom interferometers /5/. Recently, there has been a resurgence of interest in light traps which offer the possibility of containing polarized atoms /6/ or higher density samples /7,8/. Overcoming the density limit of ~10^{11} atoms/cm^3 in a MOT may open the way to study collective effects like Bose-Einstein condensation and spin waves, and free-bound transitions in long-range molecules.

The density limit is set by two processes: firstly, by collisions between ground- and excited-state atoms in which part of the excitation energy can be transformed into kinetic energy, resulting in a trap loss rate per atom $\beta \cdot n$ with $\beta \approx (1\text{-}5) \cdot 10^{11}$ cm^3/s /9/. For densities n approaching 10^{11} atoms/cm^3, the loading time of the trap is limited to less than 1 sec. The second limit is due to repulsive forces between the atoms caused by reabsorption of scattered photons (radiation trapping) /10/. At a certain atomic density, the outward radiation pressure of the fluorescence light balances the confining forces of the trapping laser beams. Further increase of the number of trapped atoms leads to larger atom clouds, but not to higher densities. As a practical matter, the power of the rescattered light sets a limit to the *number* of atoms which can be confined in a magneto-optical trap: 10^{11} atoms scatter about 100 mW of near-resonant laser light.

In this paper, we demonstrate a dark **SP**ontaneous-force **O**ptical **T**rap ("dark SPOT"), in which all the above-mentioned limitations are mitigated by confining the atoms mainly in a ("dark") hyperfine ground state which does not interact with the trapping light. The key idea is that optimum confinement of atoms is not necessarily achieved with the maximum light force because of the limitations mentioned above. Light forces which are orders of magnitude smaller than the saturated scattering force are still strong enough to confine

atoms tightly, e.g. 1 m/s sodium atoms (corresponding to a temperature of 1 mK) can be stopped in a distance of 100 μm at 1 % saturation. All spontaneous-light-force traps realized so far have operated with close to saturated excitation, whereas our dark SPOT works at scattering rates two orders of magnitude smaller.

The simple model used to explain the density limit in a MOT /10/ is readily generalized to include a "dark" and a "bright" hyperfine ground state. The trapping force is $\vec{F}_T = - k\ p\ r\ \hat{r}$, where p denotes the probability that the atom is in the bright hyperfine state and k the spring constant of the normal MOT (i.e. for p=1). Attenuation of the trapping light and radiation trapping give rise to a density-dependent repulsive force which is quadratic in p because it involves two scattering events: $\vec{F}_R = k\ (n/n_0)\ p^2\ r\ \hat{r}$, where n_0 is a constant. From the stability criterion $|\vec{F}_T| > |\vec{F}_R|$, one obtains one limit for the maximum atom density in a MOT: $n < n_0/p$. For a very large number of atoms, the *column density* of atoms is limited by the fact that the atom cloud of diameter d has to be transparent for the trapping light /11/, i.e. $n\ d\ p < b_0$, where b_0 is a constant. Substituting $d^3 = N/n$, one obtains a second limit for n: $n < (b_0/p)^{3/2}\ N^{-1/2}$. Finally, for small p, the density is limited by the fact that volume of low-density gas at fixed temperature increases by $p^{-3/2}$ when the spring constant of confinement decreases p times. This results in a third limit to the atomic density: $n < N\ p^{3/2} / d_0^3$ (d_0 is the cloud diameter in a standard MOT for low N). The constants n_0, b_0 and d_0 depend on experimental parameters and are typically $5 \cdot 10^{10}$ cm^{-3}, $5 \cdot 10^9$ cm^{-2} and 200 μm /10/.

In a simplified model, the atom density in a MOT is the largest value compatible with the three limits as shown in Fig. 1. The value of p which maximizes density depends on N and is smaller for larger N. The Stanford group /12/ and our group have recently succeeded in trapping more than 10^{10} atoms in a normal MOT. For such an N, the predicted optimum p of ~0.01 corresponds to a density increase of more than two orders of magnitude over the normal MOT (Fig. 1).

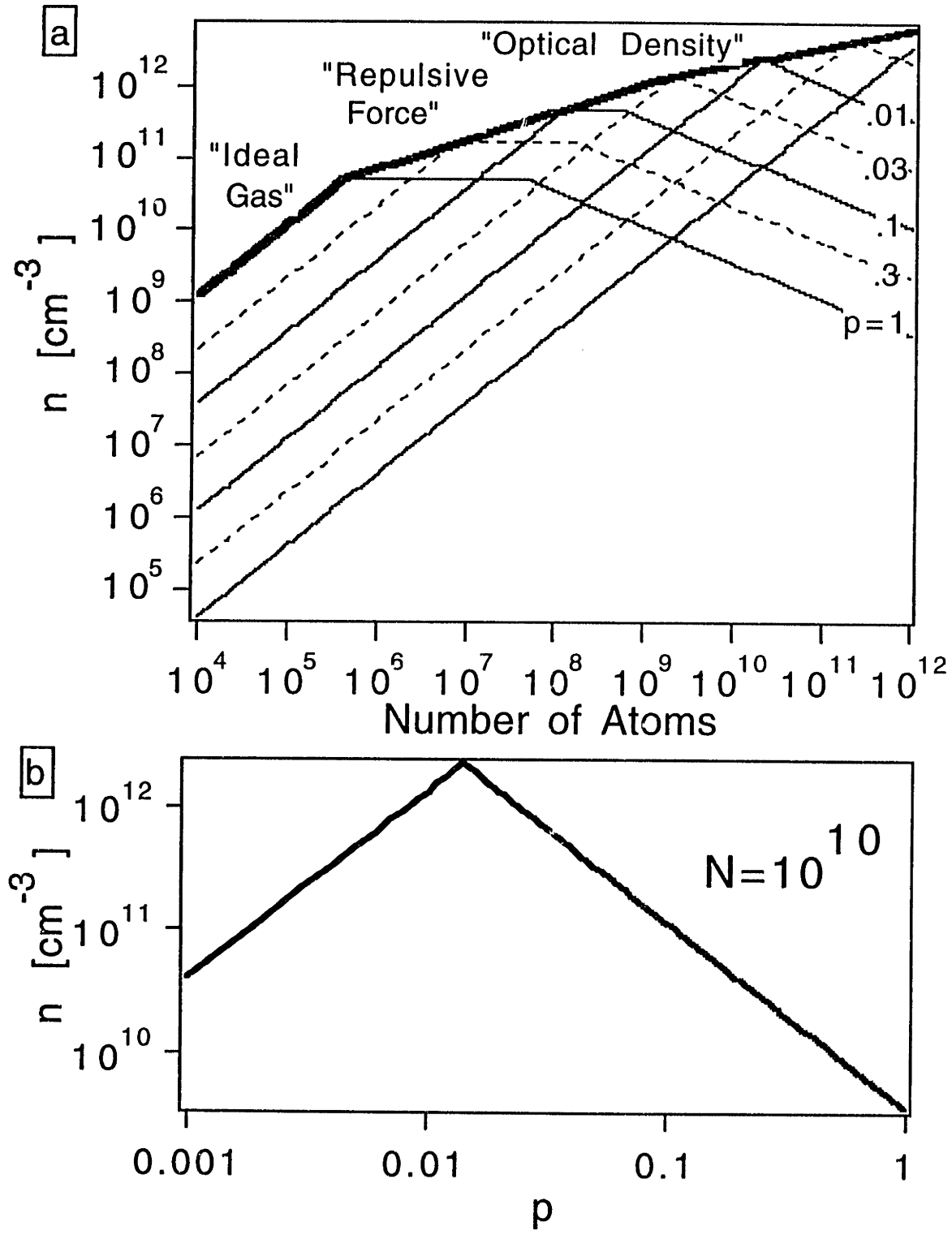

Fig. 1 (a)Atomic densities n vs. number N of trapped atoms for different values of the fractional population p of the "bright" hyperfine state. The thick line shows the highest density obtainable with an optimum value of p. For large N, this density is much higher than the one obtained in the normal MOT (p=1). For 10^{10} trapped atoms (b), the optimum trap is a hundred times "darker" than the normal MOT, resulting in more than two orders of magnitude increase in density.

In the case of sodium, the bright and dark hyperfine states are the F=2 and F=1 hyperfine levels of the $3S_{1/2}$ ground state, respectively. Spontaneous light forces are applied using the cycling F=2→F'=3 transition to the excited $3P_{3/2}$ state. Due to non-resonant excitation of the 2→2 transition, atoms are optically pumped into the F=1 ground state via a spontaneous Raman process. In all optical cooling and trapping experiments it has been necessary therefore to add repumping light resonant with the 1→2 transition to pump atoms back to the F=2 state. Usually, the intensity of the repumping light has been high enough to keep the atoms mostly in F=2. In a dark SPOT with p=0.01, the atoms spend most of their time (~99 %) in F=1; this is accomplished by appropriately reducing the intensity of the repumping light.

Although a small excitation rate is superior for confining large numbers of atoms at high density, the maximum possible excitation rate is necessary to efficiently capture atoms from a thermal background or a slow atom beam, and load them into the trap. Therefore, a dark SPOT requires a "bright" capturing region which is separated from the dark trap spatially or temporally. In the bright region, the sodium atoms are mainly in the F=2 level and experience the maximum light force. The temporal separation is accomplished by loading atoms into a normal MOT and then switching to a dark trap, and will be discussed later. Spatial separation is superior since it allows continuous loading of atoms into a dark trap. This was accomplished by using a normal MOT and applying only weak or no repumping light to the center of the trap ("a MOT with a dark spot").

In our experimental setup, a crucial part was a slow-atom source employing an increasing-field Zeeman slower /13/ capable of producing $>10^{12}$ sodium atoms/s at 100 m/s and ~10^{11} atoms/s at 30 m/s /14/. With this slower, $\geq 10^{10}$ atoms/s could be loaded into our MOT. The trap consisted of three orthogonal retro-reflected beams with diameters of ~3 cm and intensities of ~10 mW/cm^2 per beam. The frequency was tuned to the red of the 2→3 transition by 15-25 MHz. All beams were circularly polarized with helicities appropriate for magneto-optical trapping; they intersected at the center of a

quadrupole magnetic field with a gradient of 10 - 15 G/cm. Repumping light close to resonance with the $1 \rightarrow 2$ transition was passed through a glass plate with a black dot, which was imaged into the trap center with an image size of ~10 mm. With a second similar repumping beam (diameter 3 cm, intensity 3 mW/cm^2) at an angle of ~20 degrees to the first, the whole trapping region was efficiently repumped except for the center, where the dark regions of the two beams intersected.

Additional repumping light could be added to the trapping laser beams by means of an electro-optical modulator (EOM) operated at 1.71 GHz. With EOM sidebands of variable intensity, p could be smoothly varied between a value p_{min} and ~1. p_{min} was determined by two processes: (i) stray light from the repumping beams scattered by windows and the atomic beam and, (ii) spontaneous Raman transitions induced by the trapping light. With an estimated rate of $\sim 10^3\ s^{-1}$, the Raman process alone should cause ~0.1 % equilibrium population in F=2. As it turned out that p_{min} was close to the optimum value of p (see Fig. 1), most of the experiments were done without EOM sidebands.

In a normal MOT we observed a cloud of atoms ~1 cm in diameter containing roughly 10^{10} atoms. In a dark SPOT, one could clearly see a dark central region in the fluorescence of the thermal beam corresponding to the dark spots in the repumping beams. In the center was a compact ball of trapped atoms (2-4 mm in diameter) with an apparent brightness lower than the normal MOT, but still much brighter than the background fluorescence.

The density in the dark SPOT was determined by absorption spectroscopy using a weak probe beam with an intensity of ~1 $\mu W/cm^2$ and a photodiode. The probe laser beam was split off the trapping or repumping light and could be scanned by ± 120 MHz with two acousto-optic modulators. Fig. 2 shows an absorption spectrum of the trapped atoms. As at the highest densities the excited state hyperfine structure could no longer be

resolved, optical densities were deduced by fitting a theoretical spectrum to the one observed. The diameter of the cloud of trapped atoms was determined by imaging the fluorescence onto a CCD camera or by recording spatially resolved absorption giving the same result.

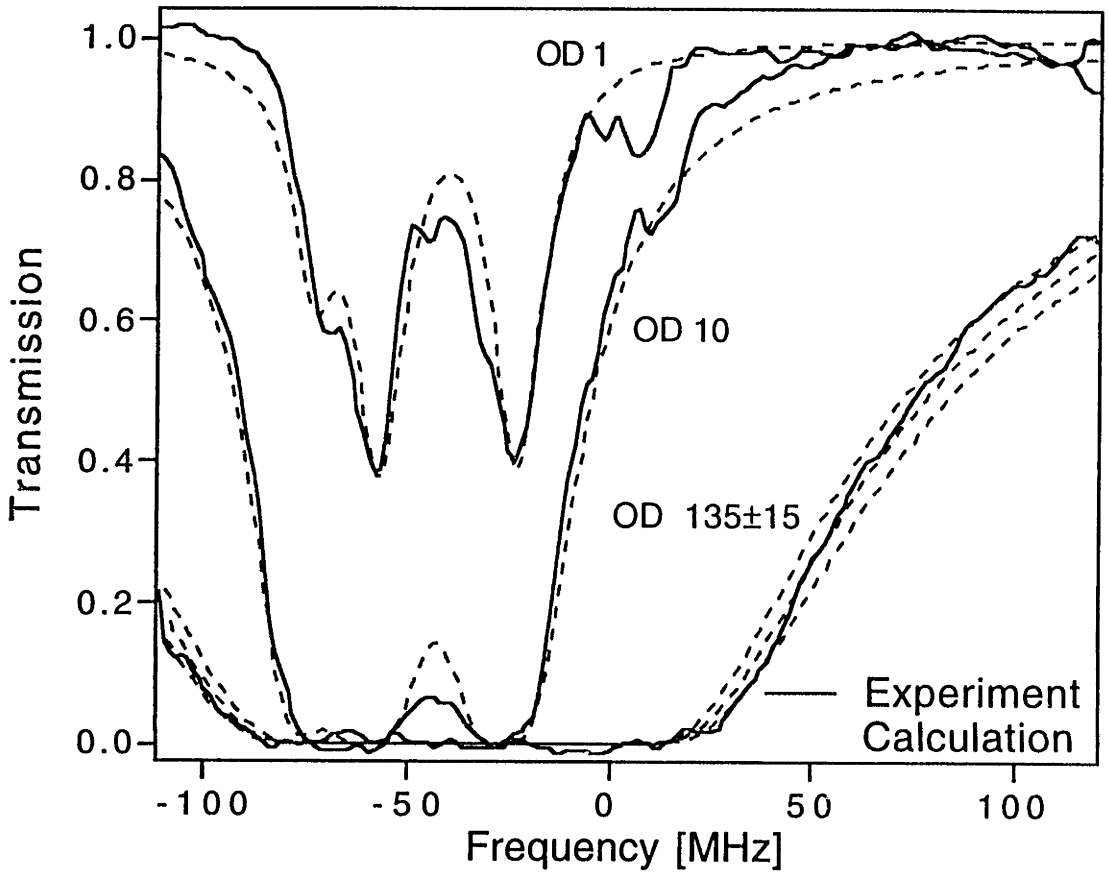

Fig. 2 Absorption spectrum of a 4 mm diameter cloud of sodium atoms trapped in a dark SPOT. The best fit yields an optical density (OD) of 135 which corresponds to an atomic density of $7 \cdot 10^{11}$ cm^{-3} and ~$5 \cdot 10^{10}$ trapped atoms. Traces with lower OD were recorded with a reduced number of atoms. The dashed lines are calculated spectra for OD = 1, 10, 120, 135, and 150, respectively.

An independent determination of the number of trapped atoms was performed by switching off the trapping and repumping beams and rapidly switching on a strong probe laser beam (diameter 10 mm, 0.5 mW/cm^2) close to resonance with F=1 atoms, optically pumping them into the F=2 state. From the transient absorption signal, the number of

absorbed photons was obtained. This number, divided by the number q of photons needed to optically pump one atom, gives directly the number of atoms in the trap. q was obtained from a knowledge of the matrix elements and a simple model of radiation trapping. The number of trapped atoms deduced should be accurate to within a factor of two.

The highest density was observed for a (3.0 ± 0.5) mm cloud of atoms with an optical density of 110 ± 10 implying a density $n = (8 \pm 2) \cdot 10^{11}$ cm^{-3}. Another (less accurate) value for n derived from the number of atoms $N = 1.5 \cdot 10^{10}$ and the diameter agreed to within 30 %. In slightly larger clouds, optical densities up to 160 and $5 \cdot 10^{10}$ trapped atoms were observed. This combination of number and density is unprecedented in light traps: Slightly smaller densities have been reported to date only for at least 100 times fewer atoms /3,7,10,15/. A similar number of atoms has been trapped by light forces only at densities 20 times lower /12/. In some of the previous work, large detunings were used /12,15,16/ to reduce the reabsorption of scattered photons. This and other ways to affect n_0, b_0 and d_0 may eventually be combined with our approach of reduced repumping to achieve even higher densities.

The maximum optical density (~2) observed when probing atoms in the bright state (F=2) was only about two times smaller than the value obtained in a bright MOT for the same experimental parameters (except for the dark spot in the repumping light). This shows that eventually the dark SPOT has similar limitations as the normal MOT, but at much higher densities. The direct comparison between dark SPOT and bright MOT showed a density ratio of about ~100 in agreement with Fig. 1. The temperature of the trapped atoms was determined by switching off the trapping light and recording the decay of the absorption signal. The temperature of (1.2 ± 0.5) mK is in agreement with the prediction of ~0.8 mK for Doppler molasses /17/ at the detuning and laser intensities used. Trap-loading and decay times were one to two seconds and limited by collisions with the thermal atomic beam rather than with residual gas at a pressure of 10^{-9} Torr. The long

trapping time clearly demonstrates the reduced trap loss by excited-state collisions in a dark SPOT since extrapolating trap losses observed in a normal MOT /9/ to our densities implies trapping times of only ~50 ms!

The repumping of the trapped atoms was mainly due to light scattered from the repumping beams into the "dark" trapping region. An absorption spectrum for F=2 atoms showed that about one percent of the atoms were in F=2, close to the optimum p predicted for $\sim 10^{10}$ trapped atoms. To vary the population in F=2, we switched off the repumping light and switched on EOM generated sidebands of the trapping light with variable intensity. In agreement with the prediction of Fig. 1, a maximum in atomic density was found for a sideband intensity of about 0.1 %. The traps with very weak repumping showed larger trap loss, probably due to the smaller potential-well depth and therefore increased radiative escape rate /18/. (Since the trapped atoms are mainly in the lowest hyperfine state (F=1), inelastic hyperfine-changing collisions cannot account for the extra loss rate observed). When atoms were loaded into a normal MOT and the intensity of the repumping light was rapidly decreased, a considerable increase in density was observed ("temporal" separation between bright capturing and dark trapping). However, the densities thus obtained were 30 % lower than those achieved by loading directly into a dark trap. The probable reason is larger trap loss during the loading phase due to both collisions and leakage of atoms out of the trap because of imperfect beam profile(one could clearly see rays of atoms leading out of the bright trap). It should be noted that the trap works even without any repumping light at all - sufficient repumping is provided by spontaneous Raman scattering of the trapping light. This offers an alternative explanation for the trapping of Rb in a MOT without repumping light reported recently /19/.

The realization of a dark SPOT for other alkali atoms seems rather straightforward. In Cs (or Rb) the atom cycles many times on the bright transition before it falls into the dark F=3 state due to the very large hyperfine splittings. This cycling time could be shortened

by using weak additional "depumping" light in resonance with the $4 \rightarrow 3$ or $4 \rightarrow 4$ transitions. The smaller rate of spontaneous Raman repumping might allow observation of trapping in a square well potential (*bounce trap*), where the atoms move freely in the central (non-repumped) region of the trap (having $p \approx 0$) and are reflected at the boundary with the outer (repumped) region. For very weak repumping the transition from the usual case of strong overdamping (damping rate α >> oscillation frequency ω) to the oscillatory regime could be observed because $\alpha \propto p$ and $\omega \propto \sqrt{p}$. Generally, it appears that a larger hyperfine splitting is advantageous for the dark SPOT because off-resonant optical pumping processes are less important and the dwell times of the atom in the bright and dark state can be controlled independently by applying additional laser frequencies.

The high densities achieved in a dark SPOT are promising for the study of cold collisions and for the observation of evaporative cooling after transferring the atoms into a magnetic trap. At densities of 10^{12} cm^{-3}, the estimated elastic collision rate is already 100 s^{-1}, much larger than the trap loss rate due to collisions with the background gas.

The dark SPOT is the first cooling and trapping scheme in which the repumping light is intentionally reduced to "shelve" the atoms, i.e. cooling and trapping forces are only exerted on a small fraction of the atoms, while most of the atoms are kept in the dark thus avoiding strong absorption of the cooling light. This concept should allow polarization-gradient cooling ot trapped atoms below increased ultimate temperatures observed at high atomic densities /15/. Another possibility for realizing a dark trap would be repumping on the $1 \rightarrow 1$ transition of the D_1 line with elliptically polarized light. This transition has a coherent dark state only for magnetic fields B=0 /20/ which inhibits repumping in the center of the trap. Recently, a new scheme in velocity-selective coherent population trapping (VSCPT) has been suggested which, in addition to the momentum diffusion process, features a weak damping force towards low velocities /21/. A simple way of combining strong damping and VSCPT would be the use of polarization-gradient molasses acting on the bright hyperfine state together with a velocity-selective repumping

scheme. Alternatively, polarized cold atoms could be obtained by using a repumping scheme which does not repump atoms from a certain m_F level (e.g. σ^+ light and a 1-1 transition). This could be implemented in the recently demonstrated vortex-force trap which confines polarized atoms at non-vanishing magnetic field /6/. Finally, a tapered two-dimensional version of the dark SPOT, a dark funnel /22/, should allow the compression of intense slow atomic beams to unprecedented brightness.

In conclusion, we have demonstrated a dark spontaneous-force optical trap, which confines atoms predominantly (~99 %) in a dark hyperfine ground state. In this way, limitations of the normal magneto-optical trap have been overcome and densities close to 10^{12} cm^{-3} for more than 10^{10} trapped atoms have been achieved.

We would like to acknowledge experimental assistance from M. Mewes. This work was supported by ONR and AFOSR through contract N00014-90-J-1642, and by NSF grant #8921769-PHY. W.K. and A.M. would like to acknowledge fellowships from the NATO Science Committee and DAAD, Germany, and from the D.G.I.C.Y.T., Spain, respectively.

References

* On leave from: Instituto de Optica, C.S.I.C., Madrid.

1. D.E. Pritchard et al., Phys. Rev. Lett. 57, 310 (1986).

2. D.E. Pritchard and E.L. Raab, in "Advances in Laser Science II", ed. M. Lapp, W.C. Stwalley, and G.A. Kenney-Wallace (AIP, New York, 1987) p. 329.

3. E.L. Raab et al., Phys. Rev. Lett. 59, 2631 (1987).

4. C. Monroe, W. Swann, H. Robinson, and C. Wieman, Phys. Rev. Lett. 65, 1571 (1990).

5. Proceedings of the Varenna Summer School on "Laser Manipulation of Atoms and Ions", ed. E. Arimondo and W.D. Phillips (North-Holland, Amsterdam) in press.

6. T. Walker, P. Feng, D. Hoffmann, and R.S. Williamson, III, Phys. Rev. Lett. 69, 2168 (1992).

7. O. Emile, F. Bardou, and C. Salomon, to be published.

8. W.D. Phillips, in Ref. 5; D.J. Heinzen, J.D. Miller, and R.A. Cline, 13th International Conference on Atomic Physics 1992, Munich, Book of Abstracts, Paper C4.

9. M. Prentiss et al., Opt. Lett. 13, 452 (1988); L. Marcassa et al., to be published.

10. T. Walker, D. Sesko, and C. Wieman, Phys. Rev. Lett. 64, 408 (1990).

11. K. Lindquist, M. Stephens, and C. Wieman, Phys. Rev. A 46, 4082 (1992).

12. K.E. Gibble, S. Kasapi, and S. Chu, Opt. Lett. 17, 526 (1992).

13. T.E. Barrett, S.W. Dapore-Schwartz, M.D. Ray and G.P. Lafyatis, Phys. Rev. Lett. 67, 3483 (1991).

14. M.A. Joffe, W. Ketterle, A. Martin, and D.E. Pritchard, 13th International Conference on Atomic Physics 1992, Munich, Book of Abstracts, Paper C9 .

15. A. Clairon et al., Proc. of the 4th European Time and Frequency Forum, J.J. Hunt ed. (1992).

16. E.A. Cornell and C.R. Monroe (private communication).

17. P.D Lett et al., J. Opt. Soc. Am. B 6, 2084 (1989).

18. P. Julienneet al., Phys. Rev. A 6, 2084 (1989).

19. P. Kohns et al., IQEC '92, Vienna, Technical Digest, p. 258.

20. A.M. Tumaikin and V.I. Yudin, Sov. Phys. JETP 71, 43 (1990).

21. F. Mauri and E. Arimondo, Europhys. Lett. 16, 717 (1991).

22. E. Riis, D.S. Weiss, K.A. Moler, and S. Chu, Phys. Rev. Lett. 64, 1658 (1990); J. Nellessen, J. Werner, and W. Ertmer, Opt. Comm. 78, 300 (1990).

Most of the things worth doing in the world
had been declared impossible before they were done.
— Louis D. Brandeis

5. DARK OPTICAL MOLASSES

5.1. GENERAL

Atoms in the magneto-optical trap or the dark SPOT are cooled by the built-in Doppler cooling mechanism: preferential absorption of red-detuned photons from a counterpropagating laser beam slows atoms down. When diffusion in velocity space arising from stochastic spontaneous-photon recoils (heating) balances the cooling the trapped sample reaches a limiting temperature. This Doppler cooling temperature T_D depends on the intensity and the detuning of the cooling light. The minimum temperature is given by:

$$k_B T_D = \frac{\hbar\Gamma}{2}, \tag{5.1}$$

where Γ is the spontaneous decay rate is achieved for low intensity and the red detuning equal to half the linewidth. For sodium $T_D = 240\ \mu K$.

Fortunately, atoms can be laser-cooled to much lower temperatures. The effect was first observed in [LWW88] and explained in [DAC89, UWR89].

5.2. SUB-DOPPLER POLARIZATION-GRADIENT COOLING

An approach to a very complicated fully three-dimensional treatment of sub-Doppler cooling has been made in [MOL91], but even the one-dimensional models [DAC89] adequately describe the experimental results. The physical effects behind these cooling schemes are subtle, so the complete treatments, even of the 1D cases, are highly mathematical, so I will provide here only the qualitative ideas .

The described sub-Doppler laser cooling mechanisms arise from interaction of the moving multi-level atom with light with space-varying polarization, which gives rise to the name: polarization-gradient cooling. Two distinctly different one-dimensional damping mechanisms have been identified: ellipticity-gradient and polarization-rotation cooling.

5.2.1. Ellipticity-Gradient Cooling

In this first case an atom is illuminated by two counterpropagating laser beams with orthogonal linear polarizations. In this case, the so-called linear-perpendicular-linear configuration, the local polarization along the beams changes in a distance of $\lambda/2$ from linear through elliptical to σ^+, to elliptical, to linear, to σ^-, to elliptical, to linear of the opposite phase (Fig. 5-1).

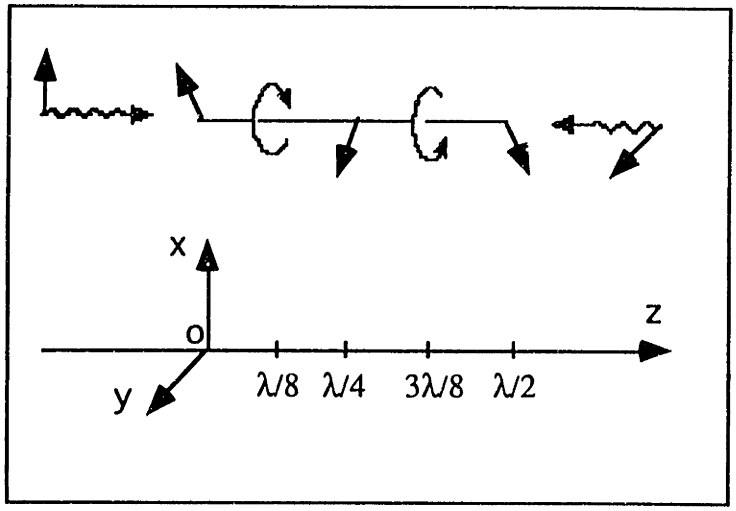

Fig. 5-1: The *Lin⊥Lin* configuration exhibits strong polarization gradients.

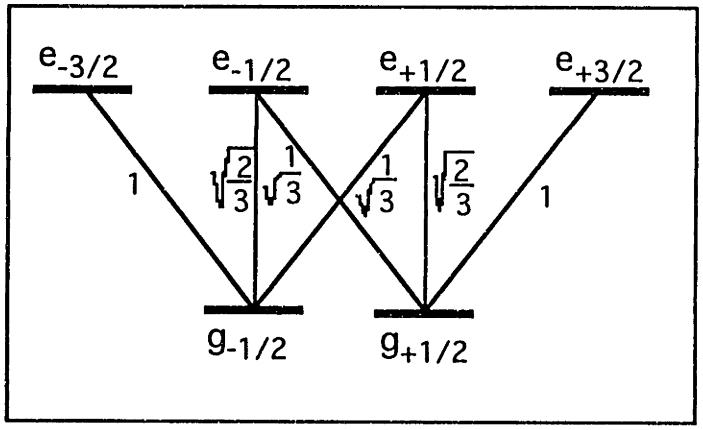

Fig. 5-2: Clebsch-Gordan Coefficients for a $J = \frac{1}{2} \rightarrow J' = \frac{3}{2}$ transition.

If an atom at rest has an appropriate level structure (e.g. $J = \frac{1}{2} \rightarrow J' = \frac{3}{2}$ optical transition) (Fig. 5-2) it is optically pumped into a distribution of m-states that depends on the local (spatially varying) polarization. Also, intense light removes the degeneracy of the Zeeman sublevels and introduces spatially varying light shifts. The light shifts depend on the Clebsch-Gordan coefficients (Fig. 5-3) and the polarization of light and, consequently, are different for different m-states. The moving atom in a certain m-state would climb the hills and descend into the valleys of the modulated potential without any energy loss. However, it turns out that for finite velocity the optical pumping rates, the energy levels and the local polarizations conspire to make the atom climb the hills more

than descend (Fig. 5-3). The cooling mechanism is called Sisyphus cooling after the mythological Greek king.

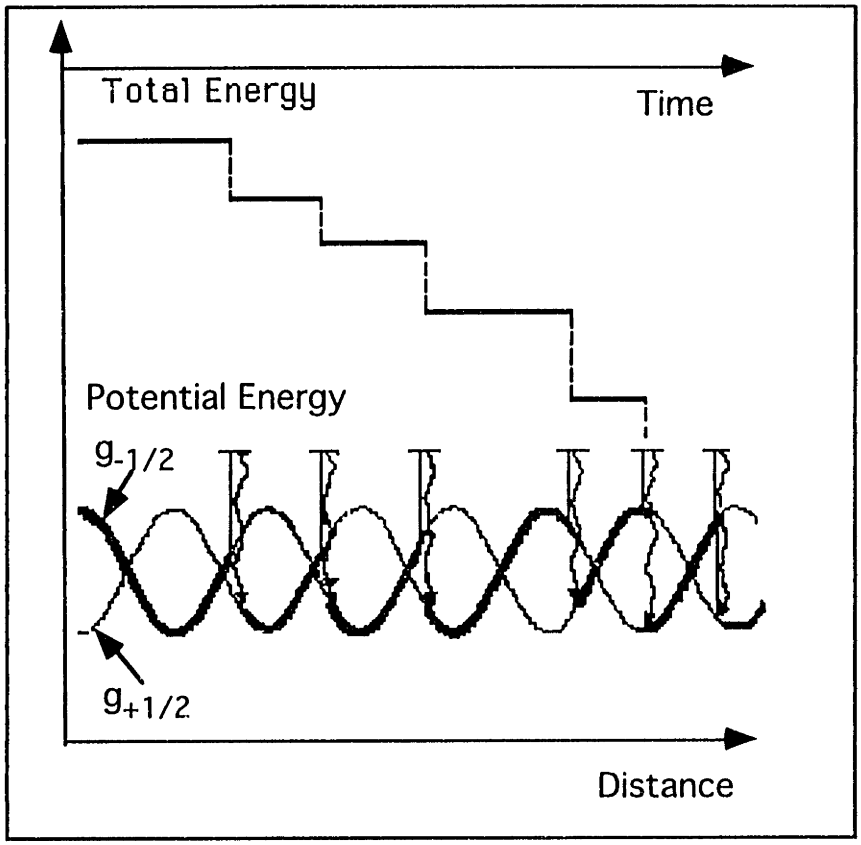

Fig. 5-3: Sisyphus Cooling effect for a moving atom. The spatially varying light shifts $E_{\pm}$ of the ground $|g_{\pm\frac{1}{2}}\rangle$ levels are induced by the red ($\delta < 0$) detuned cooling light. Because of the strong correlation between the spatial dependencies of light shifts and optical pumping rates, the atom loses potential energy when it is optically pumped from one sublevel to the other. The atom loses its kinetic energy when it climbs the hills of the potential (thick lines).

5.2.2. Polarization-Rotation Cooling

The second one-dimensional case of polarization-gradient cooling is the one with two counterpropagating waves with orthogonal circular polarization. This $\sigma^+ - \sigma^-$ configuration produces at every point a linear local polarization, whose direction rotates like in a corkscrew with a pitch of λ. A stationary atom with $J \geq 1$ (e.g. $J = 1 \rightarrow J' = 2$ optical transition) is optically pumped into a distribution of ground m-states such that there is alignment (different populations for states with different $|m|$ along the

polarization axis) but no orientation (no difference between the positive and negative m-state populations). When an atom starts moving along the laser-beam axis an orientation along this axis starts to develop, because the pumping rates have different velocity dependence for different m-states. Furthermore, the population asymmetry happens to be such that atoms in the most populated state absorb light most strongly from the circularly polarized beam opposing its direction of motion. This asymmetry of absorption accounts for the damping.

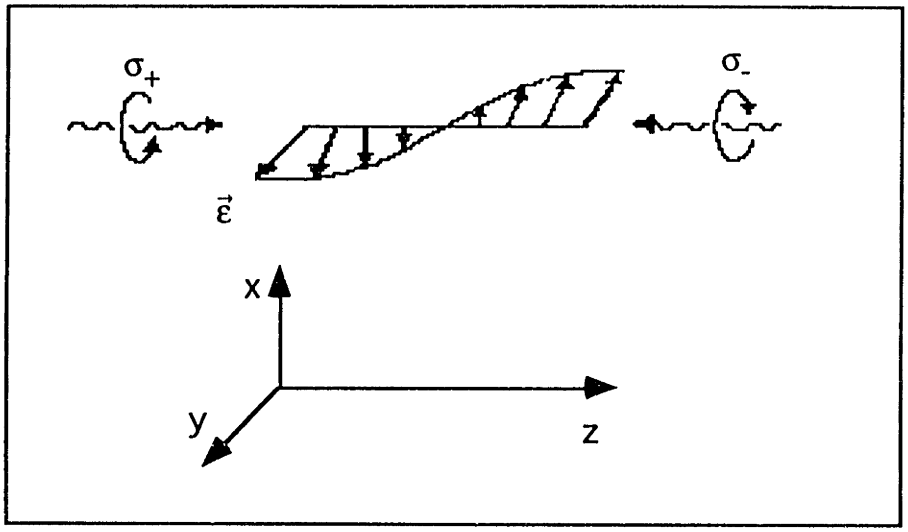

Fig. 5-4: In the $\sigma^+ - \sigma^-$ configuration the locus of the end of the polarization vector is a helix with a pitch λ.

5.2.3. Polarization-Gradient Cooling in 3D

The simple-minded approach to three-dimensional cooling is to overlap typically three orthogonal pairs of laser beams with *lin⊥lin* or $\sigma^+ - \sigma^-$ polarizations near one point, hoping that each direction of three is cooled independently. The polarization-gradient cooling in three dimensions actually works in semi-qualitative agreement with the 1D model [CSG91]. This agreement is somewhat surprising if one takes into consideration the fact that in 3D different polarizations are scrambled, because of polarized beams coming from different directions. It is hard to distinguish in this case between the

ellipticity gradient and the polarization-rotation cooling mechanisms and probably both are at work. A theoretical calculation for the 3D case has been performed in [MOL91]. Experiments on polarization-gradient cooling have been carried out with sodium, cesium and rubidium. Sodium atoms were cooled by the three-dimensional polarization-gradient molasses to temperatures ~25 μK [LPR89].

5.3. Problems With High Densities

Because polarization-gradient cooling is so efficient it is desirable to use it to cool atoms at high densities, for example in a trap. Unfortunately, straightforward implementation of this technique is not possible. The first reason is that the method works only in zero magnetic field, which is not the case in a trap. The second reason is that high density of the cooled atoms adversly effects the polarization-gradient molasses, similar to negative effect on the MOT, discribed in Chapter 4.

Most of the experimental effort to-date has been devoted to studying the mechanism of cooling itself [WRS89, LPR89, MSR90, SDP90, CSG91], with much gentler conditions than in our light trap. For this reason the parameters of the cooled sample (size, density, number of atoms) were chosen to allow for the best performance of optical molasses. For one thing, when optical molasses is loaded from a slow beam or a vapor cell, the maximum density of viscously confined atoms is many orders of magnitude lower (~10^6 cm^{-3} [CHB85]) than in our light trap (~10^{12} cm^{-3}). Sesko *et al.* have observed that the temperature of atoms in the trap increases with the number of atoms and speculated that the heating is due to radiation trapping [SWW91]. In a magneto-optical trap (MOT) the magnetic fields deteriorate the performance of polarization-gradient cooling which work best in zero field. Sub-Doppler temperatures have been observed in a MOT but only for small traps containing a small number of atoms [STF91].

It has long been expected [PRI83] that high densities of atoms will impede the efficiency of laser cooling. Optical-density effects such as radiation trapping and attenuation of cooling light, collisions between atoms and associated line-broadening all are expected to result in longer damping time and higher ultimate temperature. To our knowledge there has been only one report on the attempt to apply polarization-gradient molasses to a high-density sample of atoms: [CLN92].

In those experiments [CLN92] the optical molasses was loaded from the MOT by rapidly switching off the field gradients. The authors report that $3 \cdot 10^8$ Cs atoms were trapped in a cloud with a "radius of about 1 mm in diameter". Assuming that they actually mean 1 mm diameter it corresponds to a density of $6 \cdot 10^{11}$ cm^{-3}. At this densities the authors measured the thermalization time of 10 to 50 ms, which is 100 to 1000 times the expected typical cooling time $\tau_\alpha = M / 2\alpha$ [LPR89, CSG91], where α is the damping factor given by the cooling force $\vec{F} = -\alpha\vec{v}$. The authors attribute this anomalously long time to interatomic interactions and find a dependence of the damping time on the initial density (Fig. 3 in [CLN92]). However, on the figure cited as evidence for this temperature is plotted vs. time for different light intensities, not atom densities. The optical molasses was loaded from a MOT, but there is no reassurance given that the molasses was loaded to equal density for all the runs. Furthermore, if the MOT's laser beams intensity was changed, changes of the initial density in molasses would be expected. Thus, it is pretty difficult to interpret the results in an unambiguous way.

Another important question is what final temperature was achieved with polarization-gradient molasses at high densities. The authors report that at high detunings the minimum temperature (2.5 μK) is quite similar to the previous results. But since this temperature was measured after the molasses had been allowed to decay for awhile, it is not clear at what density this very low temperature has been achieved.

However, confusing and incomplete, this is the only piece of experimental evidence indicating that conventional optical molasses does not work as well at high atomic densities of atoms as it does at low densities.

5.4. SOLUTION: DARK COOLING

In order to cool sodium atoms efficiently at high densities with polarization-gradient molasses, we employ the same idea of shelving atoms in the dark hyperfine state used in the dark SPOT. The polarization-gradient scheme operates on the ($F = 2 \rightarrow F' = 3$) transition. When only little repumping light is provided, the majority of atoms are in the F = 1 ground state and are far-detuned from the cooling light. Consequently, the destructive effects of high atomic density on the cooling mechanisms are avoided. However, due to (weak) repumping light present the atoms are ocasionally recycled to the F =2 state where they experience the cooling force.

In our experiment we use the same configuration of light for trapping and polarization-gradient cooling. In order to reload atoms accumulated in the dark SPOT into the molasses we rapidly (< 1 ms) switch off the magnetic fields. The minimum temperature achieved by polarization gradient cooling has been shown to increase with the laser intensity [LPR89]. However, in our experiments we did not see any improvement when we simulteneously with switching off the magnetic field attenuated the intensity of the circularly polarized laser beams. Since there is no more bright fluorescence present from the outer shell of the dark SPOT, there is not enough Raman scattering to provide repumping any more. Therefore, after we load the molasses, we add to it repumping light with variable intensity.

5.5. EXPERIMENTAL RESULTS

The polarization-gradient cooling has a very visible effect on the trapped sample. If the atoms are released from the dark SPOT and probed with resonant light after ~50 ms of

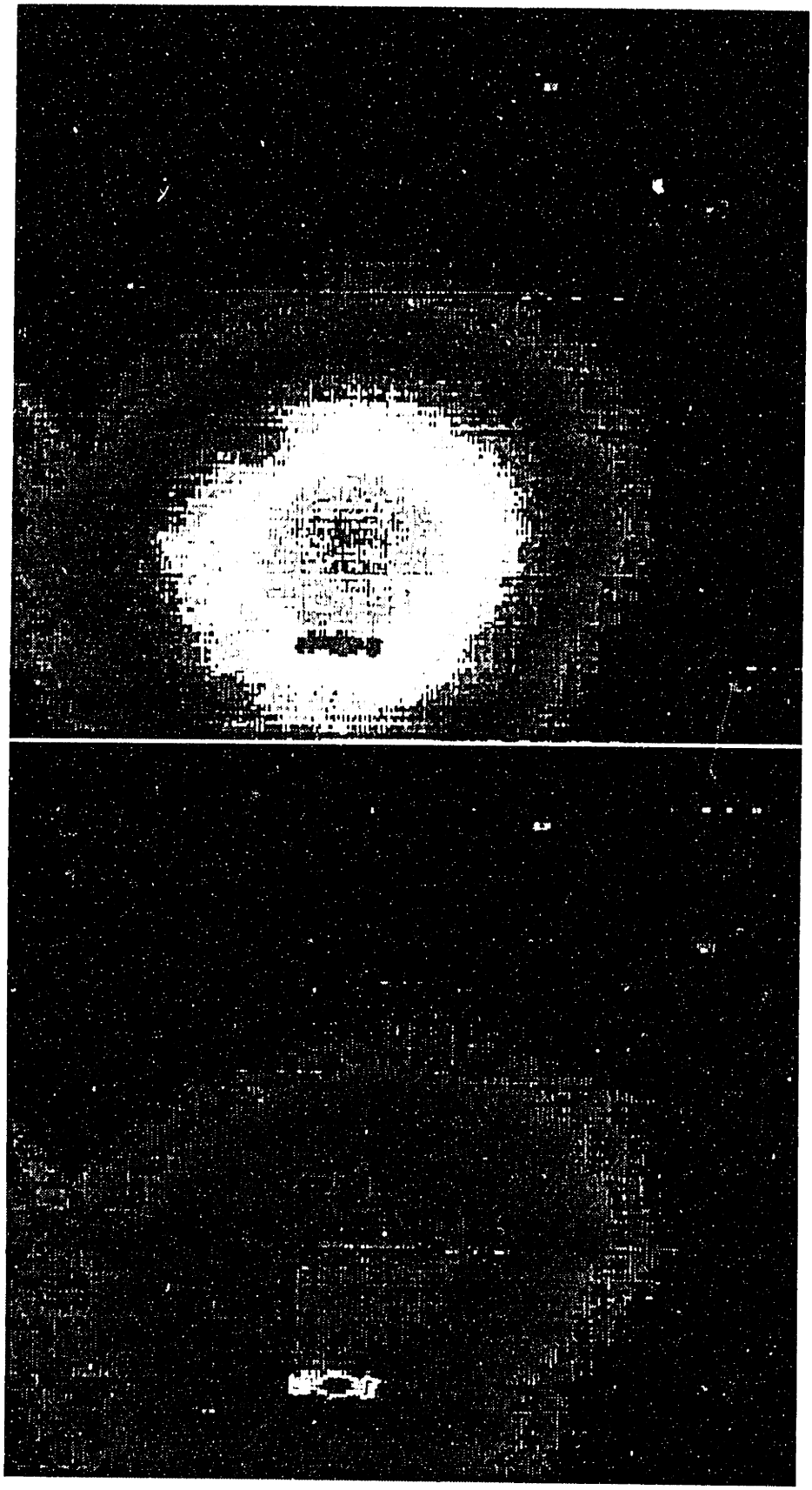

Fig. 5-5: Fluorescence images of atoms released from the dark SPOT after 50 ms of free expansion with molasses cooling for ~10 ms (top) and without cooling (bottom)

ballistic expansion, hardly any fluorescence can be seen on the TV monitor: the atoms are gone. However, if cooling with molasses is performed on the atoms for ~10 ms after the atoms are released, the fluorescence from the probe is much brighter, as shown on Fig. 5-5.

5.5.1. Optimization Procedure

Imaging of the cloud provides a very sensitive means of optimizing the dark-polarization gradient molasses. When the trap is switched off and the cooling light is turned on one can see even with the naked eye the decaying fluorescence of the viscously confined atoms. Varying the experimental parameters while observing the fluorescence enabled us to find the longest lived molasses.

It has been found [SSV90] that atoms in a weak magnetic field are cooled by polarization-gradient molasses to a non-zero velocity determined by that field. Consequently, if atoms are not in the zero magnetic field after the current in the trapping coils has been switched off, the applied cooling light gives the atoms some non-zero velocity. In order to avoid this we cancel the magnetic field in the cooling region to ≤ 30 milligauss with additional compensation coils.

The temperature of the polarization-gradient cooled atoms was measured using the ballistic expansion method described in Chapter 3. After the molasses has been applied for 5-10 ms, the cooling light is rapidly shut off and the diameter of the cloud as a function of time gives the value of the temperature. The lowest obtained temperature ~50 μK, is only a factor of 2 higher than the best value of 25 μK achieved for low-density sodium atoms with polarization-gradient molasses [LPR89]. The ultimate temperature depends on the cooling-laser beam profiles because inhomogenuities in the light intensity may create local heating or create routes for leaking from molasses. Consequently, an

ultimate temperature might be improved by spatial filtering of the laser beams and higher quality optics.

We have not found a strong dependence of the molasses temperature either on the cooling light intensity or on the sideband intensity. The lowest temperature was achieved for near-saturation intensity 5-10 mW/cm^2 of the cooling light with ~0.1% sideband intensity. The damping time of the dark polarization-gradient cooling is ~2 ms, much shorter than the value reported in [CLN92] for conventional "bright" molasses. It will be shown in the next chapter that during this short time the slow atoms do not move far away, so the initial density $\sim 10^{12}$ cm^{-3} does not significantly decrease.

The best performance of dark molasses was observed when the cooling light was red detuned by 4-5 linewidths (40-50 MHz). At this detuning, the effects of the nearby $F' = 2$ upper level may be significant and further investigation is desirable. A more careful study of the effects of the detuning and the light intensity on the dark polarization-gradient molasses is currently under way in our group.

Where we cannot invent, we may at least improve.
— Charles Caleb Colton

6. MAGNETIC TRAPPING

6.1. GENERAL

Magnetic traps confine atoms with a magnetic moment in a conservative potential well. There is no light present, so all the limitations and complications of the light traps do not apply any more. Atoms can be magnetically trapped in a single quantum state which makes magnetic traps attractive as a tool for precision measurements. The weak magnetic forces do not perturb atoms significantly, which makes magnetic traps a nearly ideal environment for studies of cold atomic interactions. Also, in a conservative potential the spread of atoms is defined by the energy distribution of the sample. So, important information about the energy distribution can be obtained using the imaging techniques in a 3D potential well of known shape. The most important property of magnetic traps as a means of achieving high densities of cold atoms is the possibility to implement evaporative cooling.

In principle, a magnetic trap is a three-dimensional minimum of the potential energy $U(\vec{r})$ of an atom with a magnetic moment $\vec{\mu}$ in a magnetic field $\vec{B}(\vec{r})$:

$$U(\vec{r}) = -\vec{\mu} \cdot \vec{B}(\vec{r}). \tag{6.1}$$

An atom is a quantum system, so the magnetic moment associated with the total spin of the atom is quantized. In small magnetic fields ($\leq$100 G, typical for magnetic traps without a bias field) the value of the magnetic moment of the state with total spin F and projection m_F is:

$$\mu = -g_F \mu_B m_F, \tag{6.2}$$

where g is the Landé g-factor of the state and μ_B is the Bohr magneton. For the (F=1) ground state of sodium $g = -1/2$. Thus, atoms with the projection of the total spin along the magnetic field $m_F = -1$ are weak-field seekers and can be confined around a minimum of the magnetic field. Since the rate of spontaneous transitions between the Zeeman levels is very small, the magnetic moment of an atom remains constant.

In order for moving atoms to be confined by the static magnetic field the direction of the magnetic moment has to follow the direction of the magnetic field adiabatically. The adiabaticity condition requires that the direction of the magnetic field in the moving atom's reference frame does not change faster than the Larmor precession frequency of the atom's magnetic moment in the magnetic field:

$$\frac{\left|(\vec{v}\cdot\nabla)\vec{B} - \nabla\vec{B}\cdot\frac{\vec{v}}{v}\right|}{B} \approx \left|\frac{(\vec{v}\cdot\nabla)\vec{B}}{B}\right| < \frac{\mu B}{\hbar} \tag{6.3}$$

For a typical optically cooled sodium atom, the velocity is $v = 30\,\text{cm/s}$. Assuming a field gradient such that magnetic trapping force is ten times stronger than gravity $|\nabla B| = {}^{10mg}/_{\mu} = 40\,\text{gauss/cm}$, the above condition is satisfied if $B > 0.05$ gauss. In smaller magnetic fields the atom may undergo nonadiabatic spin flips (Majorana

transition) and the resulting sign change of the potential expels the atom from the trap. Traps with a field minimum at a non-zero value of the magnetic field are advantageous in this respect.

6.2. MAGNETIC FIELD CONFIGURATIONS

A number of static field configurations for magnetic traps have been suggested and demonstrated experimentally. Different field configurations are discussed in detail in [BEM87].

The first demonstrated magnetic trap [MPP85] consisted of two coils with currents. This anti-Helmholtz coils configuration is simple and can be readily implemented. The resulting spherical quadrupole field has a local minimum in the center and can be used to confine atoms. But since the atoms are trapped around a point of zero magnetic field, they can escape the trap because of Majorana flops. Near the origin the field (and consequently the potential energy) is linear with the distance:

$$B(x,y,z) = \frac{B'_z}{2}\sqrt{x^2 + y^2 + 4z^2} \tag{6.4}$$

The Maxwell equation $\nabla \cdot \vec{B} = 0$ implies that the field gradient along the axis of the coils B'_z is twice that along x and y axis. The linear field is steeper than quadratic, so the effective volume is smaller for a linear-field trap than for a parabolic-field trap with similar size coils. As a result, the same number of atoms at the same temperature is confined at higher density in a spherical-quadrupole trap than in a harmonic trap. Furthermore, as a result of more favorable scaling of the effective trap volume with current through the coils in a spherical-quadrupole trap ($V \propto I^{-3}$, compared to $V \propto I^{-\frac{1}{2}}$ for a harmonic trap), similar attainable currents could be used more efficiently to adiabatically compress trapped atoms [MON92]. Finally, a practical advantage of this field configuration is that it is identical with the field used in a magneto-optical trap.

Thus, the same pair of anti-Helmholtz coils can be used for both traps and switching from one trap to another can be done by simply increasing the current.

Cylindrical-quadrupole trap configuration has been suggested in [PRI83] and has been successfully used for trapping sodium [BLM87] and hydrogen atoms [HKD87]. This trap configuration has many advantages. The non-zero minimum field suppresses the losses due to Majorana transitions. The traps of this kind can be made to have a large volume and confine a large number of atoms. This trap also allows for implementation of efficient optical cooling schemes [HMP92b]. Furthermore, the axial symmetry of this field configuration allows for efficient loading of the trap from a stopped atomic beam. But probably the major advantage of this trap configuration is that longitudinal and radial confinement can be varied independently, which allows implementation of forced evaporative cooling [MDS88].

Another type of non-zero-field magnetic trap, so called "baseball" trap, have been used [MON92] to trap cesium atoms. The magnetic coil in this trap has the shape of a baseball seam which gives rise to the name. Like in a cylindrical quadrupole, the trap loss due to nonadiabatic transitions is suppressed. The potential in this trap is almost harmonic if the gravity is balanced by an additional linear gradient magnetic field. High point symmetry of this magnetic trap makes allows for efficient transferring atoms into it from a point source such as an optical trap. The Colorado group has also experimented with some hybrid field configurations, such as coil+bars and opposite-coils traps [MON92].

6.3. IN SITU LOADING OF THE MAGNETIC TRAP

The valuable properties of magnetic traps are somewhat offset by the fact that they are typically several times weaker than light traps. The implications of the trap shallowness are twofold: (a) high magnetic field gradients and ultra-high vacuum are necessary to

ensure reasonable confinement times; (b) atoms loaded into a magnetic trap have to be pre-cooled to much lower temperatures compared to optical traps. The first aspect has been discussed in the Chapter 3: here I will discuss the loading of the magnetic trap.

The magnetic trap for sodium demonstrated in our laboratory [BLM87] was loaded continuously from a stopped atomic beam. In order to operate effectively the trap required high magnetic fields achievable only with superconducting magnets. The cryogenic technology associated with the superconducting magnets, although commercially available, is expensive, bulky, and pretty demanding. Hence, as a practical matter, it is better to postpone using it, if possible, until high-temperature superconducting magnets become available.

An alternative to the beam-loading is to capture atoms in a light trap and then transfer them into a magnetic trap. The robust and efficient light trap in this case works as an atom "integrator": it accumulates atoms during its loading time and cools them down to temperatures acceptable for magnetic trapping, thus preparing the magnetic-trap-ready sample. Better yet, in order to avoid losses associated with the transfer, it is possible to load a magnetic trap *in situ*, by substituting one trap with the other at the same point of space. This is the approach we chose for our experiment.

This intuitive approach has its own drawbacks. Of course, not all the atoms from the light trap can be recaptured by the magnetic trap. In the light trap spontaneous emission acts randomize the direction of the atom's magnetic moment, whereas only atoms with "correct" projections of the magnetic moment along the field direction (weak-field seekers) are magnetically trapped. For (F = 1) sodium atoms only atoms with $m_F = -1$ can be magnetically confined, while atoms with $m_F = 0$ and 1 can not. It means that only one atom out of three can be recaptured, setting the maximum transfer efficiency at 33%, unless special efforts are undertaken to optically pump atoms into the desired state. Also, in situ loading of the magnetic trap is inherently a pulsed method, as opposed, for

instance, to continuous loading from the slowed beam. But, the extremely high loading rates arising from accumulating ~10^{11} cold atoms in the light trap and transferring them into the magnetic trap in ~1 ms well make up for the drawbacks.

As I have described in Chapter 4, we can accumulate a large number of atoms at a high density in the dark SPOT with 5-cm-diameter trapping laser beams to ensure efficient capturing of atoms from the slow beam. The diameter of these beams sets a constraint on the minimum diameter of the magnetic coils. For magnetic confinement, on the other hand, one would like to have a small, compact coil which can produce higher field gradients and, consequently, make a deeper trap. Unfortunately, we have found that a small (~1 cm) wire loop inserted in the laser beams scatters too much light and deteriorates the dark SPOT performance. With magnetic trap coils made around the light-trap coils it would be practically impossible to achieve the high field gradients desired for tight magnetic confinement. The compromise, then, is to use the same pair of coils for both optical and magnetic traps and to optimize them to achieve as large magnetic field gradients as possible. The possibility to use the same coils for both traps is an obvious asset from the experimentalist's point of view, but the disadvantages have to be evaluated. For this purpose, it is necessary to estimate the losses associated with Majorana flops in a spherical quadrupole trap.

6.4. MAJORANA FLOPS

The probability of a Majorana transition for an atom passing near the point of zero field can be estimated using the Landau-Zener picture of rapid non-adiabatic passage. Consider a trapped atom following a trajectory characterized by a coordinate q (Fig. 6-1). The weak-field seeking atom stays on the potential energy curve with a minimum at the point of the smallest magnetic field along the trajectory. For a strong-field seeking state the potential energy is the mirror image with the maximum at the same point. The atom

can stay on the upper curve and remain trapped or undergo the non-adiabatic transition to the lower curve and escape.

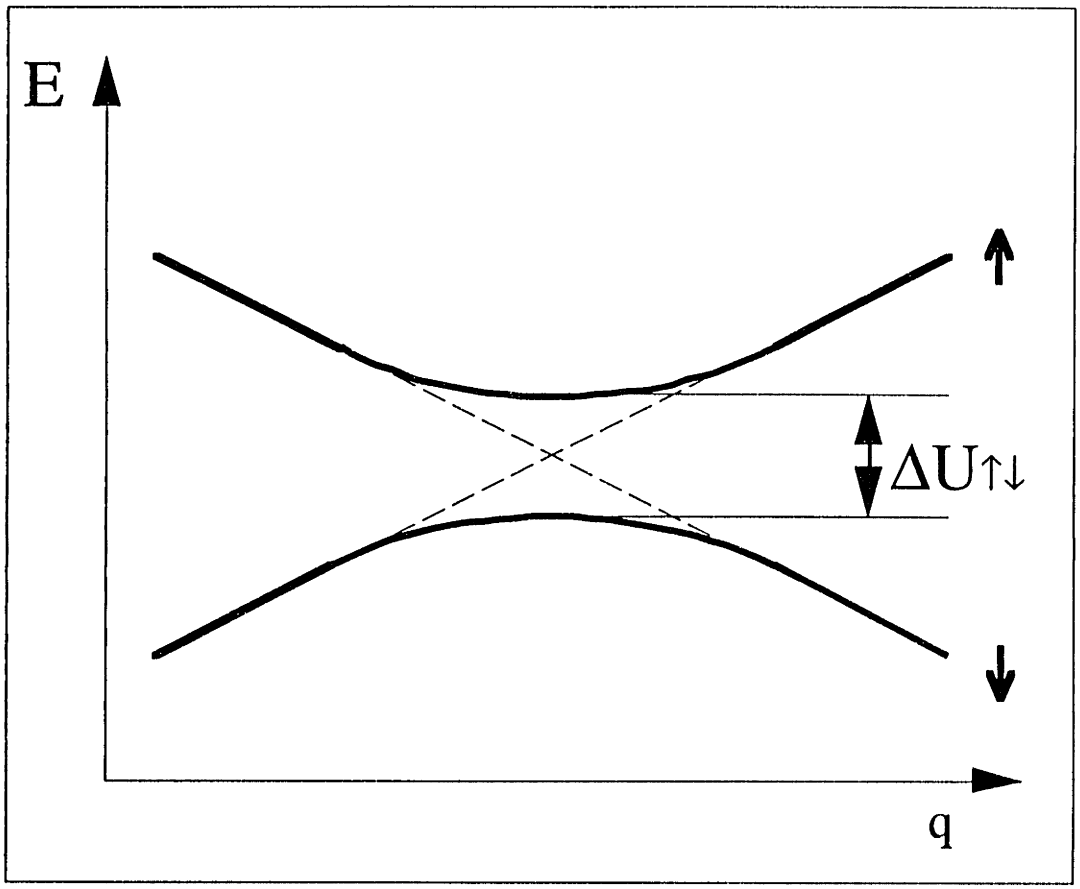

Fig. 6-1: "Avoided crossing" picture of non-adiabatic Majorana transitions.

If we define the impact parameter b as the distance from this point to the origin of the trap, the energy splitting between the curves is:

$$\Delta U_{\uparrow\downarrow} = 2 \cdot \frac{1}{2} \mu_B B(b) = \mu_B \left\langle \frac{\partial B}{\partial r} \right\rangle b \tag{6.5}$$

For a spherical quadrupole the average field gradient is

$$\left\langle \frac{\partial B}{\partial r} \right\rangle = \frac{\frac{1}{2} + \frac{1}{2} + 1}{3} \frac{\partial B}{\partial z} = \frac{2}{3} \frac{\partial B}{\partial z} \tag{6.6}$$

The level splitting then can be written as

$$\Delta U_{\uparrow\downarrow} = \beta b, \tag{6.7}$$

where $\beta = \frac{2}{3}\mu_B \frac{\partial B}{\partial z}$. The Landau-Zener probability for the non-adiabatic transition is

$$p = e^{-\frac{2\pi(\Delta U_{\uparrow\downarrow})^2}{\hbar(\frac{dE}{dt})}}. \tag{6.8}$$

The denominator in the exponent can be evaluated as

$$\frac{dE}{dt} = \frac{dE}{dq}\frac{dq}{dt} \approx \frac{1}{2}\beta\bar{v}, \tag{6.9}$$

where $\bar{v}$ is the average thermal velocity of atoms in the trap. Combining (6.5-9) we obtain the probability of the non-adiabatic transition as a function of the impact parameter b:

$$p(b) = e^{-\alpha b^2}, \tag{6.10}$$

with $\alpha = \frac{\pi\beta}{\hbar\bar{v}}$. The next step is averaging the transition probability over the whole ensemble of atoms. All atomic trajectories can be characterized by their closest-to-the-origin points $\vec{b}$. The average probability is then

$$p = \frac{2\pi}{r_o^3}\int_0^{r_o} p(b)\cdot b^2 db, \tag{6.11}$$

where r_o is the radius of the trapped cloud. Assuming typical values $\bar{v} = 30\,\text{cm/s}$ and $\frac{\partial B}{\partial z} = 50$ gauss/cm we obtain $\alpha = 5\cdot 10^7$. Since the trap radius is typically $r_o \approx 0.1\,\text{cm}$, we can replace the upper limit of integration in (6.11) with infinity. The integral can then be easily evaluated and we arrive at

$$p = \frac{2\pi}{r_o^3}\frac{1}{2\alpha}\frac{1}{2}\sqrt{\frac{\pi}{\alpha}} \approx \frac{8\cdot 10^{-12}}{r_o^3}. \tag{6.12}$$

The value p is the probability of the non-adiabatic transition for one passage, so the total loss rate due to Majorana flops per atom R_{MF} can be estimated as

$$R_{MF} = \frac{2r_o}{\bar{v}} p = \frac{1}{r_o^2 \bar{v}} \left(\frac{\pi}{\alpha}\right)^{\frac{1}{2}} \approx 5 \cdot 10^{-11} [\text{sec}^{-1}] \qquad (6.13)$$

for a cloud with a radius $r_o = 0.1$ cm. This loss rate would limit the lifetime of the trap to $\sim 2 \cdot 10^{10}$ s, which is much larger than the trapping time of ~30 s due to background collisions. It is also important to point out that the rate (6.13) becomes relatively more significant for smaller traps. Furthermore, the estimate is pretty conservative, since computer simulations (our and ref. [GAS90]) show that the majority of atoms follow trajectories that do not bring them close to the potentially dangerous zero-field point. We can thus conclude that the Majorana transitions do not constitute a problem, at least for our experimental conditions.

6.5. COOLING ATOMS DURING THE TRANSFER

During the last decade quite a few different techniques for handling (slowing, trapping, cooling, launching, etc.) atoms have been developed. Naturally, all these techniques have their advantages and drawbacks, but what is an advantage and what is the drawback depends on the application. Recalling the discussion in Chapter 1, the goal of our experiments is to maximize the number of trapped atoms, maximize their density, and minimize their temperature. Here I would like to briefly address the issue of integration and compatibility of different methods as a means of advancement along this path.

The magneto-optical trap (dark SPOT, Chapter 4) has excellent capturing capabilities, can store a large number of atoms and is a natural choice for the first step. It even has a built-in cooling mechanism (Doppler Molasses), which cools atom well enough to allow reloading atoms into the magnetic trap. The magnetic trap is a very good choice for the

last step because it is a "clean" environment, it permits easy compression and expansion of the sample, and allows for implementation of highly effective evaporative cooling.

As far as the temperature of the trapped sample is concerned, there is an efficient method of laser cooling that has been developed: polarization-gradient cooling (Chapter 5). The more than an order of magnitude decrease in temperatures achieved with this technique make it very attractive. But the problem is that this method requires a carefully nulled magnetic field, whereas both magneto-optical and magnetic trapping necessarily use non-zero magnetic field. We have shown, however, that it is posible to apply this kind of laser cooling *between* the optical and magnetic trapping stages, by shutting off (nulling) the magnetic fields for a short time. While neither trap is working the atoms are viscously confined by the optical molasses. So, while being cooled without any trap turned on, the atoms do not fly away, at least not too far, if the cooling makes them slow enough and does not last too long. In other words, atoms are efficiently cooled by polarization-gradient molasses during the transfer from the light trap to the magntic trap. The issue of atoms transfer has to be addressed now more quantitatively.

If one had to define the single parameter of merit for experiments in trapping and cooling, it would probably be phase-space density $\zeta = \frac{N}{(\Delta x \Delta p_x)^3} \propto \frac{n}{T^{\frac{3}{2}}}$. This is the parameter that has to be maximized, for example, for observation of collective effects. Without dissipation, phase-space density is at best conserved, so ζ is a quantitative measure of cooling efficiency. Since phase-space density is proportional to the atom density n, it is also a measure of trapping and transferring efficiency from one trap to the other.

As I have been discussed above atoms can be efficiently transferred from the light trap into the magnetic trap. The shapes of the potentials are most probably different for the two traps, so the equillibrium spatial distributions (trap "modes") do not necessarily coincide. As a result, the atoms can slosh in the new trap after the transfer from the old

one, acquire additional potential and kinetic energy, or, more generally, heat up. However, even if the two traps are carefully "mode-matched" so that no additional heating is introduced the temperature of magnetically trapped atoms is limited to the temperature of atoms in the light trap (1.2 mK for our dark SPOT). Fortunately, we have an effective way to cool atoms with dark polarization-gradient molasses discussed in Chapter 5. The dark molasses cools atoms to ~ 60 μK in ~5 ms. In such a short time, even in the worst case, an atom with an initial thermal velocity at 1.2 mK of ~150 cm/s will move only by a 4 mm, comparable to the typical diameter of the cloud. But since the temperature falls exponentially during these 5 ms, the atoms do not move significantly compared to the size of the cloud. In other words the cloud does not have time to expand significantly, so the density decreases by less than on order of magnitude. The temperature, on the other hand, drops by a factor of ~20. So, by introducing a ~5 ms cooling stage between the time-separated light and magnetic traps we can achieve an order-of-magnitude gain in the phase-space density.

When the trapping magnetic field is turned on around the polarization-gradient-molasses cooled cloud of sodium atoms in the F = 1 state, a factor of 3 in the phase-space density is lost as discussed above because only atoms with only one projection of magnetic moment out of three can be captured. The challenge, however, is not to loose any more. Qualitatively, if the magnetic potential is too shallow the cloud spreads and its density decreases. On the other hand, if the magnetic confinement is too tight the cloud is compressed and consequently heated, again resulting in decrease in the phase-space density ζ. It is reasonable to expect that there is an optimum magnetic field gradient, and I will describe here a simple model that quantifies the transfer of atoms from molasses into a magnetic trap.

Consider a cloud of N atoms with a characteristic size x_i cooled by molasses to a temperature T_i. The energy of the cloud in the free space is purely kinetic:

$$E_i = \frac{3}{2} N k_B T_i. \tag{6.14}$$

The rms value of one-dimensional momentum p_i is then given by

$$p_i^2 = m k_B T_i. \tag{6.15}$$

The initial phase-space density ζ_i of the cloud is

$$\zeta_i = \frac{N}{p_i^3 x_i^3}. \tag{6.16}$$

Now let us calculate the final phase-space density ζ_f of the cloud after a linear magnetic trap has been suddenly switched on. Let us assume, for simplicity, that all atoms have the correct projections of their magnetic momenta and can be captured. Also, we assume that the magnetic field gradient is the same along all axes. The total energy of the cloud now consists of the same kinetic energy and the newly acquired potential energy. After the sample has thermalized it can be characterized by a new final temperature T_f and has a new characteristic dimension x_f. For a spherical-qudrupole trap with the potential $V \propto r$ we then have [TOM86 and Appendix A]:

$$E_f = \frac{3}{2} N k_B T_i + 3 k x_i = \frac{9}{2} N k_B T_f, \tag{6.17}$$

where k is the stiffness parameter of the magnetic trap proportional to the field gradient:

$$k = \frac{1}{2} \mu_B B_x'. \tag{6.18}$$

Also, for the linear trap [TOM86]:

$$k x_f = k_B T_f. \tag{6.19}$$

The rms value of one-dimensional momentum p_f then becomes

$$p_f^2 = mk_B T_f. \tag{6.20}$$

From the expressions (6.17) and (6.19) for p_f and T_f we obtain for the new phase-space density ζ_i of the cloud:

$$\zeta_f = \frac{N}{p_f^3 x_f^3} = \frac{N}{(mk_{BT_f})^{\frac{3}{2}}(\frac{k_B T_f}{k})^{\frac{3}{2}}} = \frac{N}{m^{\frac{3}{2}} k_B^{\frac{9}{2}}} \frac{k^3}{(\frac{T_i}{3} + \frac{2}{3} k \frac{x_i}{k_B})^{\frac{9}{2}}}. \tag{6.21}$$

The function $\zeta_f(k)$ obviously has a maximum, so differentiating (6.21) with respect to k we find that the maximum is achieved at the optimum value of

$$k_{opt} = \frac{k_B T_i}{x_i}. \tag{6.22}$$

Plugging this value back into (6.21), we come to the conclusion:

$$\zeta_{f,\max} = \frac{N}{(mk_B T_i)^{\frac{3}{2}} x_i^3} \equiv \zeta_i. \tag{6.23}$$

So the atoms can be recaptured from molasses by the (optimized) magnetic trap without the phase-density loss! The optimal value for the field gradient can be derived from (6.18) and for typical values of $T_i \approx 50$ μK and $x_i \approx 0.1$ cm is found to be $B'_{opt} \approx 15$ gauss/cm, which is well within the range of field gradients attainable with our coils.

6.6. Computer Simulation of Magnetically Trapped Atoms

Once the atoms are transferred into and confined by the magnetic trap, it is important to understand their behavior in it. Atoms are moving along three-dimensional trajectories in

a potential well of complex shape and, in addition, ellastically scatter on each other. Both the non-perturbed motion and the collisions affect the shape of the cloud which we can observe in the experiment. It is necessary, therefore, to distinguish the two effects. An atom at 50 μK travels across the trap of 0.3 cm in size with an average thermal velocity of 30 cm/s in ~10 ms. It will be shown in Chapter 7 that for the density 10^{11} atoms/cm^3 and temperature 60 μK the frequency of the elastic collisions per atom is ~0.1 Hz, i.e. 1 collision every ~10 s (Fig. 7-4). Consequently, at these density and temperature both kinematic motion and and scattering occur on the same time scale and the effect on the shape of the cloud of neither can be neglected compared to the other.

Furthermore, the shape of the real magnetic trap potential has to include gravity. For sodium atoms in a magnetic trap with the field gradient 25 gauss/cm the gravitational potential energy $mgh = 3.76 \cdot 10^{-20} h$ [erg] (h is in cm) is comparable to the magnetic potential $\mu B'_r r = 11.6 \cdot 10^{-20} r$ [erg] (r is the distance from the origin in cm). The atoms are cold enough to feel this assymetry: their gravitational hight $\frac{k_B T}{mg} = 0.2$ cm is approximately equal to the radius of the cloud.

Even without collisions, atoms in an asymmetric potential constitute a system that can hardly be analyzed analytically. To learn about the atoms' trajectories we have undertaken a computer simulation. An atom with a permanent magnetic moment that adiabatically follows the field can be described classically, just like a ball in a bowl. The computer model solved the Hamiltonian equations for a three-dimensional potential including gravity. To acquire statistics the initial conditions (initial position and velocity of the atom) were chosen randomly. The equations were integrated using the forth-order Runge-Kutta algorithm with a fixed step. The integration step was chosen and verified to be small enough not to affect the results. Simulation of 10 sec of atoms trajectory took about 90 sec on the Macintosh Quadra 800 computer.

The question very important for understanding (and implementation) of evaporative cooling is whether the system is ergodic or not. To put it in other words, will a single atom in the magnetic trap pass (in a certain finite time) through every point of the space permitted by its total energy or will it stay on its closed orbit forever. To address this questions we calculated a number of trajectories for different initial conditions.

In an ideal spherical quadrupole trap with an axis of symmetry along z the projection of the atom's angular momentum along the z axis is conserved. It is easy to see then that at least some atoms will stay on a closed quasi-periodic trajectory, such as a closed circle in the plane parallel to the $z = 0$ plane. Indeed, with gravity put equal to zero the trajectories are very symmetric (Fig. 6-2).

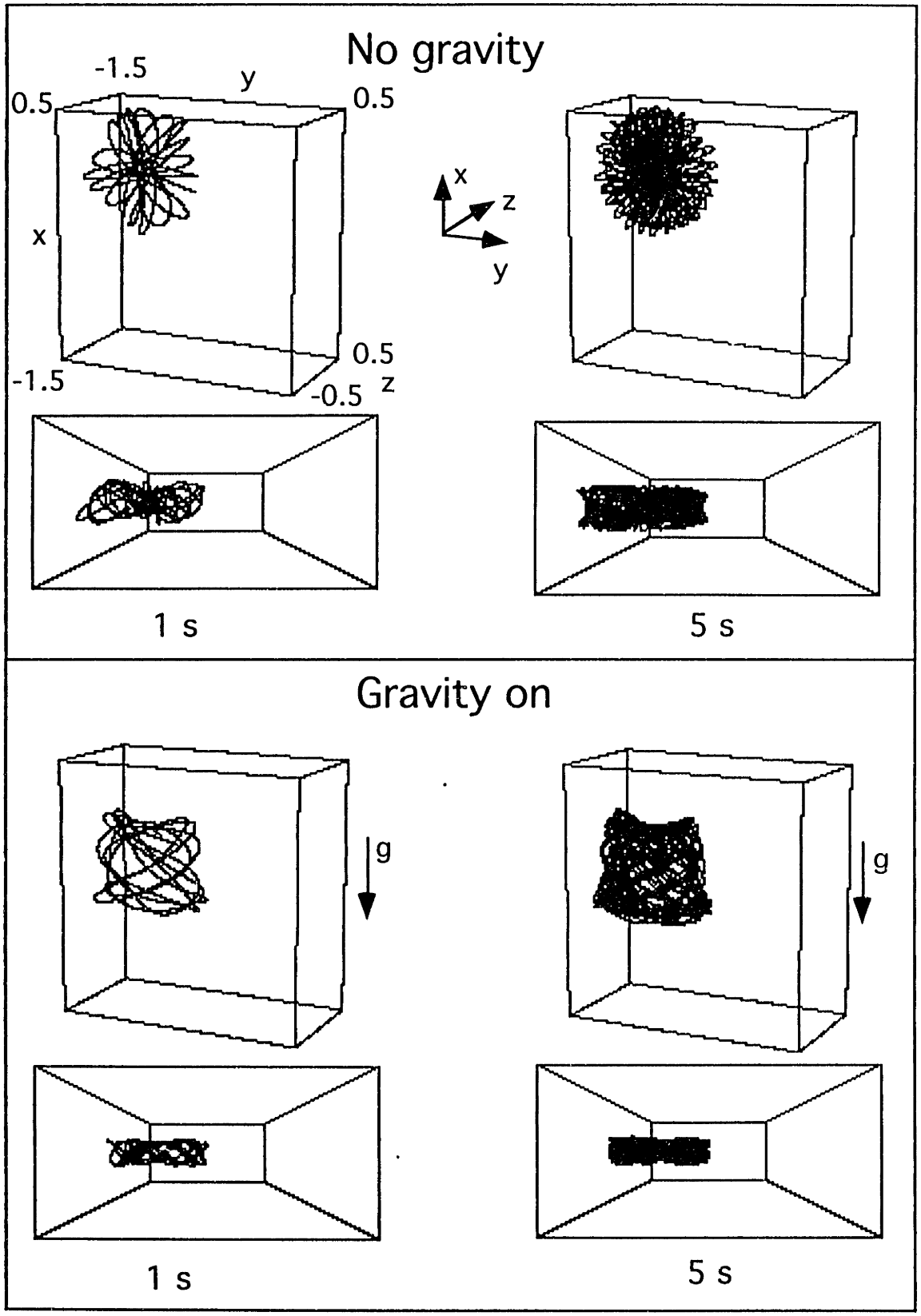

Fig. 6-2: Side and bottom views of typical trajectories of an atom in a spherical quadrupole magnetic trap with vertically-oriented coils with or without gravity. The purpose of the boxes is to guide the eye when interpreting the three dimensional pictures. The center of the trap is at the origin.

The situation does not change much when the gravity is "turned on" along the symmetry axis, which can be done with marvelous ease on a computer. However, the real coils are positioned vertically, so the there is no symmetry axis any more. It can be shown that no projection of angular momentum is conserved any more. The trajectories are very asymmetric and vary depending on initial conditions (Fig. 6-2). The actual trajectory is strongly dependent on initial conditions. Fig. 6-3 shows trajectories of an atom starting at the same point in space with the same value of velocity pointing in different directions.

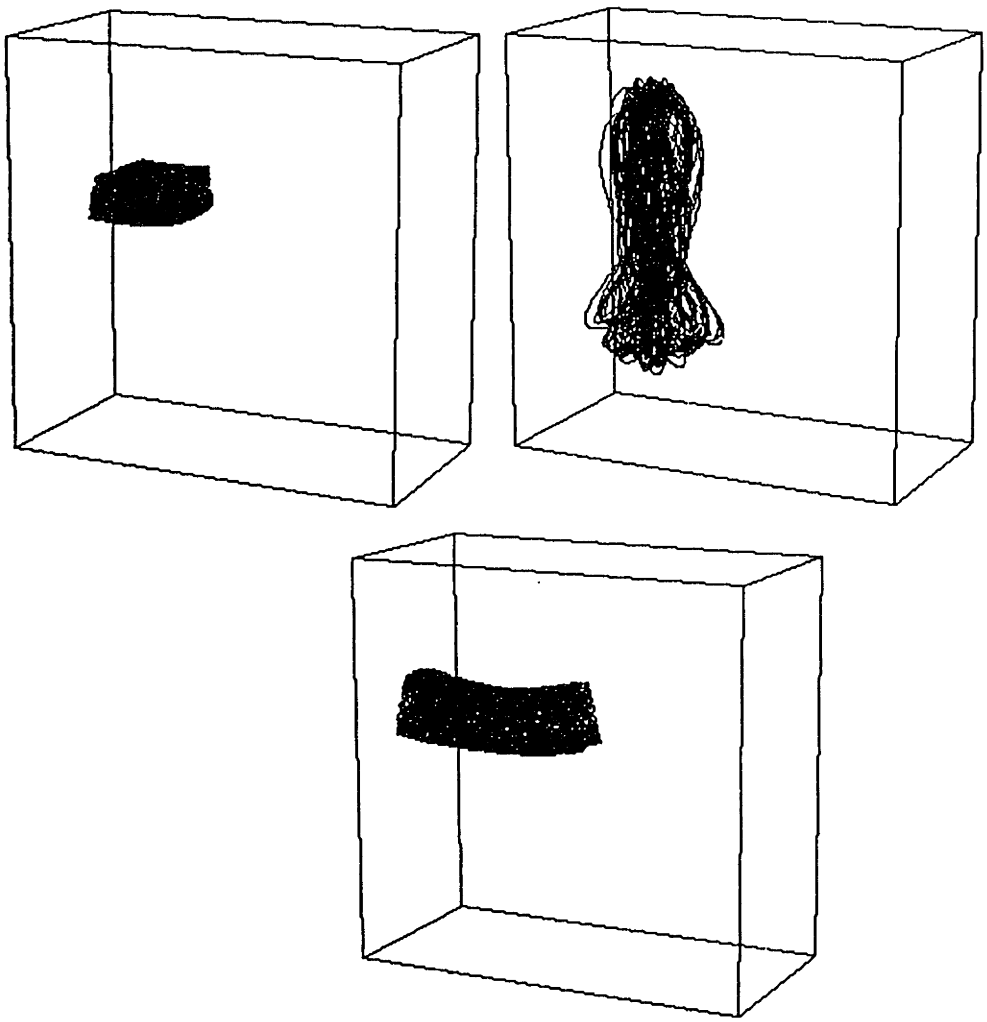

Fig. 6-3: Trajectories strongly depend on initial conditions. In this case the initial position and the velocity value are the same but the direction of the initial velocity is different.

In order to accumulate enough data we calculated and analyzed a fair number of trajectories for different initial conditions. They all look different, however, some conclusions can be made from analysis of typical trajectories shown on Fig. 6-4.

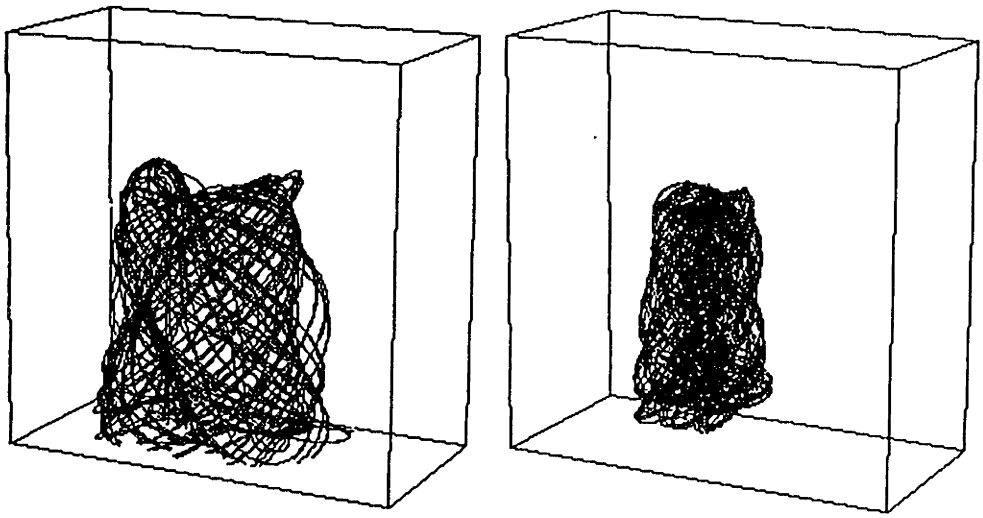

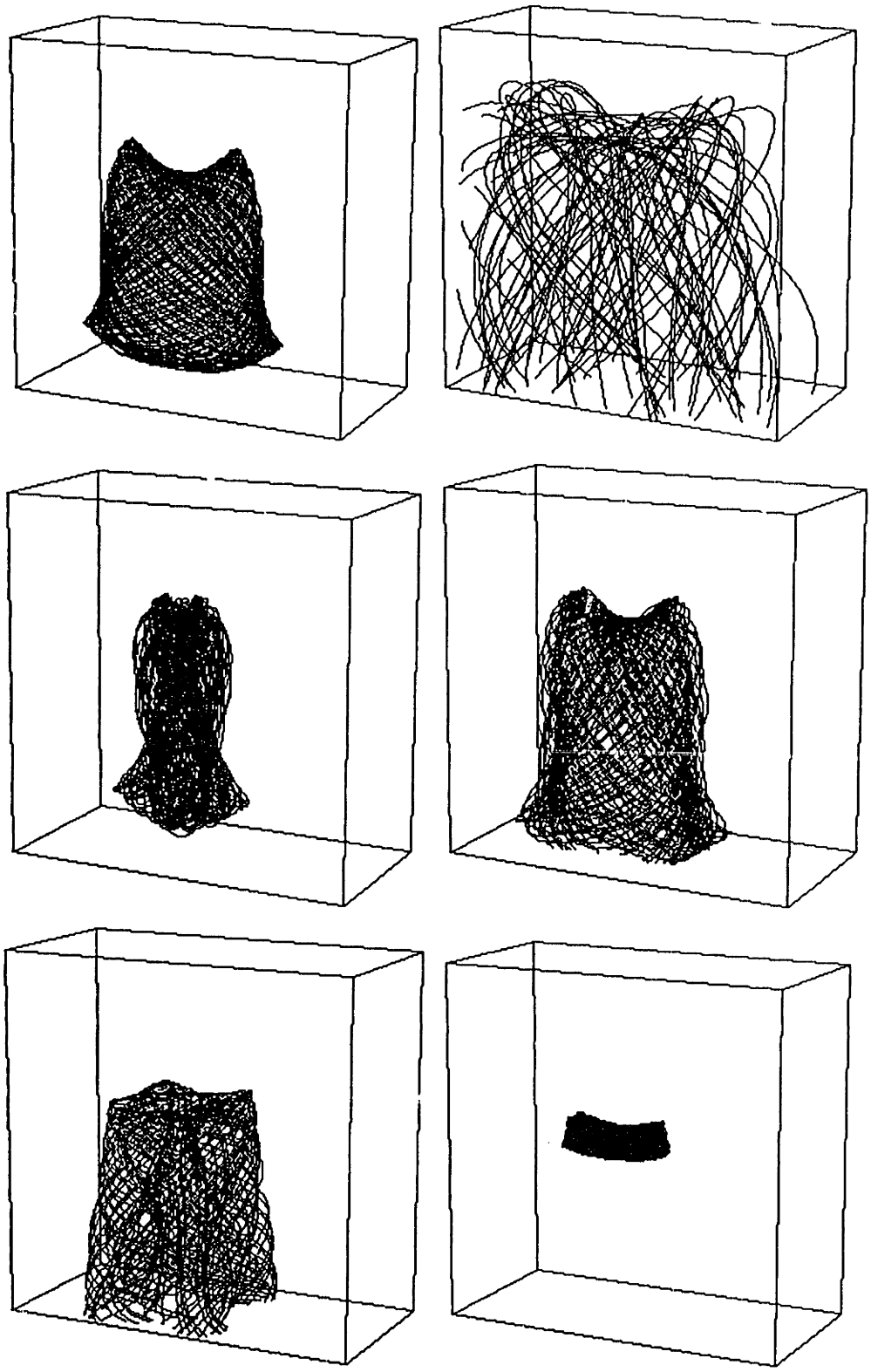

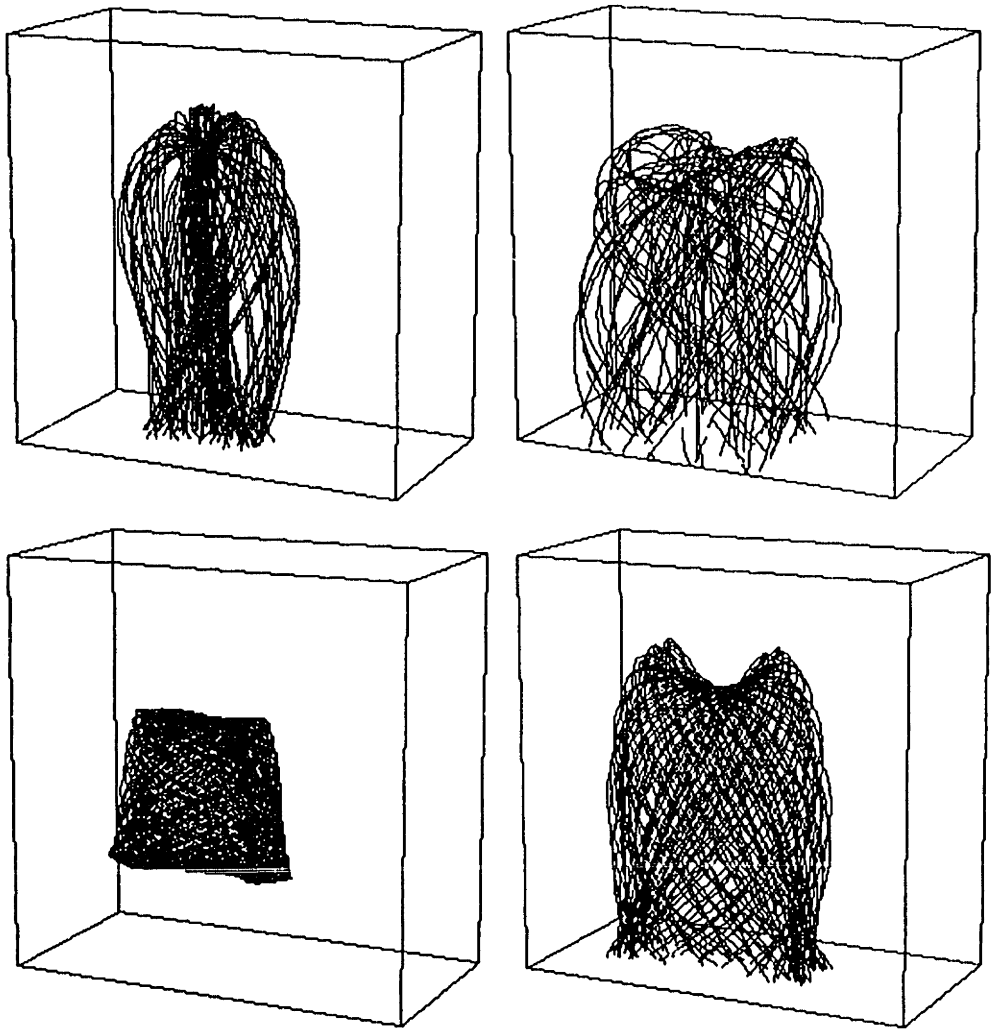

Fig. 6-4: The Gallery of Atomic Trajectories.

The trajectories are three-dimensional in the sense that gravity mixes the three directions and makes the atom sweep the volume inside some shell of irregular shape defined by the initial conditions. The trajectories remain confined by this shape, at least on a time scale of interest for trapping (~50 s). The atoms do not reach all the points allowed by energy conservation, so the system is not ergodic on this time scale. The other observation, important for example for radiative spin-flip discussed in the next Chapter, is that the atoms cover a significant part of their trajectory's volume in a matter of seconds. It means that if we want to probe or affect atoms at one point of space, an atom either passes within ~0.1 mm in the first few seconds or it will never make it there at all. This

conclusion sets a time frame for experiments on radiative truncation of the trapped cloud discussed in the next Chapter.

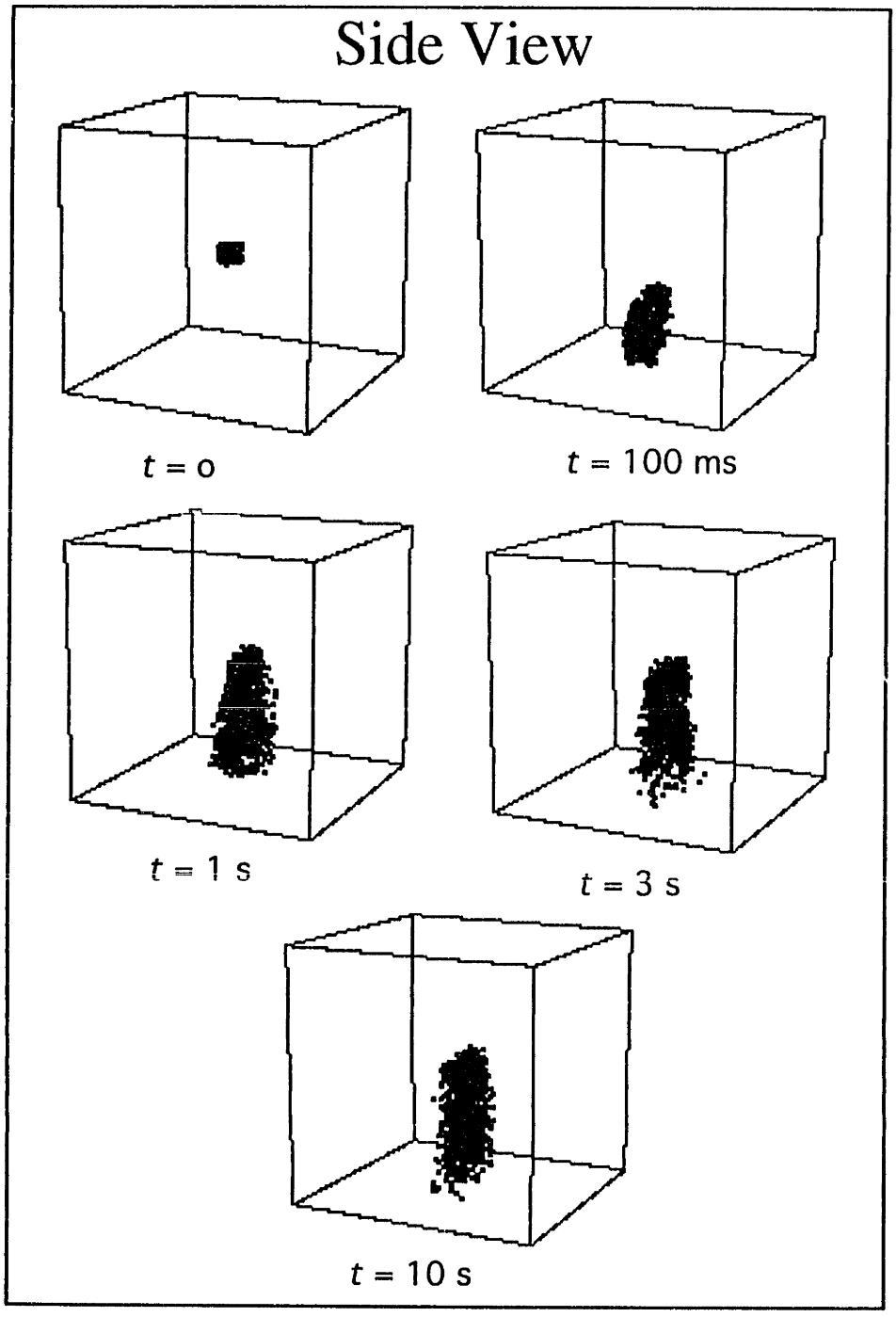

Fig. 6-5: Computer simulated spreading of the magnetically trapped cloud. The dashed circles denote the approximate position of the magnetic coils. The size of the box is 6 cm.

Another computer experiment is to calculate trajectories for a large ensemble of atoms and plot the initial and final points for these trajectories. The result then illustrates spreading of a magnetically trapped cloud with time (Fig. 6-5). For this run the cloud of 1000 atoms was "displaced" along the axis of the coils and let go at t = 0. As can be seen from the figure the cloud sags along gravity, as expected, and spreads due to sloshing of the initially displaced cloud. It is important that the typical spreading time is ~ 100 ms. The cloud shape stays practically unchanged after t = 1 s. Another important conclusion can be drawn if we look at the same clouds at a different angle, namely from the top (Fig. 6-6).

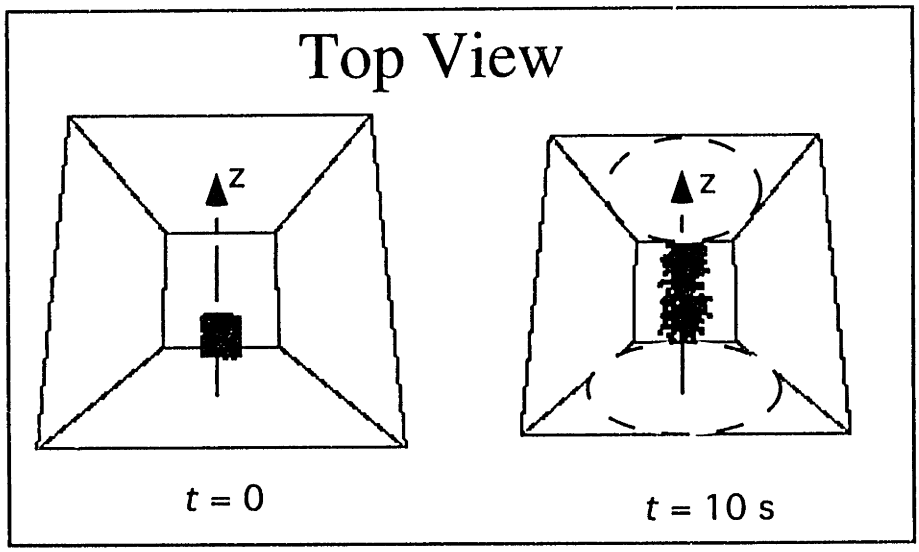

Fig. 6-6: The top view of the cloud spreading indicates that there is practically no radial spreading of the cloud.

It is clear that, while the cloud spreads in the direction along which it has been displaced (the coils axis), there is practically no spreading of the cloud along the other (radial) direction. This conclusion is important for choosing the observation point for the videocamera in a real experiment. Also, should any significant spreading be observed along this axis in the real experiment it should be attributed to inter-atomic collisions, rather than single-atom trajectories. The real-life experiment of this kind should thus

provide valuable information about the cross-section of elastic collisions between ultracold sodium atoms.

6.7. EXPERIMENTAL RESULTS

6.7.1. Loading from the Optical Trap

The first experiment in magnetic trapping is pretty straightforward. Atoms are first accumulated and held continuously in a dark SPOT, then the trapping light is shut off and at the same time the current through the magnetic coils is increased. From that moment on the atoms are confined magnetically (Fig. 6-7). The result is very encouraging, since the optical density of the cloud practically stays the same after switching to magnetic confinement. The optical density drops, however, pretty quickly. The apparent decay is, however, an artifact of the short observation time. If the observation time was increased, it became obvious that the atoms are not being lost: the optical density increases again, almost to the initial level (Fig. 6-8). The reason is that we observe sloshing of the atoms in the magnetic trap. The trap is strongly anharmonic, so due do fast dephasing of atoms oscillating in the trap, the optical density averages out and settles at some intermediate value.

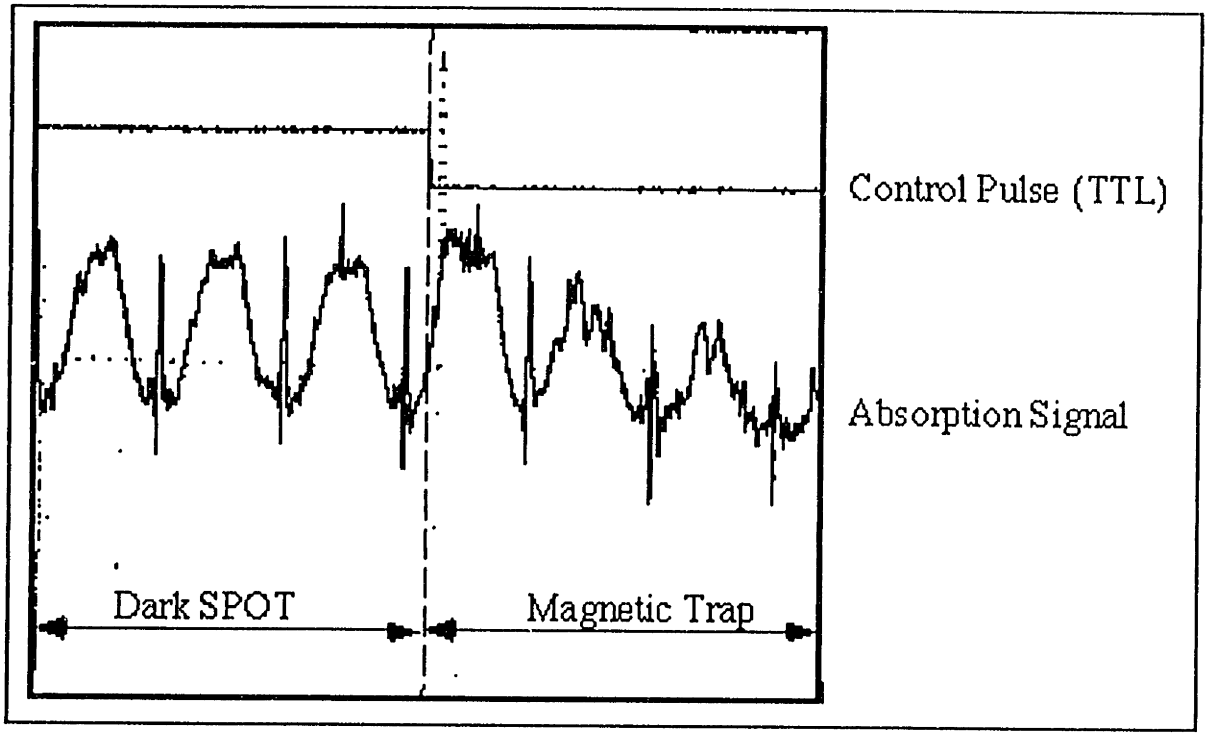

Fig. 6-7. Loading atoms from a dark SPOT to a magnetic trap. The absorption probe frequency is repetitively swept with a saw-tooth pattern (10 ms/sweep) while the signal is continuously recorded. At a falling edge of the control pulse the trapping light is turned off and the coil current is increased. The absorption of the magnetically trapped atoms deceases in each of the two successive sweeps.

The effective sloshing frequency depends on the stiffness of the trap and increases with the magnetic field gradient. The result is in qualitative agreement with a simple one-dimensional model which predicts that the recurrence time scales as $\tau \propto (B_z')^{-\frac{1}{2}}$. In order to evaluate the transfer efficiency we have to compare the initial optical density in the dark SPOT with the optical density in the magnetic trap after the oscillations settle down. As shown on Fig. 6-8 the best results are achieved with high (~80 gauss/cm) field gradients. This does not contradict the estimate given in section 6.5 since the dark SPOT is hotter then the 50-μK value assumed in those calculations.

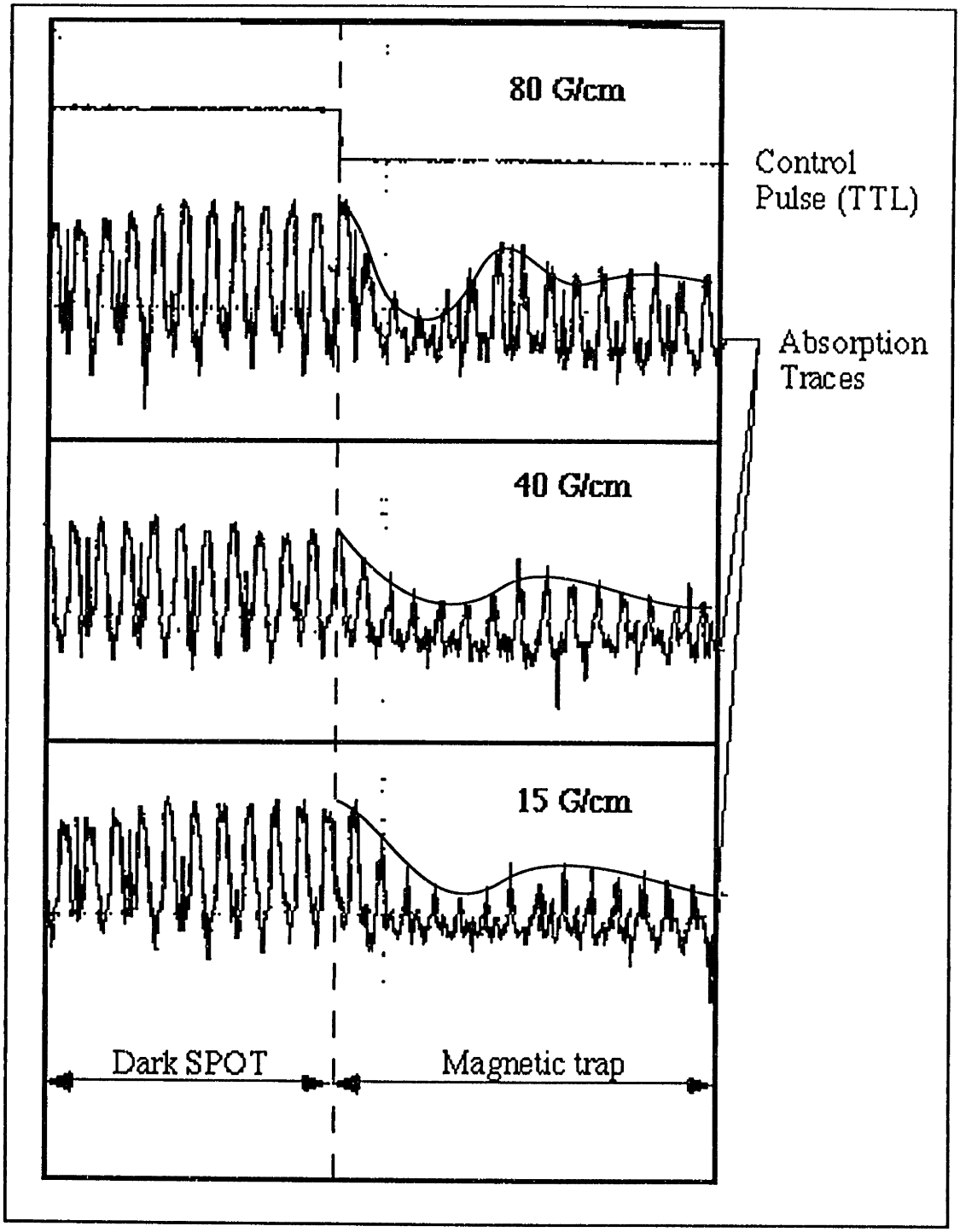

Fig. 6-8: Sloshing of atoms in the magnetic trap immediately after they are reloaded from the optical trap. The envelope of the interrogation pulses is sketched to guide the eye.

6.7.2. Loading from the Dark Molasses

As I have discussed, the transfer of atoms from the light trap to the magnetic trap can be significantly improved if polarization-gradient cooling is introduced in between. The results are shown in Fig. 6-9. The atoms are first collected in a dark SPOT (Fig. 6-9 a). The magnetic fields are rapidly turned off for ~10 ms to give the optical molasses enough time to cool atoms, after which the confining magnetic field is turned back on. After the atoms are captured in the magnetic trap they are illuminated with a flash of near-resonant laser light and the resulting fluorescence is observed with the video camera. The digitized image is shown on Fig. 6-9 b. With cooling, the cloud does not spread significantly after the atoms are transferred from the light trap to the shallower magnetic trap. Furthermore, the intensity of fluorescence of the cloud excited by the probe is almost the same (~1/3), which means that atoms are transferred without significant additional losses, other than due to angular momentum projection selection.

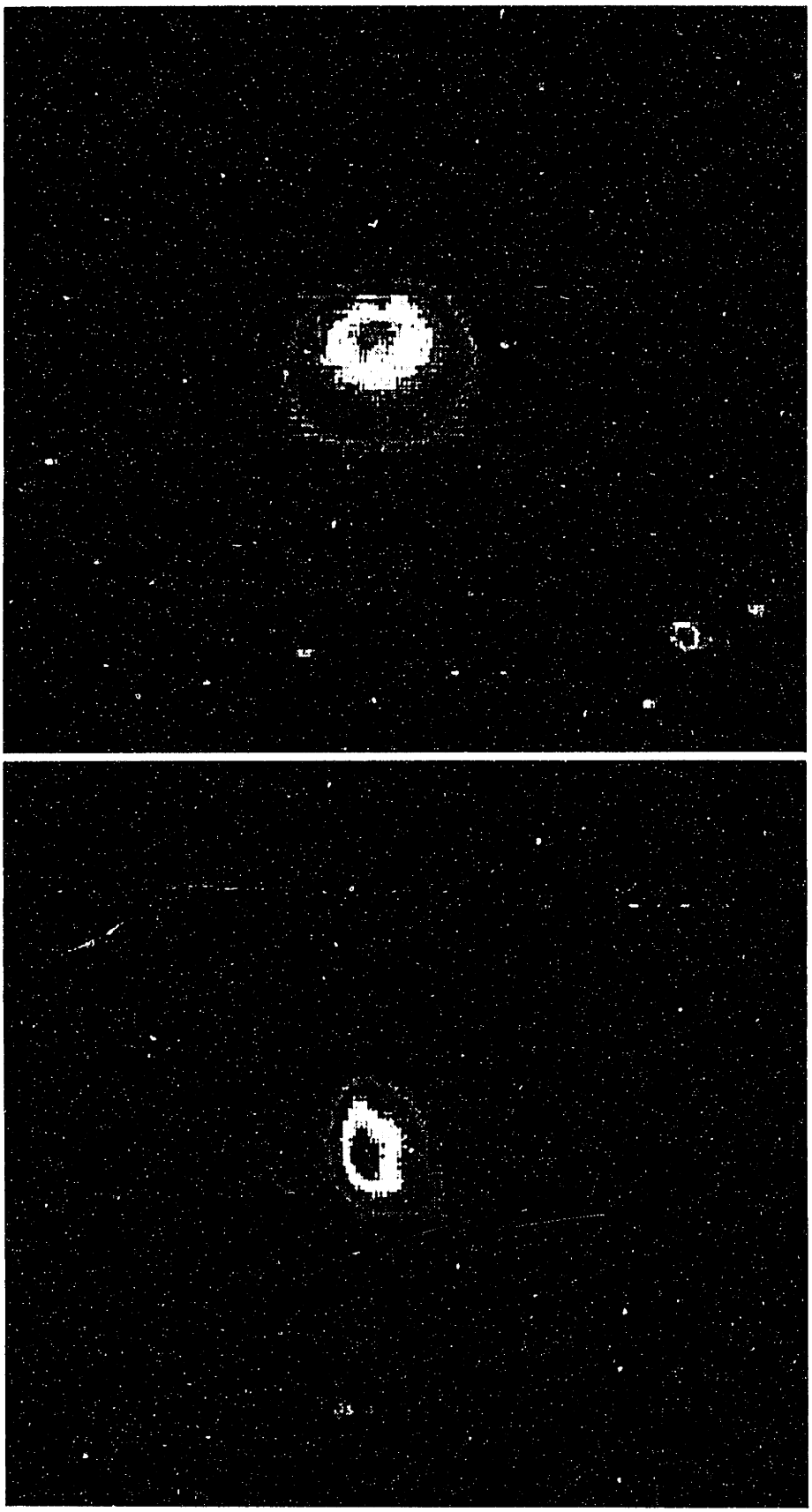

Fig. 6-9: Fluorescence images of atoms in the light trap (top) and after the transfer into the magnetic trap (bottom) with optical molasses cooling during the transfer

To quantify the transfer efficiency we took absorption spectra of atoms after they were recaptured from optical molasses by the magnetic trap. The result, shown on Fig. 6-10, demonstrates that the sample was loaded from the light trap to the magnetic trap with less than an order-of-magnitude loss of initial density of ~10^{11} cm^{-3}.

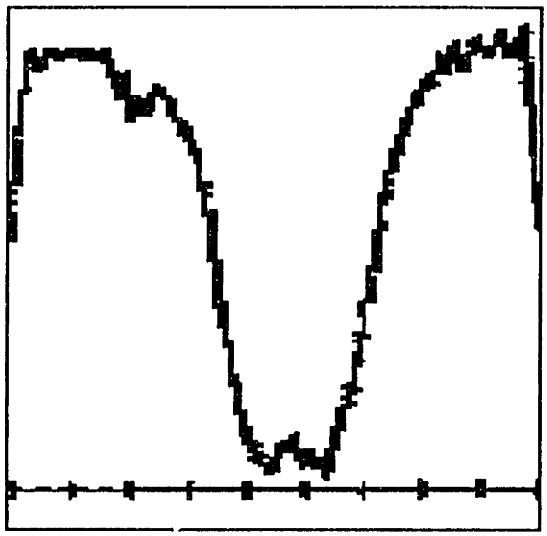

Fig. 6-10: An absorption spectrum of magnetically trapped atoms.

The next measurement we made was the number count of atoms in the trap. Using the photon titration technique described in Chapter 3, we measured a total number ~10^{10} of magnetically atoms. Comparison with the starting number of atoms in a dark SPOT gave the resulting transfer efficiency of ~25%, very close to the theoretical limit of 33%.

The next checkpoint is the temperature of the atoms. After confining the atoms in a trap for some time (>20 ms, to allow the transients caused by the transfer to die out) we released them from the trap and measured their temperature by imaging the ballistically expanding cloud as described in Chapter 3. The results are shown on Fig. 6-11. The temperature (as expected for a conservative potential) did not depend on the confinement time and was found to be ~60 μK for a magnetic field gradient ~30 gauss/cm. So, with the magnetic field gradient close to the value (15 gauss/cm) predicted by the simple

model described in section 6.5, we have accomplished efficient transfer of atoms from the molasses practically without heating.

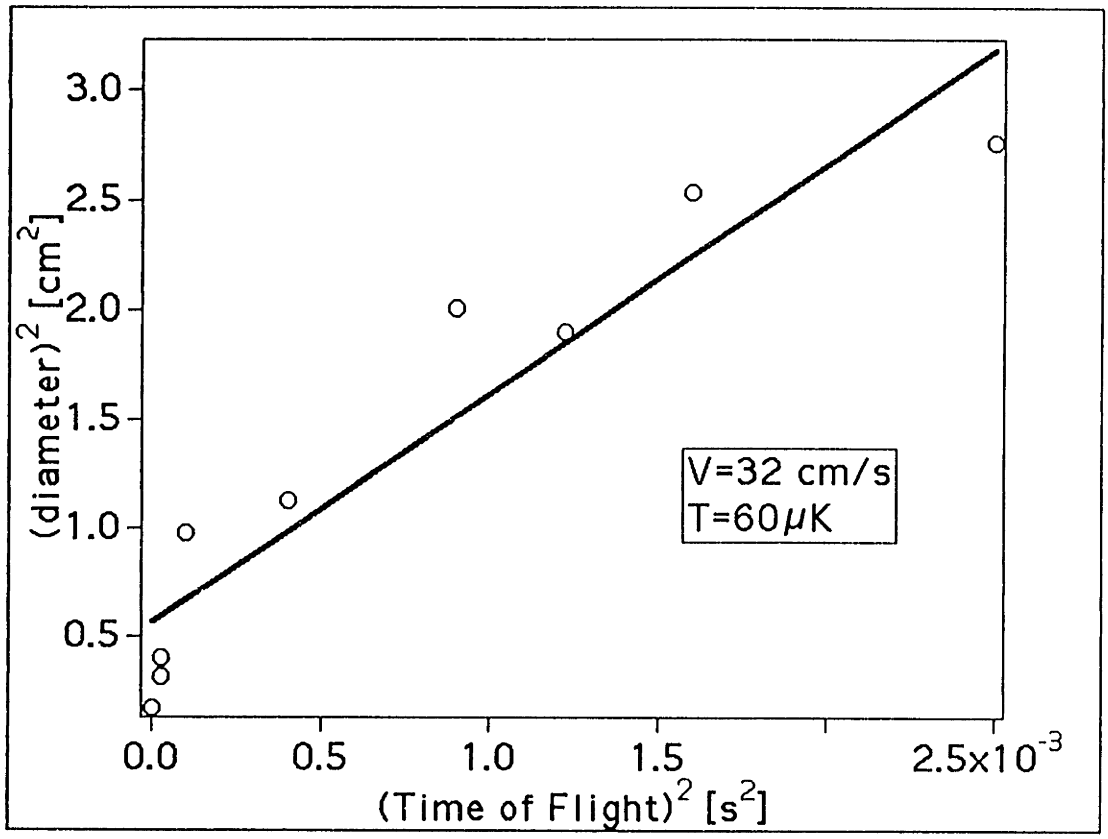

Fig. 6-11: Temperature measurement of magnetically confined atoms by fluorescence imaging. Atoms are magnetically trapped for 35 ms and then released from the trap.

In summary, we have magnetically trapped ~10^{10} of sodium atoms at densities ~10^{11} cm^{-3} and temperature ~60 μK. This is a two-order-of magnitude improvement in density and a factor of 30 in temperature for the same number of sodium atoms compared to the previous result achieved in our laboratory two years ago in a cryogenic magnetic trap [HMP92b]. These parameters combined with the trapping time of several minutes allowed us to go on to new exciting experiments described in the next Chapter.

The whole is simpler than the sum of its parts.

— Willard Gibbs

7. EVAPORATIVE COOLING

7.1. REVIEW

As of this writing, evaporative cooling of trapped atoms seems to be the most promising scheme to take the sample across the Bose-Einstein Condensation (BEC) barrier. The idea of evaporative cooling is very simple. When the hot atoms escape the trap over the edge of the potential well, they take with them higher-than-average energy thus effectively cooling the remaining sample and leaving behind a truncated Boltzmann energy distribution (Fig. 7-1). The condition, of course, is that the remaining sample is dense enough to rethermalize so that the concept of temperature remains meaningful. Thermalization and the resulting replenishment of the truncated energy distribution are crucial for sustaining the cooling process.

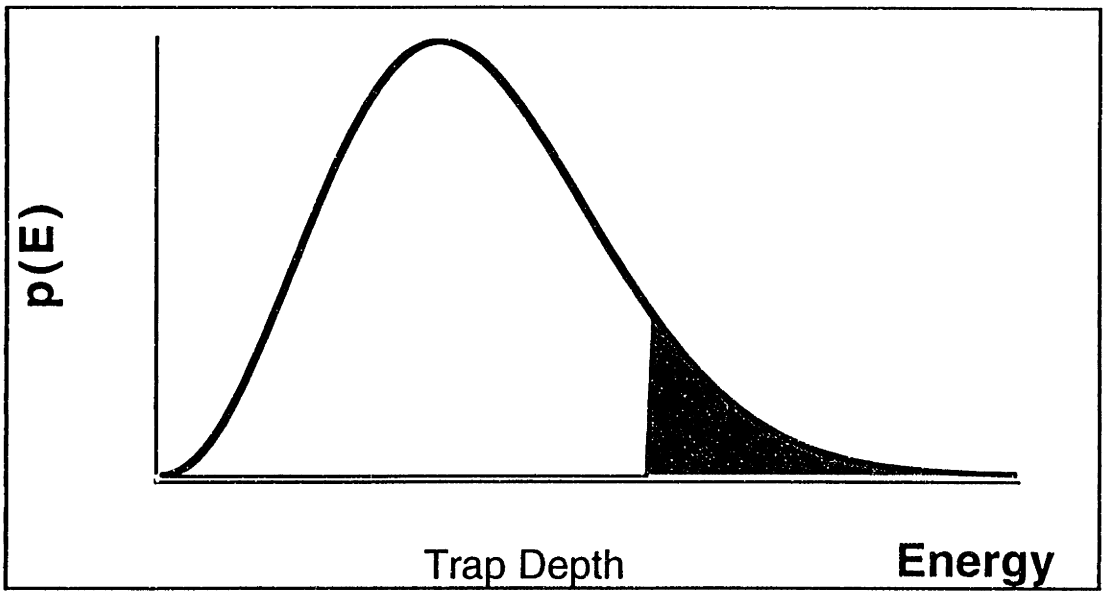

Fig. 7-1: The truncated Boltzmann distribution in a finite-depth trap. Atoms with energy higher that the trap depth (shaded area) evaporate from the trap.

Evaporative cooling of a magnetically confined gas was first discussed in [LMT85]. Soon thereafter the details for implementating in magnetically trapped hydrogen have been worked out in [HES86, TOM86]. In 1988 the MIT group successfully implemented the scheme for the first time [MDS88] and has used it to achieve record densities and temperatures of spin-polarized hydrogen atoms in a magnetic trap.

7.2. FORCED EVAPORATIVE COOLING

It is highly desirable to conduct evaporative cooling at the highest rate possible, since the sustained evaporation has to compete with loss processes. The losses such as background-gas collisions and spin-flip dipole-dipole collisions not only decrease the number density by removing atoms from the trap, but also heat up the sample. Dipole-dipole collisions occur more often near the bottom of the trap where the local density is higher, so they preferentially remove the colder atoms (anti-evaporation). The elastic collisions with hot background gas molecules can knock atoms out of the trap, but, in

addition, they can heat the sample up if the energy transferred in the collision is smaller than the trap depth.

In order to carry out evaporative cooling of the sample in a time-efficient way, two parameters of the trap should be varied with time (Fig. 7-2). The first is the trap depth. As the evaporatively cooled atoms condense near the bottom, the trap becomes for them effectively deeper and deeper, and so fewer and fewer atoms have the energy to escape. This process slows down the evaporation, so to sustain the rate the trap depth has to be lowered as the temperature of the sample decreases.

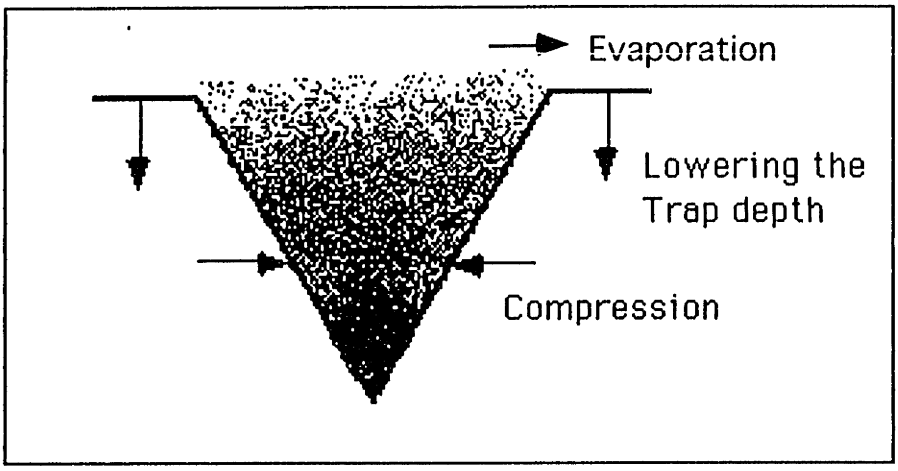

Fig. 7-2: The idea of Forced Evaporative Cooling is to lower the trap depth and adiabatically compress atoms at the same time to sustain the high rate of evaporation.

The second parameter of the trap that has to be varied in time is the trap stiffness or, in three dimensions, its volume. The rate of elastic collisions between atoms and, thus, the rate of evaporative cooling depends on the atomic density. So, when the volume of the trap is (slowly) decreased, the sample is adiabatically compressed and the density increase speeds up evaporation. On the downside, the sample is adiabatically heated at the same time, so the resulting temperature increase has to be corrected by subsequent evaporative cooling.

The scheme where the trap width and depth are altered in time in such a way that a high rate of evaporative cooling is sustained is called forced evaporation. The optimal path for simultaneously changing of these two closely coupled parameters can be found from a computer simulation of the process which described in Section 7.4. But before we start looking for the optimum we have to figure out the way the trap depth and width could be actually varied in real experiments.

7.3. RF-INDUCED EVAPORATION

In Ioffe bar magnetic traps, such as those used for trapping hydrogen [DSM89] and sodium [BLM87], the field for radial confinement is created by a long quadrupole magnet and the capping field for longitudinal confinement is provided by a pair of pinch solenoids. Fields from these two sources can be varied independently. For example the sample can be compressed by increasing the radial field, while atoms are allowed to evaporate through the weakened cap fields.

This is not the case in a spherical quadrupole, where increasing the field gradient for compression results in simultaneous increase of the trap depth. Hence, while the compression can be conveniently performed by simply increasing current through the coils, some mechanism of lowering the trap depth has to be provided. Such a mechanism - radiative evaporation - has been proposed in [PHM89]. The idea is to apply electro-magnetic radiation (radio frequency in the case of sodium) that can induce spin-flip transitions to the non-trapped states. If the linewidth of the radiation is narrow, the Zeeman shift ensures that for a given frequency only the atoms that reach a point in the trap where the magnetic field shifts the levels into resonance with rf radiation can experience a spin-flip and leave the trap. In case of an ideal, symmetric quadrupole field (without gravity) the rf frequency effectively limits the trap depth uniformly over the whole trap.

In a real spherical-quadrupole trap, where gravity is important, the potential well is asymmetric: the trap is weaker downward than it is upward. As a result, the equifield oblate spheroid (defined by the resonance condition $\mu|\vec{B}| = \hbar\omega_{rf}$) on which evaporation occurs is no longer an equipotential: $U = \mu|\vec{B}| + mgh$ is lowest at the bottom. For radiative evaporation, however, only the magnetic field is relevant, so instead of limiting the height of the potential well the resonant rf radiation "pokes a hole" in the trap near its bottom.

Let us now concider the rf-induced transition in more detail. Even if an atom happens to be in the place where its transition is in resonance with the rf, the probability of the transition is still less than unity and depends on the intensity of the rf radiation. The system can be described using the dressed atom picture, in which an intense radiation results in avoided level crossings (Fig. 7-3).

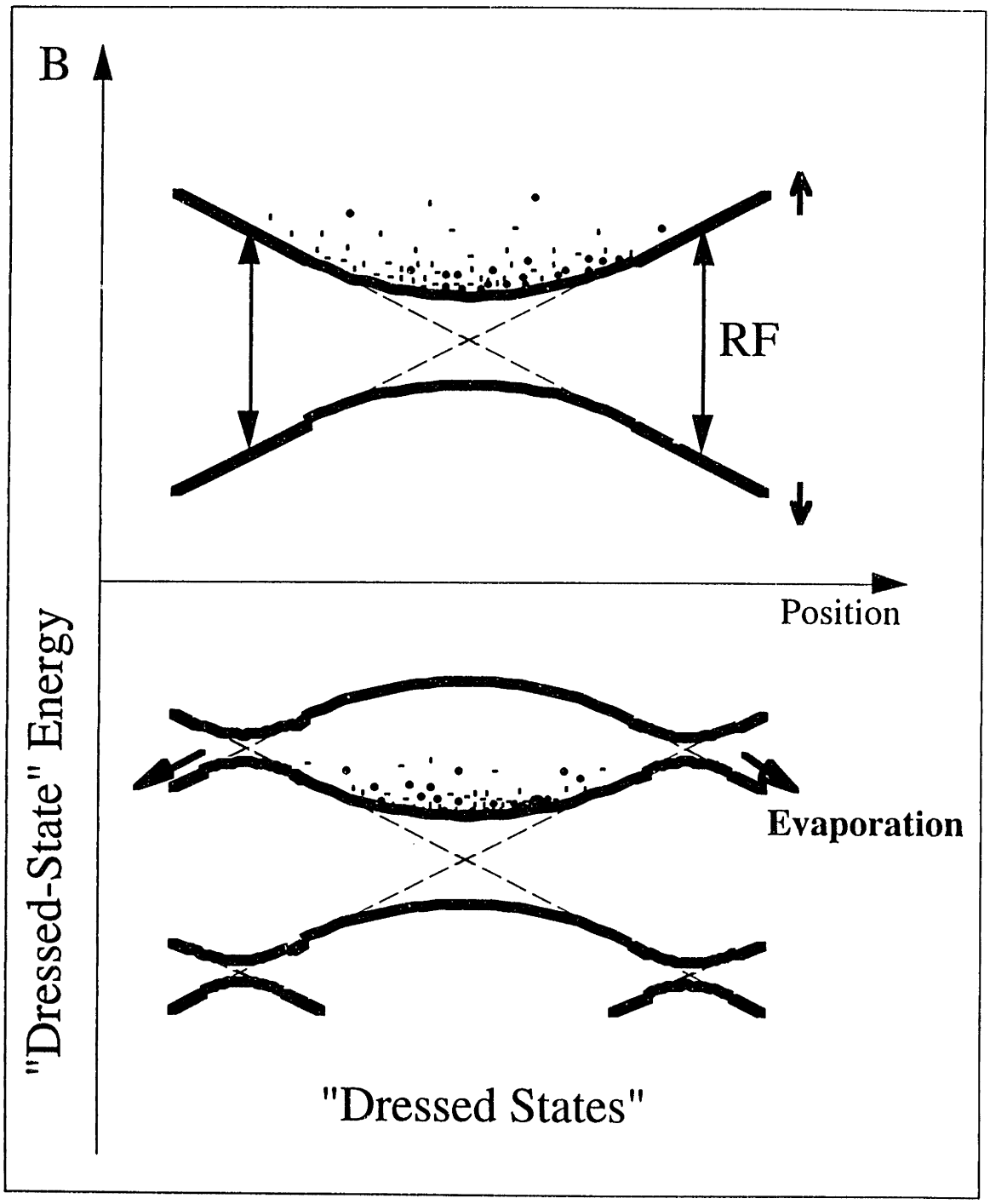

Fig. 7-3: Radiative evaporation in a magnetic trap.

The splitting is defined by the strength of the coupling interaction and increases with the rf power. Estimates of the probability of the non-adiabatic spin-flip transition in a single pass through the rf resonance region can be made using the Landau-Zener formula

$p = e^{-\frac{2\pi(\Delta U_{\uparrow\downarrow})^2}{\hbar(\frac{dE}{dt})}}$, where $\frac{dE}{dt} = \frac{dE}{dx}\cdot\frac{dx}{dt} \approx \mu B_z' \bar{v}$ and $\bar{v}$ is an average thermal velocity (~30 cm/s). Since the rf radiation couples two spin states, the splitting can be estimated as $\Delta U_{\uparrow\downarrow} = 2\mu B_{rf}$, where B_{rf} is the rf Magnetic field created by the antenna (Fig. 3-20). The estimate indicates that with the present antenna and ~1 W of rf power the level splitting is large enough so that the probability for the atom to stay on the adiabatic curve $(1-p)$ is close to unity (~0.7).

By sweeping the rf frequency from high to low one can lower the effective trap depth in time, i.e. realize forced evaporative cooling of the trapped atoms.

7.4. MODEL OF EVAPORATIVE COOLING

A computer model for evaporative cooling of hydrogen has been developed and its predictions compare favorably with the experimental observations [DOY91]. In order to develop a quantitative approach to evaporative cooling of sodium, this model has been adapted to include the features of our atomic system and experimental apparatus. The model described below has been coded into a computer program in C language. The numerical integration using the forth order Runge-Kutta algorithm took about a minute of CPU time on the Quadra 800 computer.

The environment desribed in the previous chapter can be characterized by external parameters like field gradient, rf frequency, background pressure, etc. The cold trapped atom sample can be described by two internal parameters: the total number of atoms N and (in the assumption of thermal equllibrium) temperature T. The purpose of the model is to solve numerically a set of equations for N and T as functions of time t.

After the trap is loaded, the initial conditions N_o and T_o are defined. In the magnetic trap there are four kinds of process leading to changes in the number of atoms: collisions with background molecules, dipole-dipole spin-flip collisions, evaporation of atoms from the trap, and the three-body collisions. So the rate of decrease of N is the sum of the respective rates of these processes:

$$\dot{N} = -(R_b + R_d + R_{ev} + R_{3b}). \tag{7.1}$$

All these processes also change the total energy of the sample $E = N\overline{E}$, where $\overline{E}$ is the average energy, so we can define the corresponding energy flows Q_b, Q_d, Q_{3b} and Q_{ev}. Also, the energy of the sample changes during the adiabatic compression of the sample. So the rate of change of the total energy is described by the equation:

$$\dot{E} = Q_b + Q_d + Q_{ev} + Q_{3b} + Q_{ad} \tag{7.2}$$

The loss rates and the energy flows are functions of the variables N and T, as well as time-dependent parameters of the trap. The equations (7.1) and (7.2) constitute the set of equations to be solved for variables N and T as functions of time t as a parameter. The next step is to find the expressions for these rates.

Evaporating Collisions

The assumption of the model is that atoms that populate the high-energy tail of the Boltzmann distribution are evaporated from the trap if their energy is higher than the trap depth E_t. The rate of collisions that produce evaporating atoms is then a fraction f of the total rate of elastic collisions in the trap R_{el}:

$$R_{ev} = f \cdot R_{el} \tag{7.3}$$

The value of f depends, among other things, on the temperature of the sample, the trap depth, and the shape of the potential. It can hardly be expressed analytically so a

numerical simulation has been used to calculate it in the assumption of hard-sphere collisions [HES86], [DOY91]. The range of validity of the model is given by the relative trap depth $\eta = \frac{E_t}{k_B T} > 4$. For a cylindrical potential it was found that

$$f = 0.14\eta^{2.09} e^{-\eta}. \tag{7.4}$$

It means that for the relative trap depth $\eta \approx 5$ it takes about 40 elastic collisions (occuring in one collision time) to repopulate the truncated tail of the Boltzmann distribution. For our calculations we used:

$$f = 0.02 \cdot e^{5-\eta}. \tag{7.5}$$

Every evaporating atom takes with it an average energy $\overline{E}_{ev}$. The same computer simulation [DOY91] gives the value:

$$\overline{E}_{ev} = E_t + 2k_B T. \tag{7.6}$$

The factor of two in (7.6) is approximate but the exact value is not important since the model is valid only for $E_t >> k_B T$.

For the energy flow out of the system due to evaporation we then obtain:

$$Q_{ev} = -R_{ev}\overline{E}_{ev} \tag{7.7}$$

Both the evaporation rate and the average energy of evaporating atoms depend on the depth of the trap E_t . The trap depth is defined by the frequency of the swept rf as a function of time. This is an external parameter of the model that we can vary and experiment with in order to find the optimum function for the rf frequency vs. time.

Elastic Collisions

The rate Γ of elastic collisions in a volume of ultracold gas of density n is:

$$\Gamma = \frac{1}{2} \cdot 4\pi a^2 \cdot \sqrt{2}v \cdot n^2 \cdot V., \tag{7.8}$$

where $\sigma = 4\pi a^2$ is the cross section, a is the scattering length of s-wave collisions, $\sqrt{2}v$ is the average relative thermal velocity, and the factor of one half takes care of overcounting. The value of the scattering length a for sodium is not known. However, the corresponding values for H [FRE80] and Cs [TMV92] have been calculated. The calculations predict the elastic collision rates per atom $\Gamma = \frac{1}{2}\sigma \cdot \sqrt{2}v \cdot n$ at 60 μK to be $\sim 10^{-10} \cdot n$ [s^{-1}] for (heavier) cesium and $\sim 10^{-13} \cdot n$ [s^{-1}] for (lighter) hydrogen.

Elastic scattering is due to attractive interaction between atoms $-C_6 / r^6$, and the cross section scales as $(C_6)^{\frac{2}{5}}$ [PRI83]. The value of C_6 for sodium (1580) is closer to that for cesium (7380) than for hydrogen (6.5) [VIG86]. Rescaling the cross section calculated in [TMV92] for cesium using these values of C_6 we obtain the value of cross section $\sigma = 10^{-12} \cdot [cm^2]$, in agreement with the estimate given in [PRI83]. This rate corresponds to the scattering length $a \approx 2 \cdot 10^{-7}$ cm, more than an order of magnitude larger than for hydrogen ($a \approx 0.72 \cdot 10^{-8}$ cm). The theoretical calculations for Cs has been recently confirmed by experimental measurements. A value $\sigma = 1.5 \cdot 10^{-12} \cdot [cm^2]$ for the elastic collision cross section for cesium has been found in [MCS93].

In the trap the local density $n(\vec{r})$ varies according to the Boltzmann distribution:

$$n(\vec{r}) = n_o e^{-\frac{U(\vec{r})}{k_B T}}. \tag{7.9}$$

So the total rate of thermalizing elastic collisions R_{el} is:

$$R_{el} = \frac{1}{2} \cdot 4\pi a^2 \cdot \sqrt{2}v \cdot \int_V n^2(\vec{r}) d^3\vec{r}. \tag{7.10}$$

In order to simplify the calculations, it is convenient to introduce an effective volume of the trap as:

$$V_{eff} = N/n_o = \int_V e^{-\frac{U(\vec{r})}{k_B T}} d^3\vec{r}. \tag{7.11}$$

For the spherical quadrupole field (6.2) without gravity the integral can be done analytically (Appendix A) and we obtain:

$$V_{eff} = 16\pi \left[\frac{-\frac{2}{b^3} - \frac{2r_o}{b^2} - \frac{r_o^3}{b}}{e^{br_o}} + \frac{2}{b^3} \right], \tag{7.12}$$

where r_o is the radius of the cloud measured along the z-axis, and $b = \frac{\mu B'_z}{k_B T}$.

For the spherical quadrupole trap with approximation $r_o \to \infty$ we arrive at the expression for the elastic-collision rate(Appendix A):

$$R_{el} = \frac{1}{2} \cdot 4\pi a^2 \cdot \sqrt{2} v \cdot \frac{N^2}{2^3 V_{eff}}. \tag{7.13}$$

Dipole-dipole Collisions

The rate of dipole-dipole collisions can be written as

$$R_d = \int_V \frac{1}{2} n^2(\vec{r}) g(\vec{r}) d^3\vec{r}, \tag{7.14}$$

where $g(\vec{r})$ is the dipolar decay rate constant. It is written as a function of position because it has been predicted to have a weak dependence on magnetic field [TKV91]. Near the origin of the trap, where the magnetic field is small, we can approximate $g(\vec{r})$ with a constant $g = 3 \cdot 10^{-15}$ [cm^3/s] [TKV91]. Again taking an integral over all space we obtain:

$$R_d = \frac{1}{2} g \frac{N^2}{2^3 V_{eff}}, \tag{7.15}$$

The average energy of the atom lost in each dipole collision is a sum of the average thermal energy and the average potential energy. This average potential energy is different, however, from the average potential energy in the trap because atoms escape through two-body collisions which occur preferentially near the center . This average is calculated in the Appendix A. Here I just give the final result:

$$\overline{E}_d = \frac{3}{2}k_B T + \frac{\int \varepsilon_{pot} n^2(\vec{r}) d^3\vec{r}}{\int n^2(\vec{r}) d^3\vec{r}} = 3k_B T \tag{7.16}$$

For the energy flow due to dipole loss we can write:

$$Q_d = -\overline{E}_d R_d, \tag{7.17}$$

Background Collisions

Atoms can be knocked out of the trap by collisions of residual molecules in the vacuum chamber with the trapped sample Because their room-temperature energy $k_B T_o$ by far exceeds the depth of the confining potential, we assume for this model that all collisions are "deadly" for trapped atoms, i.e. every collision with a background gas molecule knocks an atom from the trap. We thus neglect the heating of the trapped sample by grazing collisions with the background molecules. As discussed in [MON89] this assumption is only approximately correct for the vapor cell, where the predominant background-gas collisions are with the same heavy (Cs) atoms, but is justified for much lighter He atoms or, in our case, H_2 molecules.

The decay rate due to background collisions does not depend on the density of the sample, but does depend on the background pressure P in the vacuum chamber:

$$R_b = \sigma\bar{v}\frac{P}{k_B T_o}N. \tag{7.18}$$

Measurements of the cross section of collisions between sodium atoms and background nitrogen molecules have been performed in [PCB88] for a MOT. The residual gas in our experimental chamber consists mostly of hydrogen, besides the effective cross-section is dependent on the trap depth which is most certainly different. So the most accurate way is to define the decay rate operationally basing on the measurement results. We have observed τ~30 s 1/e-lifetime of our magnetic trap at $P \approx 10^{-11}$ Torr. So, assuming that the trap lifetime does not depend on its depth, the loss rate is taken to be:

$$R_b = \frac{1}{30}\frac{P[Torr]}{10^{-11}}N \ [s^{-1}]. \tag{7.19}$$

Since the background atoms take out trapped atoms randomly the average energy of the lost atom is equal to the average energy in the trap:

$$\overline{E}_b = \overline{E} = \frac{3}{2}k_B T + 3k_B T \ , \tag{7.20}$$

and the energy flow is then:

$$Q_b = -R_b \overline{E}_b \ . \tag{7.21}$$

Three-body Collisions

An estimate for the three-body rate constant for sodium $10^{-31\pm1}$ cm^6s^{-1} has been given in [PRI83]. For cesium, a value of $5\cdot10^{-29}$ cm^6s^{-1} has been found in [TMV92]. Since ~$1/r^6$ interaction is ~5 time smaller for sodium than for cesium [VIG86] it seems reasonable to accept the estimated value of $k_{3b}=10^{-29}$ cm^6s^{-1} for our calculations. The calculation analogous to (7.15) than gives for the:

$$R_b = 3k_{3b}\frac{N^3}{3^3 V_{eff}^2} \ [s^{-1}], \tag{7.22}$$

assuming that all three atoms are removed from the trap. The energy flow is

$$Q_{3b} = -R_{3b}\overline{E}_{3b}, \tag{7.23}$$

where the average energy $\overline{E}_{3b}$, is calculated in Appendix A:

$$\overline{E}_{3b} = k_b T. \tag{7.24}$$

Adiabatic Compression

When the field gradient of the trapping field increases, the sample is heated up because of work Q_{ad} done on the sample. When an ideal gas is slowly compressed its volume change is related to its temperature as:

$$V^{\gamma-1} \propto T^{-1}, \tag{7.25}$$

where $\gamma = \frac{5}{3}$ is the adiabatic constant. In a spherical quadrupole the effective volume is related to the temperature and the field gradient by equation (7.12) with $r_o = \infty$:

$$V_{eff} \propto \left(\frac{k_B T}{\mu B_z'}\right)^3, \tag{7.26}$$

which together with (7.20) gives for the average energy:

$$\overline{E} \propto T \propto (B_z')^{\frac{3}{1}}. \tag{7.27}$$

When the field gradient changes the energy changes as:

$$\frac{d\overline{E}}{dt} = \frac{\partial \overline{E}}{\partial B_z'}\frac{dB_z'}{dt} = \frac{2}{3}\overline{E}\frac{d(\ln B_z')}{dt}. \tag{7.28}$$

The rate of the energy increase than is

$$Q_{ad} = \frac{2}{3}N\overline{E}\frac{d(\ln B_z')}{dt}. \tag{7.29}$$

Summary of the Dynamics of the Model

In summary the model finds the solution of the set of two coupled differential equations :

$$\frac{d}{dt}N = -(R_b + R_d + R_{ev} + R_{3b})$$
$$\frac{d}{dt}\left(N\overline{E}\right) = -R_b\overline{E}_b - R_d\overline{E}_d - R_{ev}\overline{E}_{ev} - R_{3b}\overline{E}_{3b} + Q_{ad} \qquad (7.30)$$

for the variables N and T. In order to implement the Runge-Kutta algorithm the equations are rewritten to express the time derivatives $\dot{N}$ and $\dot{T}$ as functions of N ,T and time. Once the initial parameters N_o, T_o and the functions of time for compression (field gradient) and trap depth rf frequency) are defined, the computer calculates the "trajectories" $N(t)$ and $T(t)$. For the initial parameters N_o, T_o we have chosen the best typical values we have experimentally achieved to date: $N_o = 10^{11}$ and $T_o = 60\mu K$.

Analysis of the Model: Looking for the Optimum Path

As far as the computer simulation goes, we have two handles on the trapped sample: compression ($B_z'(t)$) and trap depth lowering ($\Omega_{rf}(t)$). The goal of the model is to determine the optimum combination of these two, that would yield the most efficient evaporative cooling of the trapped sample. The choice of the rf sweep $\Omega_{rf}(t)$ is not obvious and appears as a result of computer experiments, but close-to-optimal compression route $B_z'(t)$ can be determined just by looking at the rates (7.13), (7.15), and (7.19).

The rates of collisional processes are plotted as a function of the atomic density on Fig. 7-4. It is also important to keep in mind that the rate of elastic collisions (7.8) increases with temperature, while background collision, dipole-dipole collision, and three-body recombination rates are independent of temperature.

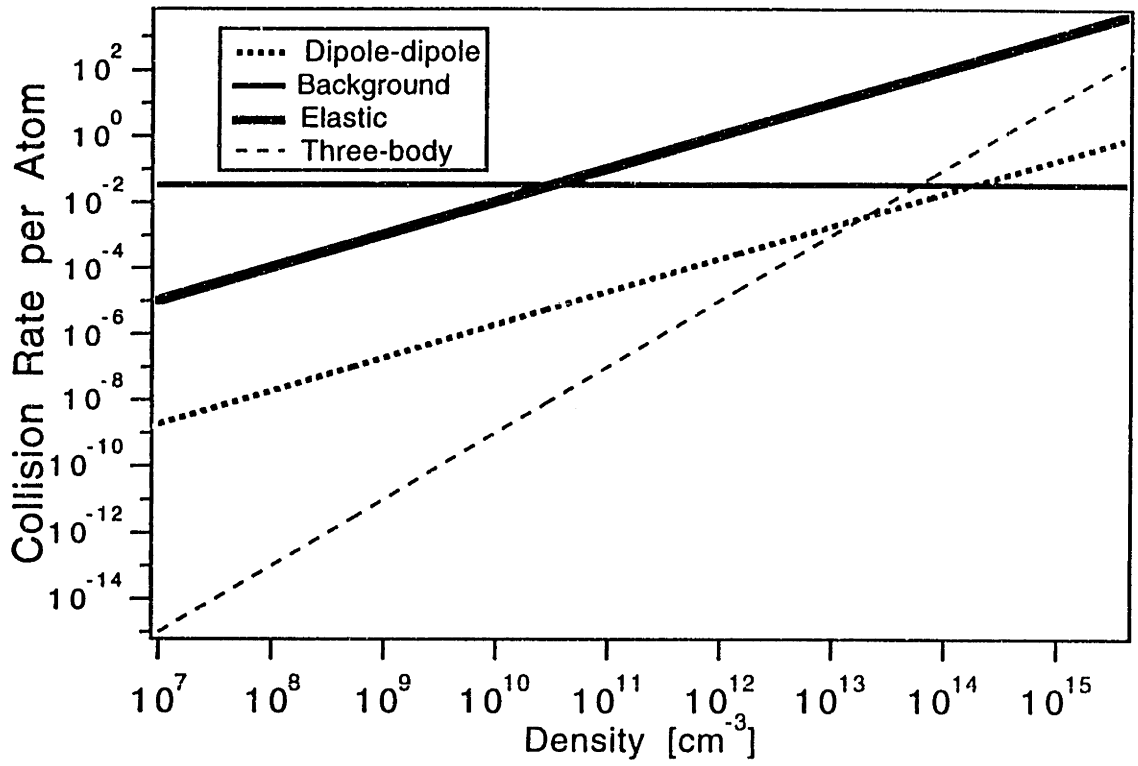

Fig. 7-4: The collisional rates per atom. Temperature of 60 μK is assumed.

The parameter that quantifies the efficiency of evaporative cooling is the ratio of the "good" elastic collisions, leading to evaporative cooling, to the "bad" collisions, leading to losses and heating:

$$\xi = \frac{R_{el}}{R_b + R_d + R_{3b}} \tag{7.31}$$

The ratio ξ as a function of atomic density is plotted on Fig. 7-5. If we start at $n_o = 10^{11}$ cm^{-3} it is advantageous to compress atoms right away as much as we can (with the current experimental setup we can not expect to increase the density more than an order in magnitude). The condition of adiabaticity is for the field gradient to change slower than the oscillation time in the trap which is ~100 ms. There is, of course, heating associated with the compression. In order to study its effect, the compression time has been varied between 1 s and 10 s. The trap depth can be controlled by changing the rf

frequency. The model allows for investigation the effects of different sweep patterns (linear, exponential, etc.) on evaporative cooling.

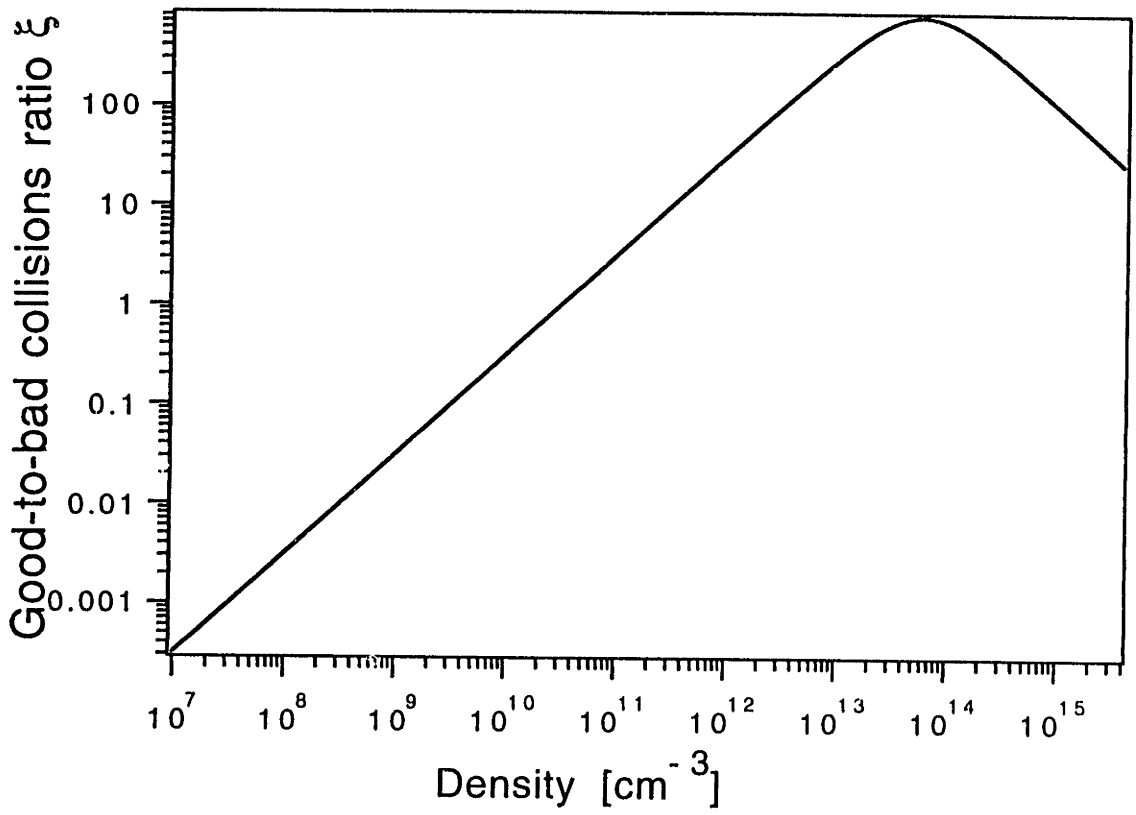

Fig. 7-5: The ratio of "good" to "bad" collisions ξ as a function of atomic density for T=60 μK.

7.5. RESULTS OF THE MODEL

In order to speed up evaporation while the background collisions remove atoms from the trap it is advantageous to compress atoms as fast as possible by ramping up the magnetic field gradient. So a compression time of 1 sec, roughly ten times the oscillation time, has been chosen.

The second observation is that the lower the trap depth the more efficient the forced evaporative cooling is. This is reasonable, since we have neglected the effect of the trap

depth on the loss, but have included its effect on the rate of evaporation. So, the lower the trap depth the larger the ratio of good-to-bad collision rates - the parameter defining the evaporative cooling efficiency. To investigate the possibility of evaporative cooling with realistic experimental conditions, the computer code has been designed in such a way that the rf frequency changes in time to maintain constant relative trap depth $\eta = 6$. Fig. 7-6 presents the results of the calculations.

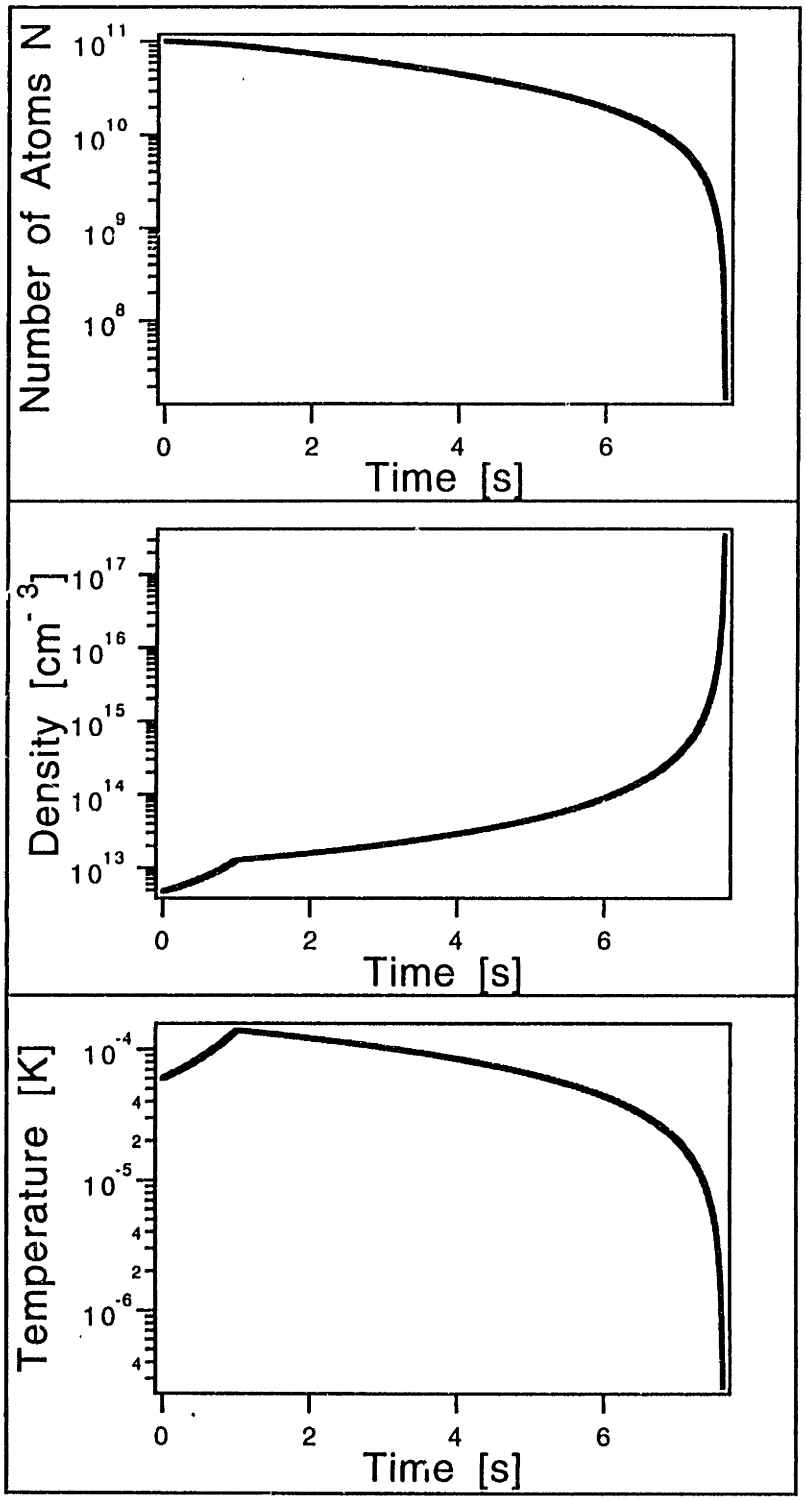

Fig. 7-6: The number of atoms N, the atomic density n and the temperature T of the trapped sample as a function of time for $T_o = 60\mu K$ and the initial number of atoms $N_o = 10^{11}$. The magnetic field gradient is increased from 30 gauss/cm to 100 gauss/cm in 1 s, while the relative trap depth $\eta = 6$ is maintained constant.

There are several distinct features of the plotted functions related to the physical processes described above. The number of atoms decreases exponentially when the loss is dominated by the background collisions. The increase in density during the first second is due to the heating during the compression. At the same time the temperature of the sample increases because of the heating associated with compression. After the compression is over, the temperature decreases due to evaporation. As can be seen from the plots the rate of evaporation increases with the density as expected. The model predicts that our experimentally achieved value $N_o = 10^{11}$ *is* high enough for achieving self-sustained "runaway" evaporative cooling(Fig. 7-6). During this runaway evaporation the temperature drops rapidly to ~1 μK. It is interesting to plot the corresponding phase-space densities as a function of time (Fig. 7-7). One should keep in mind, however, that the BEC Line is given only for reference and no conclusions about crossing it can be made within this model. The initial decrease in phase-space density during the adiabatic compression is probably due to the fact that the system is not closed and aton s are lost due to evaporation.

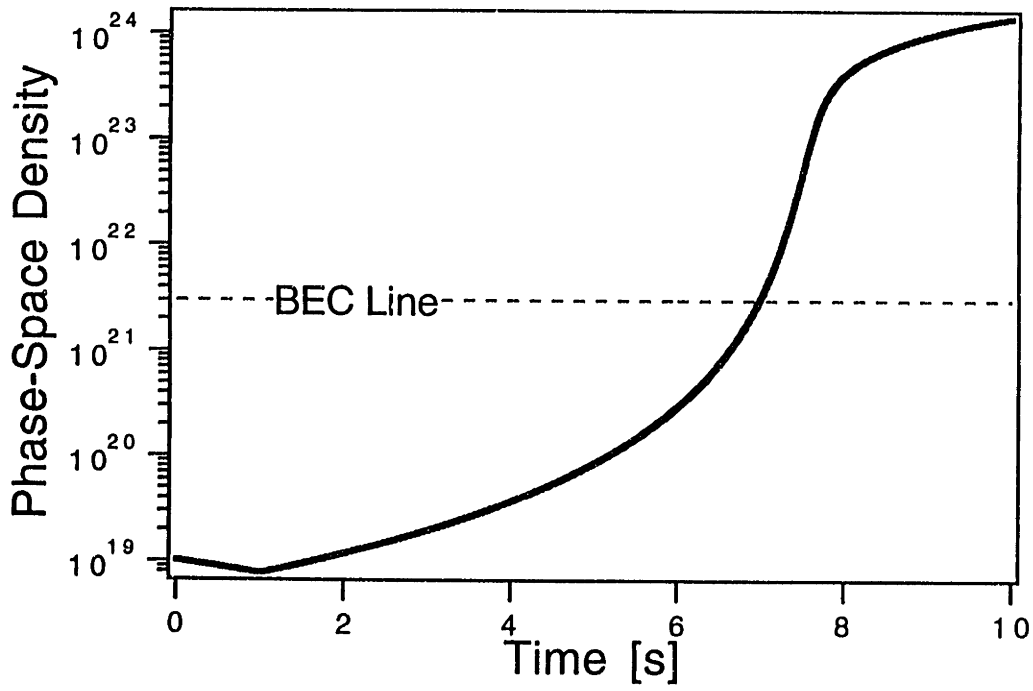

Fig. 7-7: The phase-space density as a function of time for the initial temperature $T_o = 60\mu K$ and the initial number of atoms $N_o = 10^{11}$.

The fast decrease of the number of atoms denoting the end of the runaway evaporation is not due to the BEC. It is not included in our model, since the behavior of the atomic system under BEC conditions is not well understood and is currently under intense investigations by theorists. Within the framework of our model the limit is set by the increased loss due to dipole-dipole collisions and the three-body collisions. Also, at higher densities the sample may become opaque for atoms escaping the trap via the dipole-dipole collisions, so the escaping atoms with the flipped spin accelerated by the field can knock out other atoms from the trap. This regime is somewhat similar to that in the experiments with magnetically trapped hydrogen and requires further optimization. However, the prediction of the model is favorable for cooling the sample well enough to bring it across (or at least close) to the BEC border.

The primary goal of the computer simulation is to investigate the possibility of implementing evaporative cooling with the present experimental setup and to find avenues of improvement. It is especially important because such crucial parameter as, for example, the elastic cross section is not known. It is useful than to investigate the margin of success by varying this parameter (Fig. 7-8). The model predicts, that the elastic cross section four times smaller than the assumed value is too small for implementing evaporative cooling with our present initial conditions. With that in mind the possibility of a brute-force increase of the magnetic field gradient (for example with a more powerful power supply) has been explored. The model predicts that ramping the fields up to experimentally achievable 300 gauss/cm might help to achieve the conditions required for runaway evaporative cooling even with the smaller value of the elastic cross-section. Some other possibilities are described in the next Chapter.

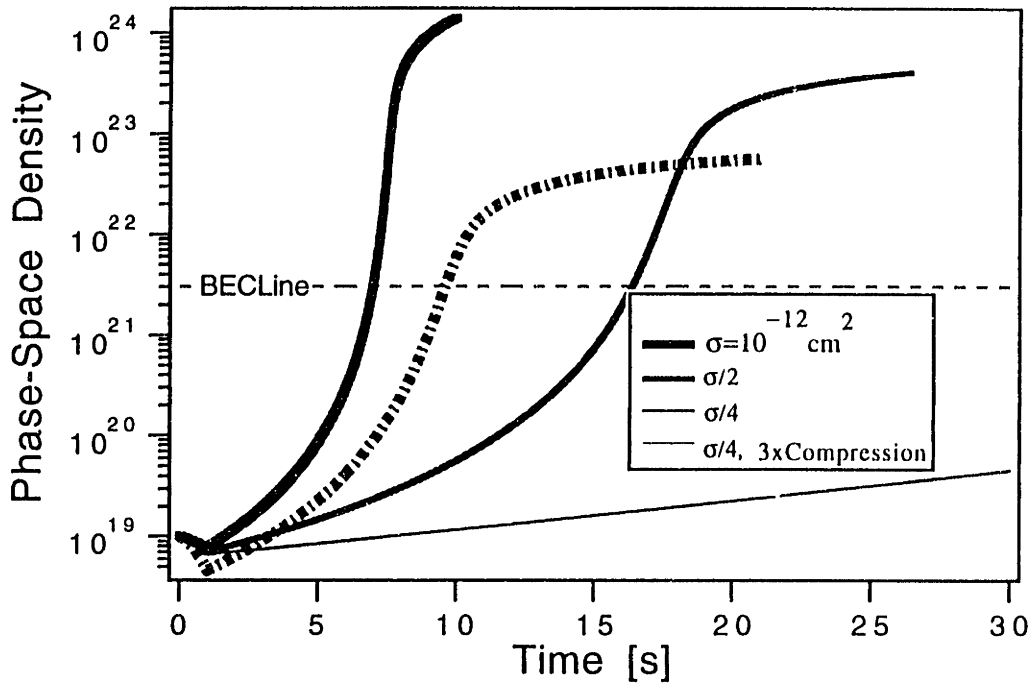

Fig. 7-8: Increasing the present maximum value of the magnetic field gradient may be a relatively simple way to achieve runaway evaporative cooling.

7.5. EXPERIMENTAL RESULTS

While actual evaporative cooling of sodium remains to be observed and, I believe, soon will be, certain steps towards the experimental realization of such cooling have been taken already. I will describe those in this Section.

The rf field applied the to the trapped sample is expected to remove the high-energy atoms from the trap. This would not only truncate the Boltzmann energy distribution, but also affect the spatial distribution of atoms in the trap. One could expect to see, instead of a gaussian cloud a ball with sharp edges. Unfortunately, there are effects that smear out the expected sharp edges. The sample is non-ergodic, so some hot atoms can be hidden from the rf on closed trajectories beyond the area of resonant spin-flips. The probability of flipping the spin is smaller-than-unity. Finally, gravity makes the area where the rf is in resonance with the Zeeman shifted atomic levels look like a spot at the

bottom of the cloud, rather than a shell. However, the first experimental results are encouraging (Fig. 7-9).

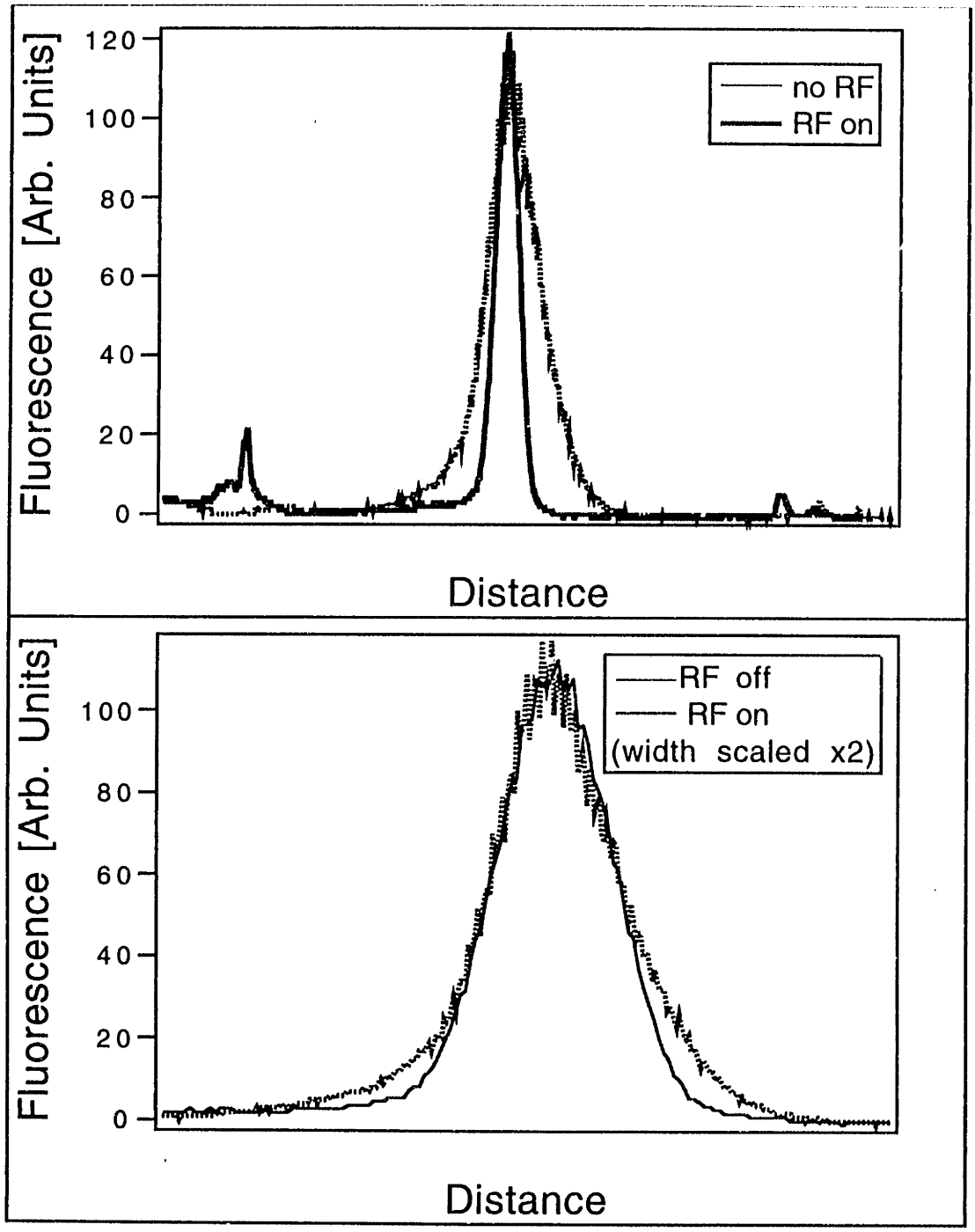

Fig. 7-9: Spatial profiles of the trapped cloud with or without the rf radiation(top). For qualitative comparison of the shapes, the profiles were scaled to have the same width as the other one(bottom).

The typical range of rf frequencies is 0.5-30 MHz and is attainable with commercial instruments. When rf radiation with frequency ~ 5 MHz is turned on an increased loss of atoms is observed. The decreased number of atoms results in smaller size of the cloud(Fig. 7-8, top). In order to compare the shapes the spatial distribution with and without the rf the narrower peak is rescaled so that it has the same width at half maximum as the other one. The difference in slope is then apparent. With the rf on, the tails of the distribution are lower, indicating the radiative truncation of the cloud. However, further, more quantitative experiments would be necessary to investigate and optimize the effects of radiative spin-flips.

The Difficult is that which can be done immediately;
the Impossible that which takes a little longer.
— George Santayana

8. SUMMARY OF THE PRESENT EXPERIMENTS AND PREDICTIONS FOR THE FUTURE

In conclusion, I would like to summarize the achievements and outline the future planned experiments. The described work constitutes serial steps towards the achievement of high densities of ultracold atoms. The Holy Grail of the field is observation of Bose-Einstein Condensation [GRE93] and it is reasonable to measure the achievements against this goal (Fig. 8-1). We have advanced by several orders of magnitude in increasing the phase-space density of the trapped sample, but there is still a (long?) way to go.

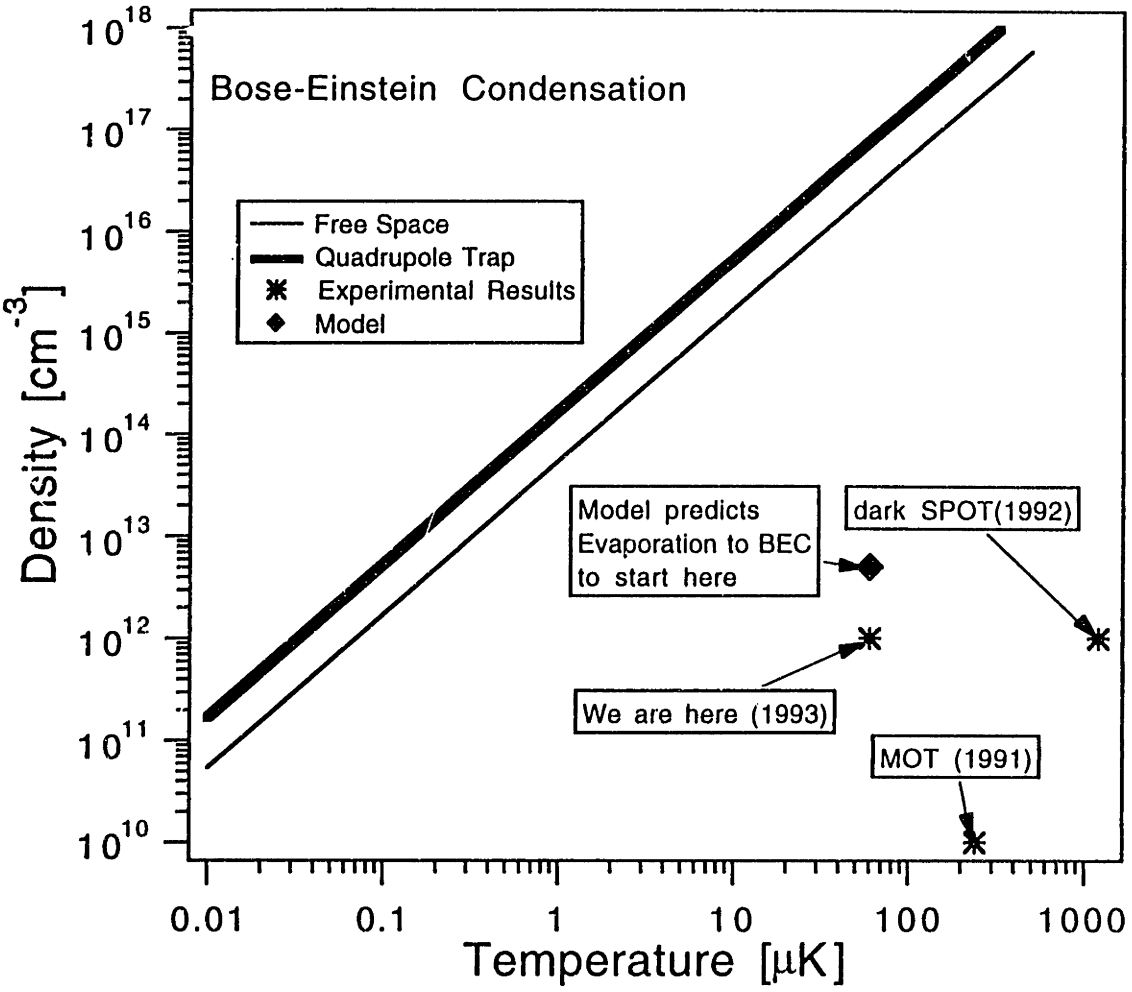

Fig. 8-1: On the way to the observation of BEC: the results of the described experiments.

Several short-term goals could be defined. It would advantageous to improve the model of evaporative by putting in accurate values for unknown parameters, such as the cross section of collisions between ultracold sodium atoms. So experiments aimed at measuring this parameters would be very useful. One possible experiment would be to measure the rate of replenishment of the truncated Boltzmann distribution by looking at the tails of the cloud's spatial profile. Another possibility is to displace the cloud in the magnetic trap by shifting the zero-field point, make the cloud slosh and measure the rate of equilibration into other directions perpendicular to the offset direction due to elastic

collisions. These experiments might significantly improve current understanding of the system.

Also, longer-term improvements can be made. A cryogenic apparatus could provide a more favorable environment by improving the vacuum and significantly cutting the rate of bad collisions. The present Zeeman slower could be replaced by an improved one that would combine the best features of the decreasing-field and the increasing-field modifications. A small-diameter, intense beam of cold atoms would provide a much higher loading rate so that more atoms might be available for evaporative cooling. Furthermore, a smaller magnetic trap of improved configuration would allow compressing atoms to higher densities. Most of these improvements are currently underway and new fascinating results may be coming out soon.

APPENDIX A

Average potential energy of the ensemble is given by the expression:

$$\bar{\varepsilon}_{pot} = k\bar{x} = \frac{\int \varepsilon_{pot} e^{-\beta\varepsilon_{pot}} d^3\vec{r}}{\int e^{-\beta\varepsilon_{pot}} d^3\vec{r}} = -\frac{\partial}{\partial\beta}\ln\left(\int e^{-\beta\varepsilon_{pot}} d^3\vec{r}\right), \tag{A.1}$$

where $\beta = \frac{1}{k_B T}$.

In a spherical quadrupole magnetic field

$$B(x,y,z) = \frac{B'_z}{2}\sqrt{x^2 + y^2 + 4z^2} \tag{A.2}$$

the potential energy looks like

$$\varepsilon_{pot} = \mu B(\vec{r}) = \mu B'_z \sqrt{\left(\frac{x}{2}\right)^2 + \left(\frac{y}{2}\right)^2 + z^2}\,. \tag{A.3}$$

The integral in (A.1) can be found analytically. Defining $b = \frac{\mu B'_z}{k_B T}$ we obtain:

$$\begin{aligned}
&\int e^{-\beta\varepsilon_{pot}} d^3\vec{r} = \iiint e^{-b\sqrt{\left(\frac{x}{2}\right)^2 + \left(\frac{y}{2}\right)^2 + z^2}}\, dxdydz = \\
&4\iiint e^{-b\sqrt{x^2+y^2+z^2}}\, dxdydz = 4\iiint e^{-br} r^2 dr \sin\theta d\theta d\varphi = \\
&16\pi\int e^{-br} r^2 dr = 16\pi\left(-\frac{2}{b^3} - \frac{2r}{b^2} - \frac{r^2}{b}\right)e^{-br}
\end{aligned} \tag{A.4}$$

For the trap depth much larger than $k_B T$ the limits of integration can be taken from zero to infinity: for $br = 6$ the difference is ~10%. So for the average potential energy we obtain:

$$\bar{\varepsilon}_{pot} = -\frac{\partial}{\partial\beta}\ln\left(\frac{32\pi}{b^3}\right) = \frac{\partial}{\partial\beta}\ln\left(\beta^3\right) = 3k_B T, \tag{A.5}$$

There are other integrals used in calculating average energies. One is the normalization integral for the two-body dipole-dipole collisions that can be easily obtained from (A.4) with substitution $b \to 2b$

$$\int n^2(\vec{r})d^3\vec{r} = \int e^{-2\beta\bar{\varepsilon}_{pot}} d^3\vec{r} = 16\pi\left(-\frac{2}{(2b)^3} - \frac{2r}{(2b)^2} - \frac{r^2}{2b}\right)e^{-2br}, \tag{A.6}$$

The other is the quadratically averaged potential energy:

$$\bar{\varepsilon}_{pot,2} = \frac{\int \varepsilon \cdot n^2 d^3\vec{r}}{\int n^2 d^3\vec{r}} = \frac{\int \varepsilon e^{-2\beta\varepsilon} d^3\vec{r}}{\int e^{-2\beta\varepsilon} d^3\vec{r}} = -\frac{1}{2}\frac{\partial}{\partial\beta}\ln\left(\int e^{-2\beta\varepsilon} d^3\vec{r}\right) = \frac{3}{2}k_B T, \tag{A.7}$$

For three-body collisions the inergrals are obtained from (A.4) with substitution $b \to 3b$:

$$\int n^3(\vec{r})d^3\vec{r} = \int e^{-3\beta\bar{\varepsilon}_{pot}} d^3\vec{r} = 16\pi\left(-\frac{2}{(3b)^3} - \frac{2r}{(3b)^2} - \frac{r^2}{3b}\right)e^{-3br}, \tag{A.8}$$

and for the average potential energy:

$$\bar{\varepsilon}_{pot,2} = \frac{\int \varepsilon \cdot n^3 d^3\vec{r}}{\int n^3 d^3\vec{r}} = \frac{\int \varepsilon e^{-3\beta\varepsilon} d^3\vec{r}}{\int e^{-3\beta\varepsilon} d^3\vec{r}} = -\frac{1}{3}\frac{\partial}{\partial\beta}\ln\left(\int e^{-3\beta\varepsilon} d^3\vec{r}\right) = k_B T. \tag{A.9}$$

REFERENCES

BDR 91 T.E. Barrett, S.W. Dapore-Schwartz, M.D. Ray and G.P. Lafyatis, "Slowing Atoms with σ^- Polarized Light", Phys. Rev. Lett. **67**, 3483-3486 (1991).

BEM87 T. Bergeman, Gidon Erez and Harold J. Metcalf, "Magnetostatic trapping fields for neutral atoms", Phys. Rev. A **35**, 1535-46 (1987).

BLM87 V. Bagnato, G. Lafyatis, A. Martin, E. Raab, R. Ahmad-Bitar, and D.E. Pritchard, "Continuous Stopping and Trapping of Neutral Atoms", Phys. Rev. Lett., **58**, 2194, (1987).

BLM89 V.S. Bagnato, G.P. Lafyatis, A. Martin, K. Helmerson, J. Landry, D.E. Pritchard, "Laser deceleration and velocity bunching of a neutral sodium beam", J. Opt. Soc. Am. B, **6**, 2171 (1989).

CBA86 S. Chu, J. Bjorkholm, A. Ashkin, and A. Cable, Phys. Rev. Lett., **57**, 314 (1986).

CHB85 Steven Chu, Leo Hollberg, John E. Bjorkholm, Alex Cable and Arthur Ashkin, "Three-dimensional viscous confinement and cooling of atoms by resonance radiation pressure", Phys. Rev. Lett. **55**, 48-51 (1985).

CLN92 A. Clairon, Ph. Laurent, A. Nadir, M. Drewsen, D. Grison, B. Lounis, and C. Salomon, "A simple and compact source of cold atoms for cesium fountains and microgravity clocks", in Proceedings of the 6th European Frequency and Time Forum, held at ESTEC, Noordwijk, Netherlands, 17-19 March 1992 (ESA SP-340, June 1992), p. 27-33.

CMW91 E.A. Cornell, C. Monroe and C.E. Wieman, "Multiply Loaded, ac Magnetic Trap for Neutral Atoms", Phys. Rev. Lett., **67**, 2439 (1991).

CSG91 A. Clairon, C. Salomon, S. Guellati, and W.D. Phillips, Europhys. Lett., **16**, 165 (1991).

DAC89 J. Dalibard, C. Cohen-Tannoudji, "Laser cooling below the Doppler limit by polarization gradients: simple theoretical models", J. Opt. Soc. Am. B **6**, 2023 (1989).

DAL88 J. Dalibard, Opt. Commun. **68**, 203 (1988).

DAV95 K.B. Davis, PhD Thesis, MIT (ca.1995), to beunpublished.

DOY91 J.M. Doyle, PhD Thesis, MIT (1991), unpublished.

DSM89 J. M. Doyle, J. C. Sandberg, N. Masuhara, I.A. Yu, D. Kleppner, and T.J. Greytak, "Energy distribtions of trapped tomic hydrogen", J. Opt. Soc. Am. B, **6**, 2244-2248 (1989).

DSY91 J.M. Doyle, J.C. Sandberg, I.A. Yu, C.L. Cesar, D. Kleppner, and T.J. Greytak, Phys. Rev. Lett., **67**, 603 (1991).

EBS92 O. Emile, F. Bardou, C. Salomon, Ph. Laurent, A. Nadir, and A. Clairon, Europhys. Lett., **20**, 687 (1992).

FRE80 D. G. Friend and R. D. Etters, "A dilute hard-sphere Bose-gas model calculation of low-density atomic-hydrogen gas properties," J. Low Temp.Phys., **39**, 409 (1980).

GAP89 A. Gallagher, D.E. Pritchard, "Exoergic Collisions of Na^*-Na", Phys. Rev. Lett. **63**, 957, (1989).

GAS90 A. Góngora-T., A. Antillón, and T.H. Seligman, "Computer simulation of magnetically trapped neutral atoms", Phys. Rev. A **42**, 3139, (1990).

GKC92 K.E. Gibble, S. Kasapi, and S. Chu, "Improved magneto-optic trapping in a vapor cell", Opt. Lett. **17**, 526 (1992).

GLJ88 P.L. Gould, P.D. Lett, P.S. Julienne, W.D. Phillips, H.R. Thorsheim, and J. Weiner, Phys. Rev. Lett., **60**, 788, (1988).

GLO92 R. Grimm,V.S. Letokhov, Yu.B. Ovchinnikov, A.I. Sidorov, "Observation of a Magneto-Optical Radiation Force", JETP Lett. **54**, 615 (1991).

GRE93 T. Greytak, "Prospects for Bose-Einstein Condensation in Magnetically Trapped Atomic Hydrogen," in Proceedings of the Workshop on Bose-Einstein Condensation, 1993, to be published.

HEE63 C.V. Heer, Rev. Sci. Instrum., **34**, 532 (1963).

HES86 Harald F. Hess, "Evaporative cooling of magnetically trapped and compressed spin-polarized hydrogen", Phys. Rev. B **34**, 3476-79 (1986).

HKD87 H. Hess, G. Kochanski, J. Doyle, N. Masuhara, D. Kleppner, and T.J. Greytak, Phys. Rev. Lett., **59**, 672 (1987).

HMP92a K. Helmerson, A. Martin, and D.E. Pritchard, "Laser and rf spectroscopy of magnetically trapped neutral atoms", J. Opt. Soc. Am. B, **9**, 483 (1992).

HMP92b K. Helmerson, A. Martin, and D.E. Pritchard, "Laser cooling of magnetically trapped neutral atoms", J. Opt. Soc. Am. B, **9**, 1988 (1992).

KAC92 M. Kasevich and S. Chu, "Laser Cooling Below a Photon Recoil with Three-Level Atoms", Phys. Rev. Lett. **69**, 1741 (1992).

KEP92 W. Ketterle, D.E. Pritchard, "Trapping and focussing ground state atoms with static fields", Appl. Phys. B, **54**, 403 (1992).

LMT85 R.V.E. Lovelace, C. Mehanian, T.J. Tommila, and D.M. Lee, "Magnetic confinement of a neutral gas", Nature, **318**, 30-36 (1985).

LPR89 P.D. Lett, W.D. Phillips, S.L. Rolston, C.E. Tanner, R.N. Watts, C.I. Westbrook, "Optical molasses", J. Opt. Soc. Am. B **6**, 2084 (1989).

LWW88 P.D. Lett, R.N. Watts, C.I. Westbrook, W.D. Phillips, P. Gould, and H. Metcalf, Phys. Rev. Lett. **61**, 169 (1988).

MCS93 C. R. Monroe, E. A. Cornell, C. A. Sackett, C. J. Myatt, and C. Wieman, "Measurement of Cs-Cs Elastic Scattering at T=30 μK", Phys. Rev. Lett. **70**, 414 (1993).

MDS88 Naoto Masuhara, John M. Doyle, Jon C. Sandberg, Daniel Kleppner, Tom J. Greytak, Harald F. Hess and Greg P. Kochanski, "Evaporative cooling of spin-polarized atomic hydrogen", Phys. Rev. Lett. **61**, 935-8 (1988).

MOL69 B. R. Mollow, Phys. Rev. **188**, 1969 (1969).

MOL91 K. Mølmer, Phys. Rev. A **44**, 5830 (1991).

MON92 C. R. Monroe, PhD Thesis, Univ. of Colorado (1992), unpublished.

MPP85 A. Migdall, J. Prodan, W. Phillips, T. Bergeman, and H. Metcalf, Phys. Rev. Lett., **54**, 2596 (1985).

MSR90 C. Monroe, W. Swann, H. Robinson, and C. Wieman, "Very Cold Atoms in a Vapor Cell", Phys. Rev. Lett. **65**, 1571 (1990).

PCB88 M. Prentiss, A. Cable, J.E. Bjorkholm, Steven Chu, E.L. Raab and D.E. Pritchard ,"Atomic-density-dependent losses in an optical trap", Opt. Lett. 13, 452-4 (1988).

PHM89 D.E. Pritchard, K. Helmerson, and A. Martin, in Atomic Physics XI, S. Haroche, J.C. Gay, G. Grinberg, eds. (World Scientific, Singapore, 1989), p. 179.

PPM85 W. D. Phillips, J. V. Prodan and H. J. Metcalf, "Laser cooling and electromagnetic trapping of neutral atoms," J. Opt. Soc. Am. B **2**, 1751-67 (1985).

PRI83 David E. Pritchard, "Cooling neutral atoms in a magnetic trap for precision spectroscopy", Phys. Rev. Lett. **51**, 1336-39 (1983).

PRK93 D.E. Pritchard and W. Ketterle, in Proceedings of the Varenna Summer School on Laser Manipulation of Atoms and Ions, edited by E. Arimondo and W. P. Phillips (North-Holland, Amsterdam, 1993), p. 473-496.

RAA88 E.L. Raab, PhD Thesis, MIT (1988), unpublished.

RPC87 E.L. Raab, M. Prentiss, A. Cable, S. Chu, and D.E. Pritchard, Phys. Rev. Lett., **59**, 2631 (1987).

RWM90 E. Riis, D.S. Weiss, K.A. Moler, and S. Chu, Phys. Rev. Lett., **64**, 1658 (1990).

SDP90 C. Salomon, J. Dalibard, W.D. Phillips, A. Clairon and S. Guellati, "Laser Cooling of Cesium Atoms below 3 mK", Europhys. Lett. **12**, p. 683-688 (1990).

STF91 A. Steane and C. Foot, Europhys. Lett. **14**, 231 (1991).

SST91 F. Shimizu, K. Shimizu and H. Takuma,"Four-beam laser trap of neutral atoms", Opt. Lett. **16**, 339 (1991).

SSV90 S-Q. Shang, B. Sheehy, P. van der Straten, and H. Metcalf, Phys. Rev. Lett. **65**, 317 (1990).

STE86 Stig Stenholm, "Semiclassical theory of laser cooling", Rev. Mod. Phys. **58**, 699-739 (1986).

SWW91 D. Sesko, T. Walker, and C. Wieman, "Behavior of Neutral Atoms in a Spontaneous Force Trap," Phys. Rev. Lett. **64**, 408 (1990).

TKV91 E. Tiesinga, S.J.M. Kuppens, B.J. Verhaar, and H.T.C. Stoof, "Collisions between cold ground-state Na atoms", Phys. Rev. A **43**, 5188 (1991).

TMV92 E.Tiesinga, A.J. Moerdijk, B.J. Verhaar, and H.T.C. Stoof, "Conditions for Bose-Einstein condensation in magnetically trapped atomic cesium", Phys.Rev. A **46**, R1167 (1992).

TOM86 T. Tommila, "Cooling of Spin-Polarized Hydrogen Atoms Trapped in Magnetic-Field Minima", Europhys. Lett., **2**, 789-795 (1986).

UWR89 P.J. Ungar, D.S. Weiss, E. Riis, S. Chu, "Optical molasses and multilevel atoms: theory", J. Opt. Soc. Am. B **6**, 2058-71(1989).

VIG86 J. Vigué, Phys. Rev. A **34**, 4476 (1986).

WHF92 T. Walker, D. Hoffmann, P. Feng, and R.S. Williamson III, "A Vortex-force Atom Trap", Phys. Lett. A **163**, 309 (1992).

WIN84 W.H. Wing, Prog. Quantum Electron., **8**, 181 (1984).

WRS89 David S. Weiss, Erling Riis, Yaakov Shevy, P.J effrey Ungar, Steven Chu, "Optical molasses and multilevel atoms: experiment", J. Opt. Soc. Am. B **6**, 2072(1989).

WSW90 T. Walker, D. Sesko, and C. Wieman, "Collective Behavior of Optically Trapped Neutral Atoms", Phys. Rev. Lett. **64**, 408 (1990).